Chem Soc Rev

REVIEW ARTICLE

View Article Online
View Journal | View Issue

Cite this: *Chem. Soc. Rev.*, 2015, **44**, 193

Strategies for interfacing inorganic nanocrystals with biological systems based on polymer-coating

Goutam Palui,† Fadi Aldeek,† Wentao Wang and Hedi Mattoussi

Interfacing inorganic nanoparticles and biological systems with the aim of developing novel imaging and sensing platforms has generated great interest and much activity. However, the effectiveness of this approach hinges on the ability of the surface ligands to promote water-dispersion of the nanoparticles with long term colloidal stability in buffer media. These surface ligands protect the nanostructures from the harsh biological environment, while allowing coupling to target molecules, which can be biological in nature (*e.g.*, proteins and peptides) or exhibit specific photo-physical characteristics (*e.g.*, a dye or a redox-active molecule). Amphiphilic block polymers have provided researchers with versatile molecular platforms with tunable size, composition and chemical properties. Hence, several groups have developed a wide range of polymers as ligands or micelle capsules to promote the transfer of a variety of inorganic nanomaterials to buffer media (including magnetic nanoparticles and semiconductor nanocrystals) and render them biocompatible. In this review, we first summarize the established synthetic routes to grow high quality nanocrystals of semiconductors, metals and metal oxides. We then provide a critical evaluation of the recent developments in the design, optimization and use of various amphiphilic copolymers to surface functionalize the above nanocrystals, along with the strategies used to conjugate them to target biomolecules. We finally conclude by providing a summary of the most promising applications of these polymer-coated inorganic platforms in sensor design, and imaging of cells and tissues.

Received 4th April 2014

DOI: 10.1039/c4cs00124a

www.rsc.org/csr

Florida State University, Department of Chemistry and Biochemistry, 95 Chieftan Way, Tallahassee, Florida 32306, USA
† Contributed equally to the manuscript assembly.

Goutam Palui

Dr Goutam Palui received his BSc and MSc degrees in Chemistry from Jadavpur University before completing his PhD from the Indian Association for the Cultivation of Science (IACS) in 2008 under the supervision of Dr Arindam Banerjee, both in Kolkata, India. During his doctoral research he worked on materials self-assemblies using synthetic short peptides and pseudo-peptides. Currently he is a postdoctoral research fellow at Florida State University, working with Professor Mattoussi, on the design and development of functional water-soluble nanomaterials (metallic and semiconductor QDs) and their applications in imaging and sensing.

Fadi Aldeek

Dr Fadi Aldeek is an organic/inorganic chemist. He received his bachelor's and master's degrees in Molecular and Supramolecular Chemistry from Louis Pasteur University, Strasbourg, France. He then pursued his postgraduate study at Henri Poincare University, Nancy, France, earning a PhD in Materials Science in 2010. He is currently working as a Postdoctoral Associate at the Florida State University. His research interest focuses on developing the technology of chemically synthesized inorganic nanocrystals. This includes challenges in making new compositions of nanocrystals and multifunctional ligands, with the ultimate goal of incorporating the nanocrystals into hybrid organic–inorganic devices and biological systems.

1. Introduction

Due to their unique physical, chemical, electronic, and optical properties nanostructures made of metals, metal oxides and metal chalcogenides have attracted a great deal of interest and much activity in the past two decades.[1–5] This has been motivated by the great promise they offer for use in numerous applications, ranging from developing optical and electronic devices to cellular imaging and biological sensing.[6–9] For example, semiconductor nanocrystals (quantum dots, QDs) exhibit size- and composition-tunable broad absorption along with narrow and symmetric emission spectra; they also exhibit a remarkable photo- and chemical-stability compared to organic dyes and fluorescent proteins.[3,10] Similarly, gold and silver nanoparticles (AuNPs and AgNPs) exhibit size- and shape-dependent Surface Plasmon Resonance (SPR) bands ranging from the UV to the near infrared (NIR) region of the optical spectrum.[9,11,12] Nanostructures made of other transition metals, such as Fe_3O_4, Mn-doped Fe_3O_4, FePt, Ni, and Co show strong size- and composition-dependent coercivity.[13–16] These unique features made them very promising to design platforms that can be applied in biology, including imaging, sensing and as diagnostic tools.[17–20]

Aqueous phase synthesis is in principle the simplest method to prepare water dispersible nanocrystals.[21] For instance, one of the earlier methods to use this route to grow QDs, including CdTe, CdSe and CdS, involved mixing of cadmium precursors in the presence of a suitable stabilizer (*e.g.*, thioalkyl acids or amines) in aqueous solutions followed by injection of tellurium, selenium or sulfur precursors. This method provides nanocrystals that are capped with small thioalkyl acids (*e.g.*, mercaptoacetic acid, 3-mercaptopropionic acid, or cystamine).[22–24] Similarly, there are several water-based chemical routes for growing Fe_3O_4 and other magnetic nanoparticles, based on the reduction of precursors such as $FeCl_3{\cdot}6H_2O$ and $FeCl_2{\cdot}4H_2O$.[25,26] However, these water-based routes tend to provide nanocrystals with rather large size distribution, and water dispersions of such materials often exhibit limited colloidal stability to pH changes and to added electrolytes and/or redox-active agents. Furthermore, this route does not allow easy, straightforward and controllable functionalization of the nanocrystals, a necessary property for further coupling to target biomolecules.

High temperature reduction of organometallic precursors in the presence of hydrophobic coordinating molecules (ligands) has thus far provided the highest quality nanocrystals, with low size dispersity and good control over size, morphology and core crystallinity.[1,4,27] Commonly used ligands in this "hot injection" reaction include trioctyl-phosphine (TOP), trioctyl-phosphine oxide (TOPO), alkylamine and alkylcarboxy for luminescent QDs, didodecyldimethylammonium bromide (DDAB) for AuNPs, and oleic acid or oleylamine for iron oxide nanoparticles.[1,27] The resulting materials are capped with hydrophobic ligands, which make them dispersible only in organic solvents. Thus, use of these materials in biomedical applications requires surface-modification with hydrophilic and biocompatible molecules. In the last two decades, this has been widely done by several groups using various chemical approaches, which can essentially be grouped into two main strategies:[3,8,28–30] (1) removal of the native capping molecules and replacing them with bifunctional hydrophilic ligands (cap or ligand exchange), or (2) encapsulation of the native hydrophobic nanocrystals within micelle structures made of amphiphilic polymers or phospholipids.

Ligand exchange requires the presence of strong anchoring groups to replace the native cap and drive the metal–ligand coordination onto the inorganic surface of the nanocrystals, along with hydrophilic segments to promote affinity to water. This strategy relies on small molecules as well as polymers. In comparison, the encapsulation strategy preserves the native cap, as these interdigitate with the hydrophobic block of the amphiphilic

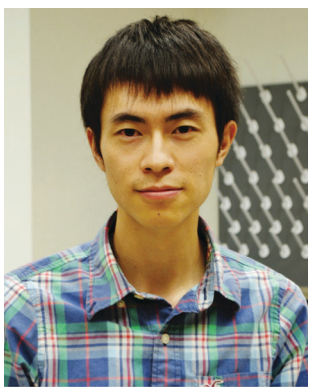

Wentao Wang

Wentao Wang received a bachelor's degree in Physical/Organic Chemistry from Jilin University, China, in 2009. He then joined the Florida State University in the fall of 2011. He has been a PhD candidate under the supervision of Prof. Hedi Mattoussi, in the Department of Chemistry and Biochemistry since January 2012. His research focuses on the design of multidentate and multifunctional polymer ligands readily adaptable to various metal-rich surfaces, including QDs, metal and metal oxide nanocrystals. He is also developing novel approaches for surface modification of inorganic nanocrystals and the development of biological sensing and imaging using these optimally designed inorganic nanoprobes.

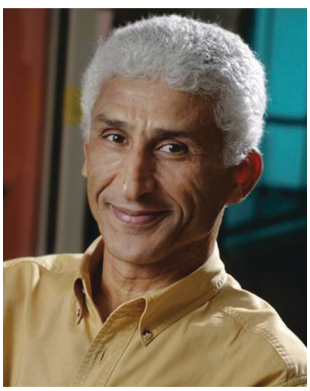

Hedi Mattoussi

Hedi Mattoussi has been a professor at the Florida State University since August 2009. Prior to that, he spent 12 years working as a senior Scientist at the Naval Research Laboratory (Washington). He received a bachelor's degree in Physics from the Faculty of Sciences in Tunis and a PhD in Condensed Matter Physics from the University of Pierre & Marie Curie in 1987. In 1994, he received a Habilitation to direct Research, Materials Physics, also from Paris. He presently focuses on interfacing inorganic nanoparticles with biological systems using chemical and photochemical means, to develop novel tools for imaging, sensing and diagnostics.

polymer or phospholipid (usually made of aliphatic chains), *via* entropy-driven hydrophobic interactions, while the hydrophilic moieties promote affinity to water media. Interdigitation between the native cap of the nanoparticles and the hydrophobic block of the amphiphilic polymers is stable enough to preserve the nanocrystal coating and impart colloidal stability in aqueous media.

Polymers, whether synthetic or biological, have provided researchers with a great platform for designing a variety of ligands capable of functionalizing various nanocrystals *via* either of the strategies introduced above (ligand exchange or encapsulation). The wealth of knowledge and expertise gained over the past few decades for designing novel polymerization techniques allow remarkable control over the chemical make-up, architecture and molecular weight of the polymer materials. This can be fully exploited to develop effective surface functionalization strategies applicable to a wide range of nanoparticles based on encapsulation or ligand exchange.[31,32] For instance, simple or more complex chemical transformations have allowed groups to design and test several amphiphilic polymers with control over the hydrophobic and hydrophilic blocks as well as the overall polymer size. Similarly, simple chemical coupling allowed the development of several polymer ligands, where the ability to insert several anchoring groups along a single polymer chain can enhance the ligand-to-nanoparticle interactions and provide materials with great colloidal stability.

We will start by summarizing the synthetic strategies developed so far to prepare inorganic nanoparticles, including water-based routes as well as those relying on the high temperature reduction of metal precursors (also referred to as hot injection routes). We then summarize the recent advances in the synthesis of several amphiphilic block copolymers and their use to promote water solubilization *via* either ligand exchange or an encapsulation process. We then conclude by providing a summary of a few representative biological applications using those polymer-functionalized nanoparticles.

2. Growth of inorganic (metal, semiconducting and magnetic) nanocrystals

Reduction of metal salts in water media (*e.g.*, growth in inverse micelles or *via* arrested precipitation) was one of the initial routes developed to grow several metal, metal oxide and semiconductor nanocrystals.[33–35] This route is easy to implement, often carried out using slight heating, and has the advantage of providing materials already dispersed in aqueous media. It requires water-soluble precursors and suitable capping ligands for stabilizing the nanoparticles. In comparison, the growth of nanocrystals at high temperature (or *via* hot injection method) relies on the reduction of organometallic precursors at high temperatures; it is primarily carried out in organic hydrophobic solutions. This growth route has been applied to an array of materials, including magnetic nanocrystals, semiconductor quantum dots as well as gold and other metal nanoparticles; it has been shown to reproducibly provide homogeneous materials with crystalline cores and, more importantly, low size dispersity. This involves a temporally discrete nucleation event driven by saturation in the precursor concentrations, followed by slower controlled growth and ripening with further annealing. Rapid injection of precursors into the reaction vessel increases their concentrations above the nucleation threshold. A short nucleation burst partially relieves this saturation, and subsequent annealing at high temperatures promotes the growth of more homogeneous and uniform nanocrystals.

The ability of this growth route to provide homogeneous crystalline nanocrystals with reduced size dispersity has allowed researchers to carry out sophisticated characterization studies and probe the fundamental photophysical, spectroscopic and chemical properties of such nanoparticles. The collected results have been tested against proposed conceptual models,[36–45] which have permitted scientists to develop a much better understanding of these systems. This experimental success has also brought these nano-structured materials closer to the realm of targeted applications, including integration into electronic, optical and biological systems.

2.1. Luminescent quantum dots (QDs)

In the last two decades, a variety of colloidal semiconductor nanostructures have been prepared; they range from spherical, cubic, rod-like, branched, tetrapod-like and platelet materials.[27,46–50] The first reports describing the effects of carrier confinement within nanometer size nanocrystals of semiconductors were published in 1981–1982. In those studies, the authors reported measurement of size-dependent optical spectra of CuCl, CdS or CdSe nanocrystals embedded into silicate glasses.[51,52] Efros and Efros showed that glass matrices containing precipitated crystallites of CdS_xSe_{1-x} can be used to build tunable optical filters where variations in the size and/or stoichiometry of the crystallites allow tuning of the corresponding absorption band.[53] During the same period similar results detailing the growth of CdSe nanoparticles precipitated in glasses were reported by Borrelli and co-workers at Corning Inc.[54,55] The growth of colloidal QDs using reverse micelles reported by Brus and co-workers, and Henglein and co-workers in the early 1980s introduced another highly important dimension into the field, as nanocrystals with size-tunable optical features that can be studied and processed from solution conditions became available.[33,34,56,57]

A major breakthrough in the growth of high quality colloidal QDs was developed in 1993 by Bawendi and co-workers. The authors showed that high temperature reduction of dimethyl cadmium ($CdMe_2$) and tri-*n*-octylphosphine–selenium (TOP:Se) in a hot coordinating solution (at 280–350 °C) made of trioctylphosphine and trioctylphosphine oxide (TOP/TOPO) can provide high quality CdSe QDs, with homogeneous core crystallinity, low size dispersity and high room temperature photoluminescence quantum yields.[27] In particular, they prepared CdSe nanocrystals that exhibit narrow and size-tunable symmetric photoluminescence (PL) spectra, a high molar extinction coefficient and high chemical stability. In subsequent studies, Peng and co-workers

further refined the synthetic rationales underlying the effectiveness of this synthetic route by showing the importance of introducing additional alkylphosphonic acid ligands into the growth reaction. They also introduced less volatile cadmium precursors (*e.g.*, cadmium oxide, CdO and cadmium acetylacetonate, $Cd(acac)_2$), which are also easy to store under ambient conditions.[58,59] A flurry of reaction modifications and adjustments followed those studies where several groups further optimized the reaction conditions and expanded those chemical rationales to grow other nanocrystals.[4,60–62] In some of those reports, researchers substituted the TOP/TOPO and hexadecyl amine (HDA) coordinating solution with other non-coordinating materials made of long alkane or alkene chains such as 1-octadecene (ODE) or even olive oil.[63,64] Those materials do not play any major role in the stabilization of the nanoparticles during the growth process. These adjustments produce a smaller number of nuclei than the ''conventional'' route where TOP–Se is used as a precursor, and this is attributed to the fact that TOP provides better solubility to selenium compared to 1-octadecene or other non-coordinating solvents.

By using different combinations of core materials (*e.g.*, CdTeSe, CdHgTe), one can expand the photoemission of the nanocrystals from the red to near infrared (NIR) region of the optical spectrum compared to those made of CdSe cores.[65–67] More recently, a few groups expanded the high temperature reduction route to grow Cd-free QDs (namely, $CuInS_2$ and $CuIn_5Se_8$ nanocrystals) with emission extending into the NIR.[62,68] However, those dots still exhibit broad emission with absorption spectra reflecting less defined crystalline structure. Further refinements will undoubtedly improve those properties.

Solution phase grown nanocrystals have a large fraction of their atoms arrayed at their surfaces that are poorly passivated by the ligands. This creates surface defects which affect the rate of exciton radiative recombination, and reduce the overall photoluminescence quantum yields (PL QYs).[69,70] Borrowing from the ideas developed for band gap engineering in semiconductor physics, several groups overcoated the native core with a thin layer (a few atomic monolayers) of wider band gap semiconducting materials to enhance the quantum yield and photochemical stability of the resulting core–shell QDs. Examples include the overcoating of CdSe QDs with a thin layer of ZnS, CdS, ZnSe, or ZnSSe.[71–74] More recently a few groups have shown that a very thick layer of CdS on a CdSe core can bring the PL quantum yield (QY) close to one.[75,76] Overcoating is usually carried out using high temperature reduction of the desired precursors, but at lower values (120–190 °C) than those used for the core growth. A variety of precursors such as diethylzinc ($ZnEt_2$), zinc acetate ($Zn(OAc)_2$), zinc acetylacetonate ($Zn(acac)_2$), zinc diethyldithiocarbamate ($Zn(S_2CNEt_2)_2$), hexamethyldisilathiane (TMS_2S), and elemental sulfur have been used for overcoating CdSe with ZnS shells.[4,71–73,77–79] We should note that overcoating with ZnS, ZnSe, CdS, CdSe, *etc.* has also been applied to other QD materials such as those made of PbSe, $CuInS_2$ and $AgInS_2$ cores.[80–82] We would like to note that the exact nature of the surface capping ligands on QDs prepared using these various high temperature strategies is still unclear. Even though the commonly accepted premise has been for a long time that TOP and TOPO constitute the majority of surface ligands along with smaller fractions of alkylamines and phosphonic acids, recent studies have indicated that TOP/TOPO may not be the dominant ligands on the nanocrystal surface.[83]

2.2. Iron oxide nanoparticles

The growth of iron-based magnetic nanoparticles initially relied on the precipitation of Fe salts, namely $FeCl_3$ in aqueous media, and materials prepared *via* this route have been used in various studies and applications.[84–87] This route provided an easy synthetic route to prepare ''ready to use'' hydrophilic nanoparticles. However, control over size, core crystallinity and size dispersity of the nanoparticles was only marginally achieved. Several iron-based magnetic nanoparticles (*e.g.*, Fe_5HO_8, $Fe_5(O_4H_3)_3$, Fe_2O_3, Fe_3O_4, and FeOOH) have been grown using various methods, including chemical precipitation,[85] sol–gel and forced hydrolysis,[84] hydrothermal techniques,[86] surfactant-mediated template synthesis,[87] microemulsion,[88] biomimetic mineralization,[89] flow injection synthesis,[90] electrochemical methods,[91] sonochemical techniques,[92] and high-temperature decomposition. Following the success of the hot injection method reported for growing QDs,[27] several groups expanded this route to grow various magnetic nanocrystals.[16,93–101] For instance, high quality iron oxide nanocrystals with homogeneous crystalline cores and low size distribution have been prepared *via* decomposition of iron precursors, such as $Fe(Cup)_3$ (Cup = *N*-nitrophenylhydroxylamine), $Fe(CO)_5$, $FeCl_3$ and $Fe(acac)_3$ at high temperature in reaction media made of organic solvents and coordinating surfactants. In one of the earlier growth strategies published by Hyeon and co-workers, the authors started by developing an organometallic iron complex, iron–oleate, prepared by reacting iron chloride ($FeCl_3{\cdot}6H_2O$) and sodium oleate in a mixture of ethanol, water and hexane at ~70 °C for four hours.[1,16] Washing the above mixture with distilled water followed by evaporation of the organic solvent(s) yields a waxy solid compound, which could be stored for further use. Briefly, in a typical reaction to grow 12 nm (diameter) NPs, the desired amount of iron–oleate complex is dissolved in 1-octadecene (a non-coordinating organic solvent) and the mixture is heated and annealed at ~320 °C. After 30 min, the colorless solution turns brownish black, indicating the formation of iron oxide nanoparticles. The size of the nanoparticles can be controlled by varying the solvent used (*e.g.*, 1-hexadecene (b.p. 287 °C), 1-octadecene (b.p. 317 °C), trioctylamine (b.p. 365 °C), octyl ether (b.p. 286 °C), and 1-eicosene (b.p. 330 °C)) and the annealing temperature; larger sizes are usually prepared when using solvents having higher boiling points. Also, the size of the iron oxide nanocrystals can be tuned by varying the concentration of oleic acid in the reaction mixture. For example, 11, 12, and 14 nm sized iron oxide nanoparticles were produced using solutions containing 1.5, 3, and 4.5 mM of oleic acid, respectively. Peng and co-workers further expanded this approach and showed that other metal oxide nanocrystals such as Cr_2O_3, MnO, and Co_3O_4 can be grown using high

temperature reaction starting with various metal fatty acid salts as precursors.[100]

The high temperature growth strategy has further been expanded to prepare metal-doped nanoparticles with enhanced coercivity, because the spin contribution from the dopants can alter the final magnetic moment per crystal unit and increases the magnetic susceptibility of the resulting nanoparticles. Indeed, the magnetic properties of iron oxide nanoparticles can be controlled by doping the core with magnetically susceptible elements, such as Mn, Ni and Co ions. The resulting transition metal-doped iron oxide nanoparticles exhibit mass magnetization values that can vary from one system to another, with the highest value measured for $MnFe_2O_4$ nanoparticles (110 emu per gram Mn, Fe), as demonstrated by Cheon and co-workers.[97,102] These magnetism-engineered iron oxide (MEIO) nanoparticles can induce significant MR contrast-enhancement effects, and the resulting nanoparticles were applied for visualizing (*via* magnetic resonance imaging, MRI) a few specific biological events.[14,103,104] Similarly, high temperature growth has been applied to prepare magnetic nanocrystals made of metal alloys, such as FeCo and FePt.[105]

2.3. Gold nanoparticles (AuNPs)

Chemical reduction of gold precursors at room temperature in either the aqueous phase or a biphasic water–organic mixture has been effectively used by several groups to grow Au nanoparticles.[9,106] In one of the early pioneering studies, Turkevich and co-workers were the first to report the growth of ~10–20 nm AuNPs using water-based reduction of chloroauric acid ($HAuCl_4$) in the presence of trisodium citrate.[107] Frens and co-workers used this synthesis route to grow several size AuNPs with the diameter ranging from 16 to 140 nm, by varying the molar ratio of citrate-to-gold precursors used.[108] There have also been instances where polymers such as poly(*N*-vinylpyrrolidone) (PVP), poly(4-vinylpyridine), poly(vinyl alcohol) (PVA), polyethyleneimine (PEI), poly(diallyl dimethylammonium chloride) (PDDA) have been used to grow and stabilize Au nanoparticles.[109,110] We should stress that the as-prepared citrate-stabilized AuNPs exhibit very limited colloidal stability to pH changes and added salts. Aggregation is often observed in even slightly acidic buffers or in the presence of low concentration of added electrolytes. They have recently been shown to strongly and nonspecifically interact with serum proteins, producing what has commonly been referred to as corona on inorganic nanoparticles in biological media.[111–113] A major development was the synthesis of hydrophobic AuNPs functionalized with thioalkyl ligands using two-phase (toluene–water) reaction reported by Brust and Schiffrin.[106] In this method, $HAuCl_4$ was transferred from water to toluene (organic phase) using the surfactant tetraoctylammonium bromide (TOAB), and then reduced by sodium borohydride ($NaBH_4$) in the presence of dodecanethiol. Recently, our group has developed a one-phase aqueous growth method of AuNPs stabilized with dithiol-terminated hydrophilic molecules (*i.e.*, PEG- or zwitterion-appended lipoic acid, LA–PEG or LA–ZW ligands). This route permitted control over the NP diameter in the range of 2–20 nm.[114] It has more recently been expanded to grow Ag nanoparticles over a broad size range as well as fluorescent clusters of Au and Ag.[12,115] Another approach for synthesizing and controlling the size and shape of AuNPs is the seed-mediated growth. Here, small metal nanoparticles are prepared first and then used as seeds (nucleation centers) along with dissolved Au precursors to grow larger size AuNPs and Au nanorods (AuNRs).[116–118] Thus far, most of the water-based growth methods used thiol-containing compounds to provide monolayer-protected AuNPs, a choice motivated by the strong metal-coordination of sulfur onto gold surfaces.[119] Peng and co-workers developed a single-phase (organic) reaction to grow AuNPs with low size dispersity. Here, tetrabutylammonium borohydride (TBAB) mixed with hydrazine (in toluene) was used as a reducing reagent and fatty acids or aliphatic amines were used as ligands.[48] Briefly, fatty acid ligands were first dissolved in toluene, followed by the addition of TBAB dissolved in didodecyldimethylammonium bromide (DDAB). Then, a gold precursor dissolved in DDAB was injected into the above solution at room temperature. Finally, thiol ligands were added to the reaction mixture to stop the growth of the nanoparticles. Improvement of the nanoparticle quality while reducing size distribution was achieved by thermal annealing at 120 °C. The size of the particles was controlled from 1.5 to 15 nm by varying the nature of the reducing agent and capping ligands, the TBAB-to-gold molar ratio, and growth temperature.

Despite the great success of the room temperature reduction route for growing AuNPs and AuNRs, it has been recently shown that the hot injection method provides better quality and more homogeneous AuNPs, as was demonstrated for QDs and magnetic nanocrystals above. For example, Williams and co-workers applied the reduction of $Au(acac)PPh_3$ at ~105 °C in a solution containing a mixture of TOPO and HDA.[120] They reported control over the nanoparticle diameter from 10 to 50 nm by varying the precursor concentration, the nature of the coordinating solvent(s) and the reaction time used. In a parallel study, Osterloh and co-workers used oleylamine as a reducing agent and stabilizer to prepare alkylamine-stabilized gold nanoparticles with low dispersity over the size range of 6–21 nm.[121,122] The Au precursor was rapidly injected into a solution containing oleylamine and toluene at 110 °C, and the reaction mixture was left stirring for two hours before cooling to room temperature. They controlled the size of the AuNPs by varying the precursor concentrations and reaction time. Recently, Swihart and co-workers reported the synthesis of homogeneous 10 nm AuNPs using a solution containing pure oleylamine. Here, the oleylamine was used as a solvent, reducing agent and stabilizer for the nanoparticles.[123]

3. Water dispersion strategies

One key requirement for the successful integration of these inorganic nanocrystals/nanoparticles into biology is the implementation of an effective surface-modification strategy that renders those materials hydrophilic and compatible with commonly used

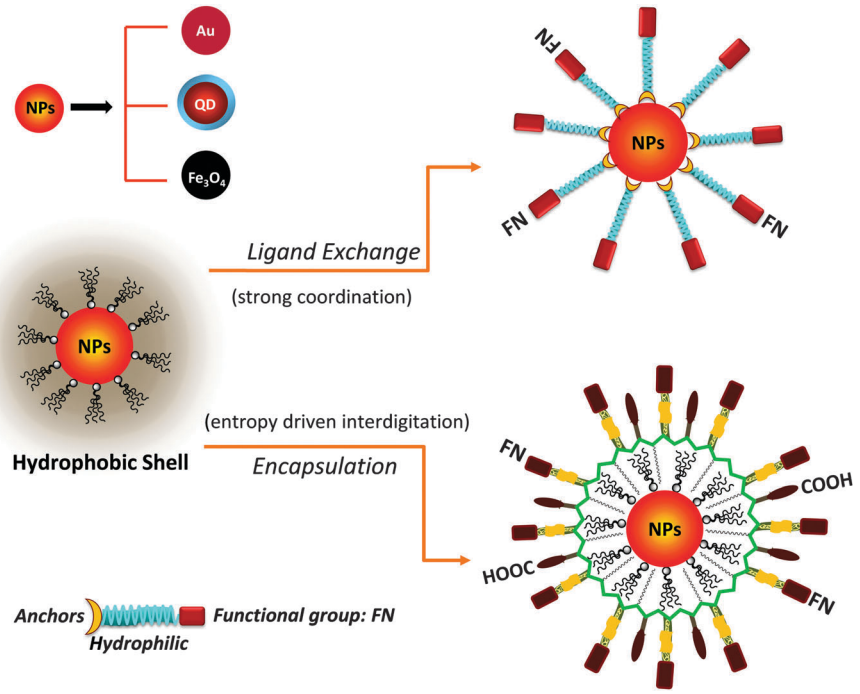

Fig. 1 Schematic representation of phase transfer *via*: (top) ligand exchange which relies on the presence of strong anchoring groups on the nanoparticle surface; (bottom) encapsulation of the hydrophobic nanoparticles (NPs) within an amphiphilic block-copolymer. Encapsulation involves the entropy driven-interdigitation between the native ligands and the hydrophobic blocks of the copolymer. Semiconducting nanocrystals (QDs), metal (Au) and metal oxide (Fe_3O_4) nanoparticles are shown.

bio-conjugation techniques to target biomolecules. This requirement is valid regardless of the initial growth method or the nature of the inorganic nanocrystals used. For example, citrate-stabilized AuNPs and cetyltrimethylammonium bromide (CTAB)-coated AuNRs, even though prepared in water they exhibit limited colloidal stability to added electrolytes and pH changes. This limits one's ability to integrate them with biomolecules, or introduce them into live cells. Additional surface-functionalization with appropriate hydrophilic ligands has been used to expand their colloidal stability and impart target specific biological activities to these materials. However, nanocrystals prepared *via* a high temperature reduction route are hydrophobic, and a judicious surface functionalization strategy is critically important to promote water-solubility and biofunctionality to these systems.

Overall, the strategies developed thus far for achieving surface-functionalization and biocompatibility of inorganic nanostructures can be grouped into two main types. The first involves the removal of the native hydrophobic organic coating and replacing it with bifunctional hydrophilic molecules, *i.e.* ligand exchange (see Fig. 1).[124–129] The second route relies on encapsulation of the native hydrophobic nanocrystals with amphiphilic block copolymers or phospholipid micelles.[10,130–132] Because the ligand exchange process requires the removal of the native organic capping shell, the bifunctional molecules used for phase transfer must present one or multiple metal-coordinating groups to anchor onto the inorganic surface, along with reactive functions for attaching the NPs to biomolecules. Conversely, encapsulation relies on the entropy-driven interdigitation between the hydrophobic segments of the amphiphilic molecules and the native cap on the nanocrystals, leaving the hydrophilic blocks (segments) laterally free to interact with the surrounding buffer and promote affinity to water (Fig. 1). In either strategy, polymers have provided researchers with a tremendous wealth of chemical and physical knowledge, along with a wide variety of structures to work with and build on. For example, there are several chemical routes that can be utilized to introduce new functional and/or coordinating groups within the polymer macromolecules (block copolymer) for optimal functionalization of the nanocrystals.[31,32] In addition, several block-copolymers have an extremely low critical micelle concentration (CMC), which makes them stable under a wide range of physiologically-relevant conditions and thus suitable for therapeutic applications.[133] A summary of the various polymer designs for either strategy is provided in Table 1.

3.1. Exchanging the native cap with hydrophilic ligands

Ligand exchange as a strategy involves the removal of the native coating (*e.g.*, CTAB, oleic acid or TOP/TOPO) from the surface of nanoparticles and its replacement with multifunctional hydrophilic ligands. Thus to be effective, this strategy requires a judicious choice of the polymer ligand. The latter must combine high affinity anchoring groups, hydrophilic blocks and reactive groups (Fig. 2 and 3). The first two components (*i.e.*, anchoring groups and hydrophilic moieties) control the stability of the nanocrystal-to-ligand binding and thus the colloidal stability of the resulting dispersions, while the reactive groups

Table 1 Summary of the strategies, based on either ligand exchange using multi-coordinating polymer ligands, or encapsulation within amphiphilic copolymers, to surface functionalize inorganic nanocrystals and promote their integration with biological systems

Surface-modification strategy	Polymer platform used	Coordinating groups/interdigitating blocks	Nanocrystals	References
Ligand exchange	Thiolated poly(L-lysine)-*graft*-poly(ethylene glycol) (PLL-*g*-[PEG:SH])	–Thiols: $(-SH)_n$	AuNPs	149
	Poly(acrylic acid)-*graft*-mercaptoethylamine (PAA-*g*-MEA)	–Thiols: $(-SH)_n$	CdSe–ZnS	153
	Multi dihydrolipic acid-*graft*-poly(methacrylate)	–Thiols: $(-DHLA)_n$	CdSe–ZnS	150 and 151
	Lipoic acid and poly(ethylene glycol) modified poly(acrylic acid) (PAA-*g*-[PEG:LA])	–Thiols: $(-LA)_n$ or $(-DHLA)_n$	AuNPs and CdSe–ZnS	152
	Sulfobetaine and lipoic acid modified poly(acrylic acid)(PAA-*g*-[LA:ZW])	–Thiols: $(-DHLA)_n$	CdSe–ZnS	155
	Methacrylate modified sulfobetaine and lipoic acid (LA:ZW)	–Thiols: $(-DHLA)_n$	CdSe–ZnS	154
	Poly(methacryloyloxyethyl phosphorylcholine (MPC))-*co*-poly(dihydro lipoic acid)	–Thiols: $(-DHLA)_n$	AuNRs	158
	Methacrylate modified poly(ethylene glycol) and imidazole (polyimidazole ligands, PILs)	–Imidazoles	CdSe–CdS–ZnS	124
	Poly(maleic anhydride)-*graft*-imidazole (PMAH-*g*-IL)	–Imidazoles	CdSe–ZnS	145
	Methacrylate modified sulfobetaine modified-graft and imidazole (SBPILs)	–Imidazoles	CdSe–Cd/ZnS	163
	Dopamine modified poly(acrylic acid)-*graft*-poly(ethylene glycol) (OligoPEG-Dopa)	–Dopamines: $(-DOPA)_n$	Fe_3O_4	143
	Dopamine-modified poly(isobutylene-*alt*-maleic anhydride)-*graft*-poly(ethylene glycol) (PEG:DOPA)	–Dopamines: $(-DOPA)_n$	Fe_3O_4	172
	Poly(L-3,4-dihydroxyphenylalanine)-*graft*-poly(ethylene glycol)	–Dopamines: $(-DOPA)_n$	Fe_3O_4	173
Encapsulation	Polystyrene-*block*-poly(acrylic acid), PS-*b*-PAA	–Hydrophobic interactions (polystyrene and alkyl chains)	AuNPs	178
	Poly(methyl methacrylate)-*block*-poly(acrylic acid), PMMA-*b*-PAA	–Hydrophobic interactions (polystyrene and alkyl chains)	AuNPs	178
	Polystyrene-*block*-poly(acrylic acid), PS-*b*-PAA block-copolymer: PS_{100}-*b*-PAA_{13}, PS_{160}-*b*-PAA_{13} and PS_{250}-*b*-PAA_{13}	–Hydrophobic interactions (polystyrene and alkyl chains) followed by chemical cross linking	AuNPs	179
	[Polystyrene-*co*-poly(4-vinyl benzophenone)]-*block*-poly(acrylic acid) [(PS-*co*-PVBP)-*b*-PAA]	–Hydrophobic interactions (polystyrene and alkyl chains) followed by photo-induced cross linking	AuNPs	180
	[Poly(styrene)-*co*-poly(4-vinyl benzophenone)]-*block*-poly-(ethylene oxide) [(PS-*co*-PVBP)-*b*-PEO]	–Hydrophobic interactions (polystyrene and alkyl chains) followed by photo-induced cross linking	AuNPs	180
	Poly(acrylic acid)-*graft*-dodecylamine	–Hydrophobic interactions (polydodecyl and alkyl chains)	AuNPs	182
	Poly(ethylene oxide)–poly(*n*-butyl acrylate), PEO–PnBA	–Micelle assembly through PnBA	AuNRs	183
	Poly(styrene sulfonate), PSS	–Electrostatic adsorption	AuNRs	190
	Poly(acrylic acid)-*graft*-octylamine	–Hydrophobic interactions (Poly alkylamine and alkyl chains)	CdSe–ZnS	10 and 200
	Poly(maleic anhydride *alt*-1-tetradecene)-*graft*-alkyl amine and/or poly ethylene glycol	–Hydrophobic interactions (poly alkyl and TOP/TOPO, oleylamine or alkane chains)	CdSe–ZnS, Fe_3O_4, AuNPs	130, 132 and 204
	Poly(styrene-*co*-maleic anhydride)-*graft*-poly(ethylene glycol)	–Hydrophobic interactions (poly styrene and TOP/TOPO)	CdSe–ZnS	205
	Poly(ethylene glycol-*b*-2-*N*,*N*-dimethylaminoethyl methacrylate) (PEG-*b*-PDMA)	–Hydrophobic interactions (poly styrene and TOP/TOPO)	CdSe, CdSe–ZnS	206 and 207
	Polyisoprene-*block*-poly(ethylene oxide) diblock (PI-*b*-PEO or PI-*b*-$(PEO)_2$ star)	–Hydrophobic interactions	CdSe–CdS/ZnS, Fe_3O_4, AuNPs	209, 211 and 212

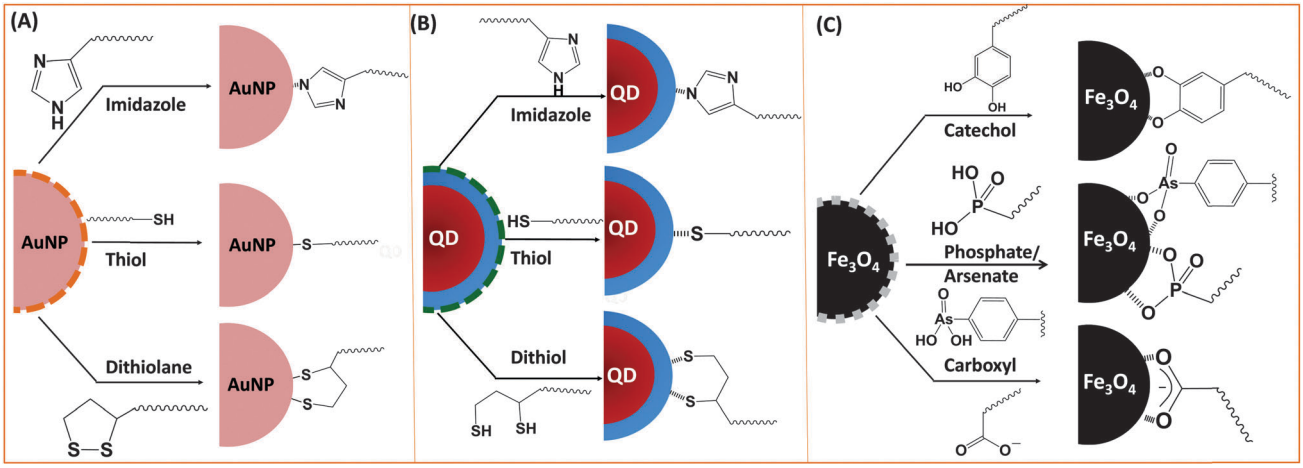

Fig. 2 Schematic representation of various metal-anchoring groups often employed using the ligand exchange strategy: (A) metallic (AuNPs), (B) semiconductor (QDs), and (C) magnetic (iron oxide) nanocrystals are shown.

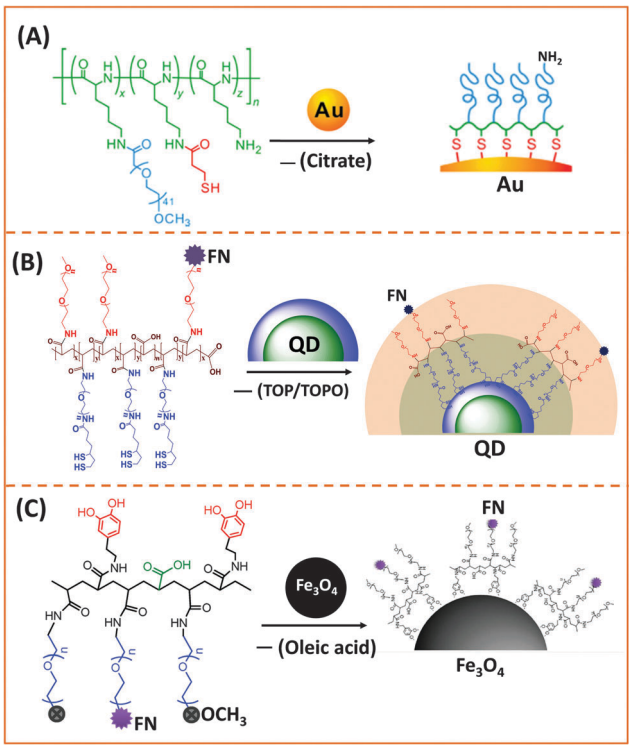

Fig. 3 Representative examples of designing biocompatible nanoparticles *via* cap-exchange applied to: (A) citrate-stabilized gold nanoparticles, (B) TOP/TOPO-capped QDs, and (C) oleic acid-capped magnetic nanocrystals.[143,149,152] (Figures are reproduced from the above references with permission from the American Chemical Society.)

allow one to apply the optimal coupling strategy for attaching the desired number and type of target molecules (*e.g.*, peptides and proteins) to the inorganic platform of interest. The selection of the anchoring group(s) depends on the nature of the inorganic surface of the nanocrystals (Fig. 2).[134–139] For example, thiol groups exhibit much higher affinity to AuNPs and to Zn- and Cd-rich QD surfaces, though coordination onto AuNPs is much stronger. Au-to-thiol (or Au–sulfur) interaction has been described in several instances as covalent binding,[119] and thiol-modified ligands are believed to be the most effective for functionalizing AuNPs and AuNRs.[140–142] In comparison, dopamine has been shown to provide strong coordination onto the surface of iron oxide NPs, but its ability to coordinate onto Au and semiconductor surfaces is rather weak. Carboxyl- and amine-appended alkyls such as oleylamine and oleic acid have been used in the high temperature growth of QDs and iron oxide nanocrystals; they provide good anchoring groups for the metal surfaces in organic solutions.[1,16,35,100,143,144] These groups have also been proposed and utilized as anchoring groups to promote the dispersion of AuNPs, iron oxide NPs and QDs in buffer media. Their effectiveness as coordinating groups in aqueous media is rather weak, nonetheless, as often nanoparticles prepared using this strategy exhibit limited colloidal stability to pH changes and in the presence of soluble electrolytes.[143] More recently, a few studies have shown that the amino acid histidine, if judiciously inserted into a polymer structure (organic or biological), can promote strong affinity to AuNPs and core–shell QDs.[124,136,145] In those studies, the authors have exploited the known metal-coordinating capacity of the imidazole group of histidine and designed a few polymer ligands laterally appended with histidine derivatives (*e.g.*, histamines). They have shown that such polyhistamine-modified polymers can coordinate onto semiconductor nanocrystals and promote their dispersion in biological media.[124,145]

3.1.1. Gold nanoparticles and semiconductor quantum dots. Thiol-appended alkyl and thiol-modified PEG molecules as ligands have been more widely used to cap exchange QDs and AuNPs. Commercially available mono-thiolalkyl acid ligands (*e.g.*, mercaptoacetic acid, 3-mercaptopropionic acid, and 11-mercaptoundecanoic acid) have been widely used to provide water solubility to QDs and AuNPs, due to a combination of easy access to those materials (commercially-available) and ease of implementation.[24,125,129,146] However, QDs cap exchanged with those small molecules suffer from

rather limited long term colloidal stability in buffer media especially under acidic conditions, because solubility in water relies on the presence of carboxylic acid fragments (at the periphery of the nanoparticles), which tend to promote solubility in water through their carboxylate form. Moreover, monothiolated ligands can be easily displaced from the NP-surface in biological media (*e.g.*, inside live cells) by competing sulfur-containing amino acids such as glutathione and cysteine. These molecules are natural reducing agents and are abundant in biological media. They can alter the colloidal stability of nanoparticles capped with weakly-coordinating ligands.[147] This ligand-to-NP stability issue can be partly addressed using bidentate and multidentate ligands.[148] For instance, derivatives of dihydrolipoic acid-appended PEG provide substantially better stability and reactivity than their monothiol–alkyl counterparts, a result attributed to the stronger binding affinity of the dithiol group (chelating effect of the bidentate group) to ZnS-overcoated QDs.[127,129,148] Polymer structures present an obvious platform for designing ligands with higher numbers of metal-coordinating/chelating groups (Fig. 3A and B).

AuNPs used for cap exchange are generally stabilized by weakly binding ligands such as citrate or CTAB, and a few groups have recently explored the use of multi-coordinating functional block-copolymers to install stronger binding cap and/or introduce hydrophilic and reactive groups for interfacing with biological entities (antibodies and DNA). In one of their recent reports Taton and co-workers tested the effectiveness of poly(L-lysine)-*graft*-poly(ethylene glycol) (PLL-*g*-PEG) copolymers to passivate and disperse AuNPs in buffer media. They incorporated several thiol groups and PEG chains (*via* amide bond formation) into the poly(lysine) backbone, by sequential addition of NHS-ester-terminated PEG-(mPEG-SCM) and a thiol linker (*N*-succinimidyl-3-(2-pyridyldithio)-propionate).[149] In addition, by leaving a few of the amine groups in the lysine residues intact, this opens up the possibility for coupling the NPs to carboxyl-terminated biomolecules (Fig. 3A).[149]

Instead of monothiol anchors, a few groups grafted lipoic acid (dithiolane) or lipoic acid-modified with a short PEG segment onto the polymer backbones. In one of the early studies, Raymo and co-workers designed a polymer construct made of the polymethacrylate backbone presenting several lateral LA groups along with few PEG segments to transfer hydrophobic QDs to buffer media.[150,151] Their synthetic strategy was based on the radical copolymerization of methacrylate monomers pre-functionalized with lipoic acid, and PEG moieties with varying chain lengths, or PEG moieties presenting lateral amine or carboxyl groups (Fig. 4A). They showed that following borohydride reduction of the LA groups the resulting polymer ligands provided QDs with enhanced long term stability compared to small mono-thiol ligands. Here the larger PEG chain tended to increase the effective hydrodynamic size of the water-dispersible QDs. To potentially reduce the hydrodynamic size of the hydrophilic nanocrystals, a few groups used poly(acrylic acid) oligomers (with a molecular weight of $\sim$1800).[152,153] For example, Liu and co-workers designed a multidentate polymer ligand made of polyacrylic acid (PAA) coupled with mercaptoethylamine (MEA) *via* carbodiimide chemistry using dicyclohexyl carbodiimide (DCC). The produced multi-thiol polymer was used to transfer QDs to buffer media.[153] The resulting PAA-*g*-MEA capped water-soluble QDs have relatively small hydrodynamic diameters (around 13 nm) and exhibit colloidal stability over a broad pH range (3–14) and added salt (up to saturated NaCl solution).

Our group used this PAA short chain to prepare a series of PEG- and LA-modified oligomer ligands having a central backbone laterally appended with combinations of LA–PEG, methoxy–PEG, amine–PEG, and azide–PEG moieties (OligoPEG ligands).[152] The use of smaller PEG moieties ($M_w \sim 600$ or 750) eventually reduces the overall extension of the polymer coating on the nanocrystals (Fig. 3B and 4B). These LA-modified OligoPEG ligands were applied either to cap AuNPs, or after borohydride reduction to functionalize QDs. This route provided colloidal dispersions of QDs and AuNPs that remained stable over a broad range of conditions and over extended periods of storage time. With the same aim of reducing the hydrodynamic size of the polymer-capping, Zweit and co-workers, and Giovanelli and co-workers, took slightly different approaches for achieving the synthesis of multi-coordinating zwitterionic co-polymers (Fig. 5A and C).[154,155] In particular, Giovanelli and co-workers synthesized a polymer containing molecular lipoic acid anchors and a sulfobetaine containing zwitterionic groups *via* a two-step process. They first modified the lipoic acid and zwitterion with methacrylamides and then performed the polymerization reaction to obtain a randomly grafted copolymer.[154] In order to functionalize the polymer with reactive groups for further conjugation with biomolecules, they introduced a methacrylamide monomer bearing a reactive amine function during the polymerization step (Fig. 5C). This functionalization has been confirmed by coupling the cap exchanged NPs with a dye (fluorescein) *via* carbodiimide coupling. Finally, the multi-LA–zwitterion appended polymer exhibited strong affinity to QD surfaces, with reduced desorption rates compared to their lower coordination ligand counterparts and increased colloidal and intracellular stability.

To perform cap exchange on CdSe and ZnS-overcoated QDs, reduction of the 1,2-dithiolane to dithiol is required, as only the thiolated form of the ligand can coordinate onto the surface of QDs; the oxidized ligands do not cap these QDs.[126,129] This chemical reduction is routinely carried out using $NaBH_4$ as a reducing agent. Though effective, chemical reduction of the dithiolane ring using $NaBH_4$ is not suitable for certain sensitive functional groups (*e.g.*, azide and aldehyde) often introduced into the ligand structure for further modification of the resulting nanocrystals. For polymeric molecules the purification process is even more tedious, and after purification the DHLA-based ligands need to be stored under inert conditions. In order to address these problems, our group has recently introduced a new strategy to transfer QDs to polar and buffer media using lipoic acid-based ligands.[156] In this strategy, the ligand exchange is promoted photo-chemically, and involves the *in situ* reduction of lipoic acid in the presence of QDs. This idea was motivated by a previous study by Sander and co-workers reporting that a

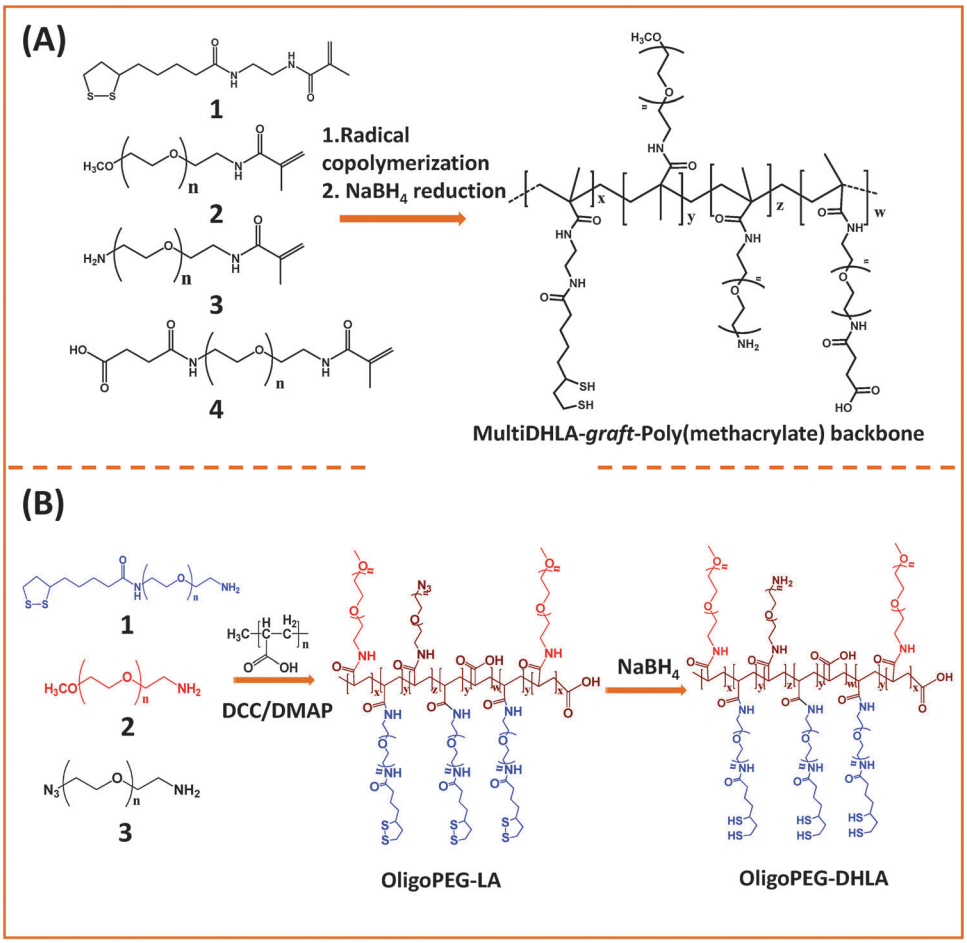

Fig. 4 Synthesis of two representative polymer ligands: (A) a block-copolymer prepared *via* radical polymerization of reactive methacrylate groups; (B) OligoPEG polymer prepared *via* carbodiimide chemistry starting from a poly(acrylic acid) backbone. Both polymers present multiple lipoic acid moieties per polymer chain.[150,152] (Figures are adapted from the above references with permission from the American Chemical Society.)

well-defined absorption at ~350 nm originating from the cyclic disulfide ring of the lipoic acid can be altered under UV irradiation.[156,157] Indeed, we found that the photoligation and cap exchange on QDs can be easily applied with our molecular scale LA–PEG and LA-zwitterion ligands. Furthermore, the resulting materials exhibit great colloidal stability over a wide range of conditions. This idea should be easily applicable to polymers bearing multiple LA groups.

Emrick and co-workers developed a multi-coordinating zwitterion polymer by appending several LA groups onto a phosphorylchlorine (PC) block co-polymer. They first prepared a hydroxyethyl methacrylate (HEMA)-terminated lipoic acid (LA) monomer *via* EDC coupling. The HEMA–LA compound was then mixed with a methacrylamide phosphorylcholine (MPC) along with 4-cyanopentanoic acid dithiobenzoate (CTP) as the chain transfer agent and 4,4′-azobis(4-cyanovaleric acid) (ACVA) as the initiator for radical addition-fragmentation chain transfer (RAFT) polymerization (Fig. 5B).[158] The authors showed that following chemical reduction of the LA groups the resulting DHLA-rich methacrylamide phosphorylcholine zwitterion polymer can be effectively applied to cap exchange CTAB-capped AuNRs, and the resulting dispersions exhibited great colloidal stability.

There is also growing interest in developing ligands that incorporate metal anchors other than the ubiquitous thiols, carboxy or amines. This idea was inspired by earlier demonstrations showing conjugation of hydrophilic QDs to polyhistidine (His_n)-tagged proteins and peptides, promoted by metal-affinity interactions. Indeed, several groups have explored this conjugation method, due to the ease of implementation and the fact that His-tagged biomolecules are ubiquitous. For instance, we have demonstrated the conjugation of CdSe–ZnS QDs with His-tagged proteins and peptides, and showed that such interactions require direct access of the histidine tag to the Zn-rich QD surfaces.[159,160] Learning from these developments, a few groups recently explored the ability of imidazole-modified ligands, or polyhistidine-appended peptides and proteins to effectively interact with core–shell QDs and AuNPs.[124,161,162]

In one of those developments, Bawendi and co-workers used RAFT polymerization to design a random brush co-polymer having both PEG and imidazole as side groups along with an aliphatic backbone (Fig. 6).[124] They started by preparing monomer precursors bearing the necessary acrylate group to endow the final copolymer with the desired multi-functionality; those precursors present an imidazole anchoring group, a hydrophilic

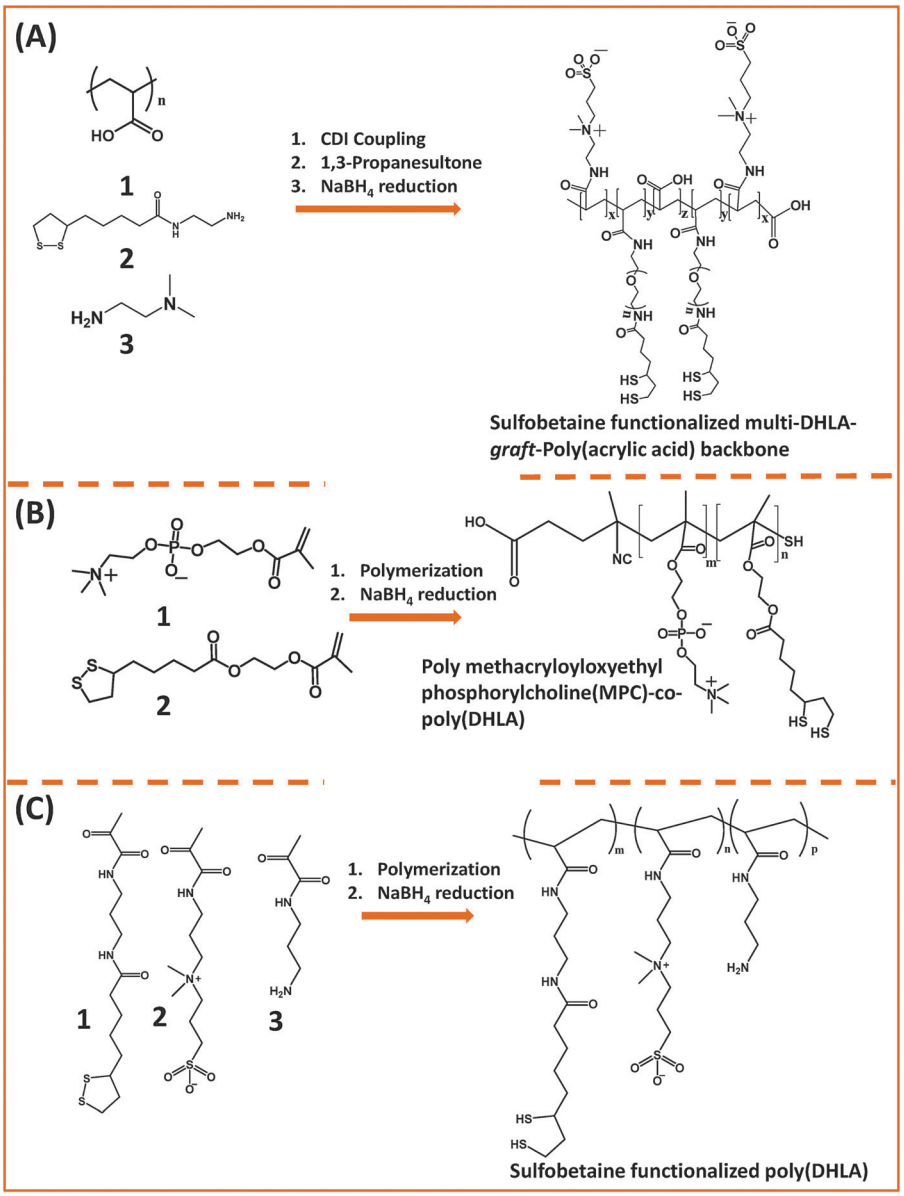

Fig. 5 Synthesis of the poly(DHLA)-zwitterionic block-copolymer using: (A) carbodiimide chemistry starting from a poly(acrylic acid) precursor; (B) and (C) radical polymerization starting with LA and ZW moieties pre-modified with reactive methacrylate groups. Sodium borohydride has been used to reduce the dithiolane ring of the lipoic acid, a process required for cap exchange on QDs.[154,155,158] (The figures are adapted from the above references with permission from the American Chemical Society.)

PEG segment, and a reactive amine group. The first monomer was prepared by DCC and NHS coupling between acrylic acid and histamine dihydrochloride, followed by imidazole nitrogen protection using di-*tert*-butyl dicarbonate (BOC_2O). The second monomer consisting of a OMe–PEG_{11}-terminated with acrylate function was synthesized *via* two modification steps: (1) transformation of the hydroxyl group of poly(ethylene glycol) methyl-ether to amine; (2) reaction of the amine–PEG–OMe with the NHS-ester of acrylic acid. The third monomer was synthesized by coupling amine–$(PEG)_{3/11}$–NH(Boc) with the NHS ester of acrylic acid. The removal of the Boc-protecting group was carried out using trifluoroacetic acid, TFA. These monomers were chosen to control three parameters: binding affinity of the polymer onto the nanocrystal, colloidal stability and functionality of surface. The stoichiometric ratio of those monomers was varied during the polymerization reaction to eventually control the relative ratio of anchors, hydrophilic and reactive groups. In addition, to minimize the potential for polymer cross-linking and aggregation of QDs after ligand exchange, small molecular weight polymers were used (a degree of polymerization smaller than 30). They showed that this imidazole-rich polymer can effectively displace the native TOP/TOPO cap and coordinate onto QD surfaces, providing water-dispersible relatively compact QDs with long term stability at pH > 5.[124] In subsequent studies, they extended that design and substituted the PEG moieties with zwitterionic groups.[163] They designed two sulfobetaine-functionalized

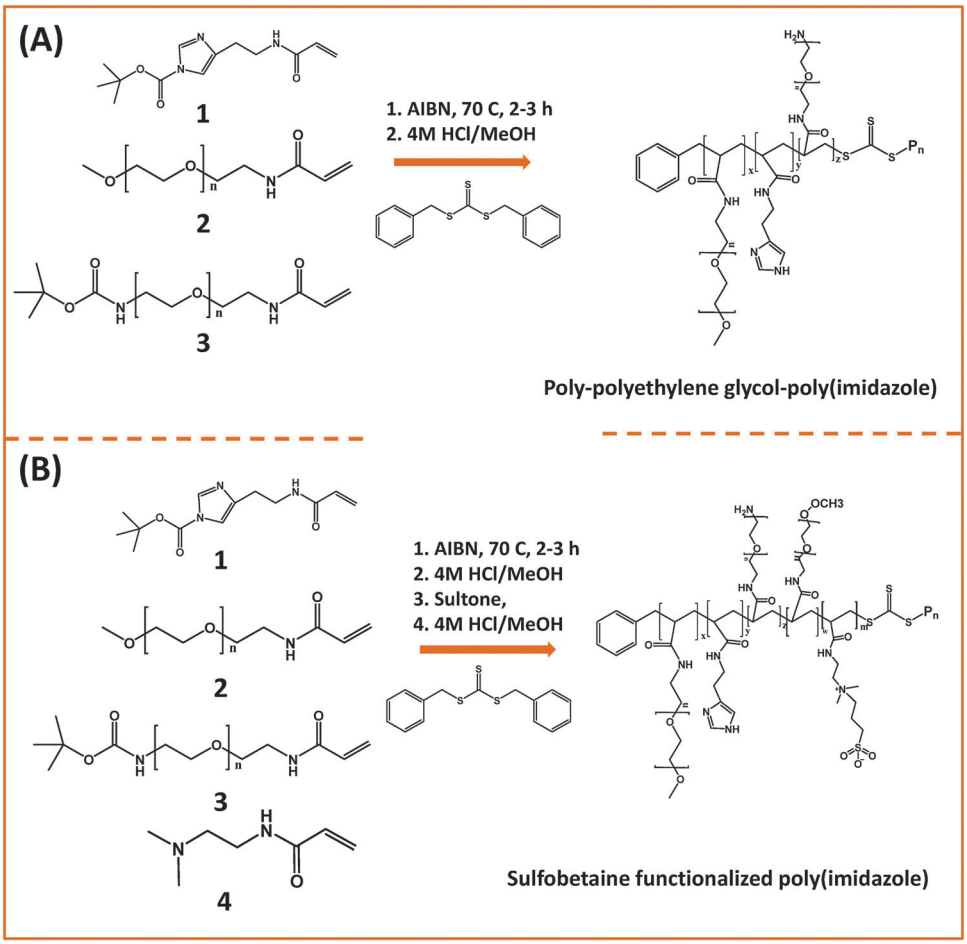

Fig. 6 (A) Synthesis of poly(imidazole) block-copolymer prepared *via* RAFT; polymerization was carried out using methacrylate groups pre-modified with imidazole or PEG moieties. (B) Synthesis of a sulfobetaine functionalized poly(imidazole) block-copolymer using a similar approach.[124,163] (Figures are adapted from the above references with permission from the American Chemical Society and from Wiley.)

poly(imidazole) ligands (BPILs) using the above methodology: sulfobetaine poly(imidazole), SBPILs, and carboxybetaine-functionalized poly(imidazole), CBPILs (Fig. 6B). These zwitterion-*co*-polymer ligands were successfully used for capping various types of QDs emitting from the near infrared to the visible region (*e.g.*, InAs–CdZnS, CdSe–CdS, and CdSe–CdZnS).

Another example using an imidazole-modified polymer as a ligand for QDs was reported by Cai and co-workers.[145] This multidentate polymer was prepared by reacting poly(maleic anhydride) (PMAH) with either pure histamine or a mixture of histamine and N_3–PEG–NH_2 to obtain azide-functionalized QDs. They examined the effects of PMAH coating on the hydrodynamic size and optical properties of CdSe–ZnS QDs with varying core size emitting at 525 nm, 605 nm, and 705 nm. They found that this ligand design produced nanocrystals with high quantum yields along with minimal increase in the hydrodynamic size ($\sim$2 nm after cap exchange). They also reported that PMAH-His-capped QDs were stable in the presence of H_2O_2 and under UV irradiation.

3.1.2. Magnetic nanoparticles. Several acid-modified alkyl molecules have been used to stabilize iron oxide nanoparticles, where ligand binding to the NPs is presumably facilitated by iron-to-oxygen affinity. Molecules presenting phosphonic and carboxylic acid have also been used to cap iron oxide and other magnetic nanoparticles in organic media.[164–167] In fact, one of the most successful high temperature growth routes for Fe_3O_4 nanoparticles uses oleic acid as a coordinating molecule.[1] However, phase transfer of hydrophobic nanoparticles to buffer media using ligands modified with dopamine groups has emerged as the most promising route for preparing relatively stable iron oxide NPs.[168] In particular, the catechol segment of the dopamine molecule is believed to exhibit the highest affinity to the Fe-rich nanoparticle surfaces. Several studies have reported the use of mono-catechol-appended single chain PEG to promote the transfer of iron oxide nanoparticles to water media, and some of these materials have been used for demonstration in MR contrast imaging and as delivery platforms.[168–171] However, the stability of these dispersions is rather modest, which has motivated the researchers to explore the design of multicatechol-based ligands or polymers to enhance the ligand affinity to the iron oxide nanocrystals, as demonstrated for AuNPs and QDs above. We, for example, have compared the effectiveness of several catechol-modified, or carboxy-modified oligomers as ligands to functionalize Fe_3O_4

nanoparticles.[143] In that study, we used a polyacrylic acid (PAA) oligomer as a backbone, which was further modified with both poly(ethylene) glycol short chains having inert or functional groups and dopamine; coupling relied on carbodiimide chemistry using dicyclohexyl carbodiimide and 4-dimethylaminopyridine (DMAP) (Fig. 7A). The resulting OligoPEG-Dopa ligands were used to cap exchange oleic acid-capped iron oxide nanoparticles. We used single chain PEG modified with either one catechol or one

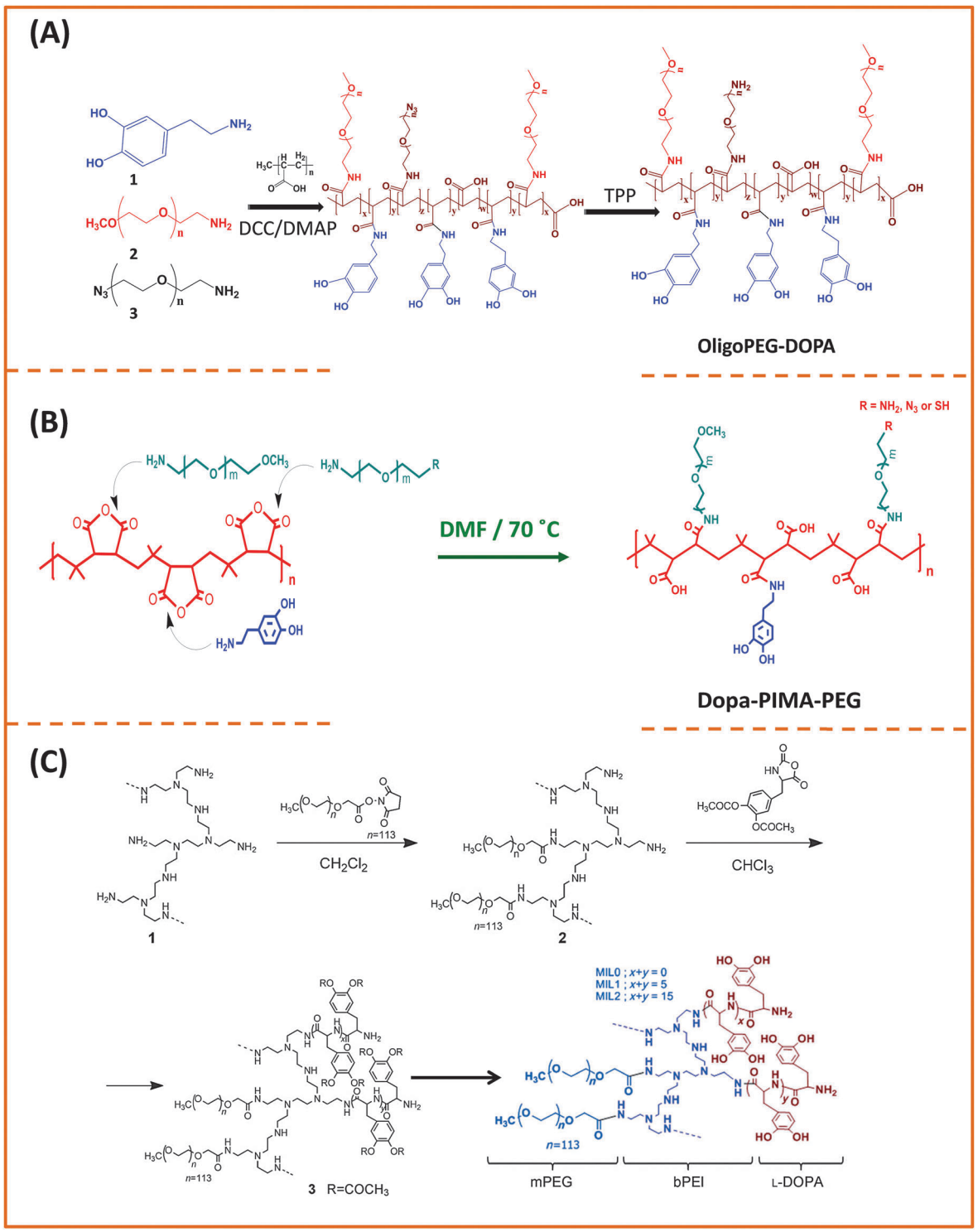

Fig. 7 Synthesis of three multi-anchoring poly(dopamine) polymers, starting with: (A) poly(acrylic)acid and DCC coupling; (B) poly(isobutylene-*alt*-maleic anhydride) and nucleophilic addition reaction; (C) poly-amine as the precursor polymer and NHS along with amine–anhydride coupling.[143,172,173] (Figures are adapted from the above references with permission from the American Chemical Society and from Wiley.)

carboxy group to prepare the control NP dispersions. Our results showed that the multi-dopamine oligomers impart better colloidal stability to iron oxide nanoparticles than either OligoPEG-carboxy (ligand presenting several COOH groups) or small molecule ligands appended with carboxy or dopamine. We also showed that insertion of azide groups in the oligomer allows click coupling with alkyne-modified dye molecules. More recently we explored the use of nucleophilic addition reaction to install several dopamine anchoring groups, polyethylene glycol moieties and reactive groups onto a poly(isobutylene-*alt*-maleic anhydride) (PIMA) chain. This chemical design is efficient and reagent-free, and this transformation greatly enhanced the ligand affinity to the magnetic NPs, while the presence of several hydrophilic and reactive groups promoted stability in buffer media and subsequent conjugation with target biomolecules (see Fig. 7B).[172] In another report, Hyeon and co-workers developed a multi-catechol polymer ligand made of poly(L-3,4-dihydroxyphenylalanine), polyDOPA, further modified with methoxy poly(ethylene glycol) units (Fig. 7C). The polymer synthesis started with the protection of the dihydroxyl groups of L-3,4-dihydroxyphenylalanine (L-DOPA) using acetic anhydride (AC_2O) followed by the treatment with triphosgene to provide (AC_2)-DOPA-*N*-carboxylanhydride (NCA). They then modified the poly(ethylene glycol) methyl ether (mPEG-OH, 5000 Da) to PEG-*N*-hydroxysuccinimidyl ester (NHS), followed by reaction with branched polyethylenimine (bPEI) yielding the final mPEG–bPEI polymer. Those two components [(AC_2)-DOPA-*N*-carboxylanhydride (NCA) and mPEG–bPEI-p(DOPA)] were finally mixed to obtain the copolymer *via* ring-opening polymerization reaction. Here too the authors reported enhanced stability of the iron oxide nanoparticles in buffer media.[173] Additional use of these materials *in vivo* will be detailed below.

There is an alternative route for designing ligands with strong coordination onto iron oxide nanoparticles, which relies on the use of phosphonic acid groups (instead of carboxyl or dopamine) as anchors.[35,174,175] In this approach, phosphonic acid groups are inserted along a polymer chain (with or without polyethylene glycol moieties) to yield multi-phosphonic acid ligands. Such phosphonic acid based polymer ligands were tested by a few groups and were shown to exhibit a higher coordinating affinity towards metal oxide surfaces than their carboxylic acid counterparts, especially under acidic conditions.[35,175] Polysaccharides have also been used for coating iron oxide nanoparticles, due to their biocompatibility.[176,177] The chelation is driven by the interaction between the hydroxyl groups and the iron oxide surface of the nanoparticles. A ubiquitous polysaccharide that has often been used in these studies is dextran; it is composed exclusively of glucopyranosyl units with varying degrees of branching and chain length. A drawback of this polymer-coating is the relatively high rate of desorption from the nanoparticle surfaces, due to the naturally weak hydrogen bonding; desorption from the nanoparticle surfaces can occur at high dilution or upon heating. However, cross-linking can be used to enhance dextran polymer coating and provide higher colloidal stability in aqueous media.

3.2. Phase transfer *via* encapsulation within amphiphilic block copolymers

The use of amphiphilic block copolymers for encapsulating various nanocrystals has been widely reported, since this strategy is believed to preserve the photo-physical properties of the native (hydrophobic) nanoparticles. The polymers must contain two distinct blocks with drastically different solubilties, and a balance between the hydrophilic and hydrophobic blocks is crucial for the effectiveness of the encapsulation strategy. We will describe a few established examples where this strategy has been applied for the encapsulation of metal, metal oxide and semiconductor nanoparticles.

3.2.1. Encapsulation of metal nanoparticles. Application of this strategy to metallic nanostructures (*e.g.*, those made of Au and Ag) has not been widely explored in the literature, which contrasts with its ''popularity'' as a means of promoting hydrophilicity and biocompatibility to semiconducting and metal oxide nanoparticles. Nonetheless, a few groups have tested its effectiveness to functionalize AuNPs and AuNRs, and developed a few amphiphilic polymer designs using an atom-transfer radical polymerization route. For example, Taton and co-workers used this idea to design and optimize the structure of two amphiphilic block-copolymers that present two different hydrophobic blocks, while sharing the same poly(acrylic acid) hydrophilic block: a polystyrene-*block*-poly(acrylic acid), PS-*b*-PAA, and poly(methyl methacrylate)-*block*-poly(acrylic acid), PMMA-*b*-PAA; the PAA block size was fixed while varying the hydrophobic PS and PMMA blocks.[178] They used these polymers to encapsulate hydrophobic AuNPs capped with dodecanethiol. Here, starting with citrate-stabilized AuNPs the authors first carried out cap-exchange with dodecanethiol to render the NPs hydrophobic and facilitate interdigitation with the hydrophobic blocks of the copolymers (Fig. 8A). This permitted formation of micelle capsules around the nanoparticles, after addition of water to a DMF solution containing the polymer mixed with the dodecanethiol-modified nanoparticles. They showed that this surface-templated self-assembly of polymers around the AuNPs provides an inorganic–polymer core–shell structure where the thickness of the coating layer can be judiciously controlled by varying the size of the hydrophobic and hydrophilic blocks, and without substantially enhancing the overall size of the AuNPs, *e.g.*, they measured a small increase in the NP size (from 12 nm to 15 nm, using TEM). In addition, they found that due to the glassy nature and higher refractive index of the hydrophobic block compared to water (n_{PMMA} = 1.49 and n_{PS} = 1.59), the SPR absorption peak, λ_{max}, of the encapsulated-AuNPs was red-shifted with respect to the value measured for citrate-stabilized NPs: λ_{max} = 540 nm for $PMMA_{240}$-*b*-PAA_{13}–AuNPs and λ_{max} = 547 nm for PS_{250}-*b*-PAA_{13}–AuNPs. They further showed that the chemical stability of the polymer capsules can be enhanced by cross-linking the polyacrylic acid block using carbodiimide/diamine coupling with 2,2′-(ethylenedioxy)bis(ethylamine).[178] In a follow-up study and focusing on the chemically cross-linked PS-*b*-PAA block-copolymer coating, they probed the effects of varying the relative size of the amphiphilic polymer used compared to the AuNP size on the structure of the surface-templated copolymer self-assembly around the AuNPs. Using a

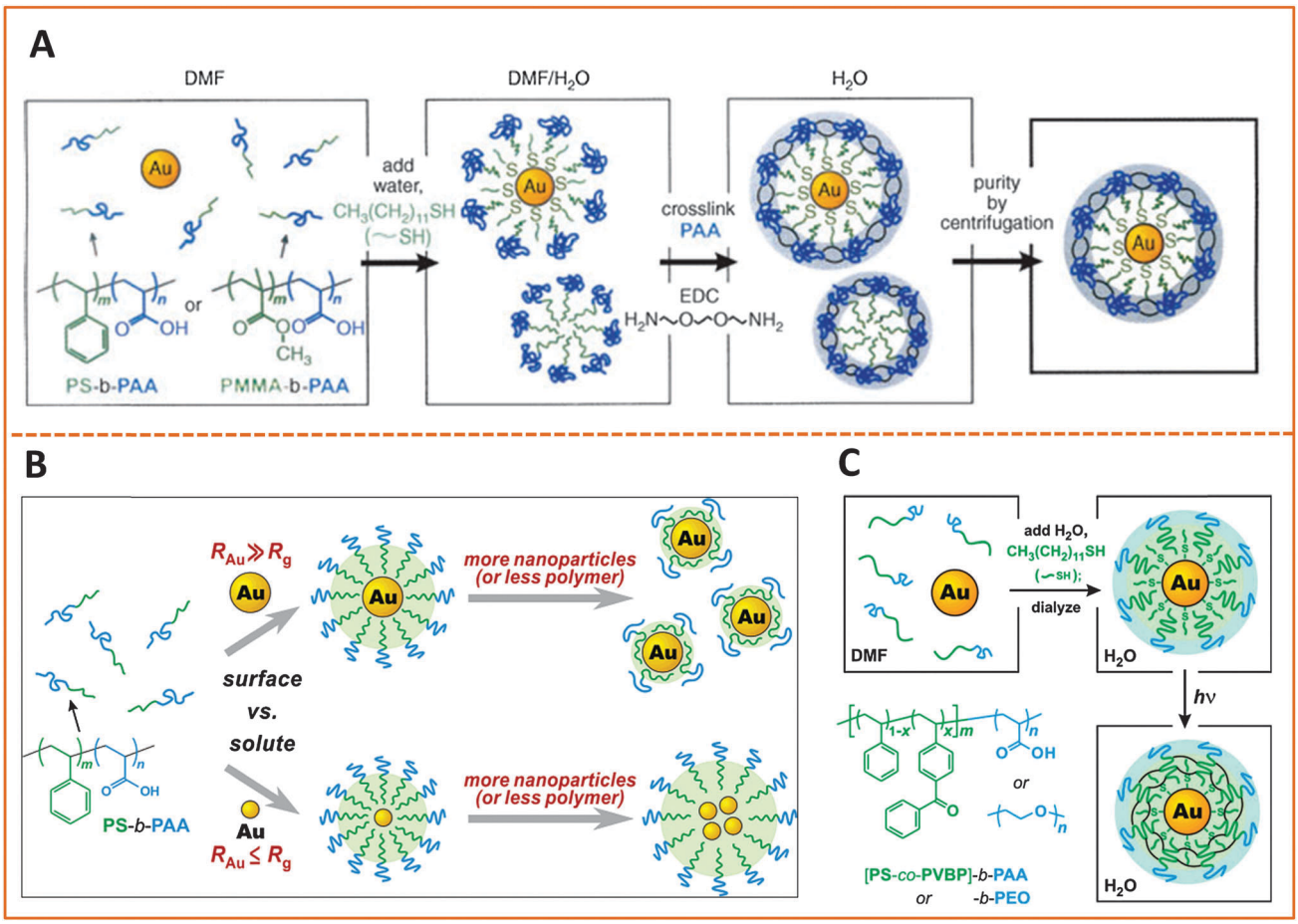

Fig. 8 Strategies for encapsulating AuNPs within amphiphilic block-copolymers. (A) Encapsulation using PS-*b*-PAA and PMMA-*b*-PAA block-copolymers, followed by EDC cross-linking. (B) Effects of varying the size of the hydrophobic block in the copolymer and/or the size of the AuNP on the structure of the polymer-templated AuNP capsules. Shown are instances where capsules containing single AuNPs *vs.* a few AuNPs are controlled by changing the ratio between the NP and polymer dimensions, R_{Au}/R_g. (C) Use of photochemically-active benzophenone as a cross linking agent to prepare AuNPs encapsulated within cross-linked PS-*b*-PAA or PMMA-*b*-PAA.[178–180] (Figures are reproduced from the above references with permission from the American Chemical Society and Wiley.)

set of AuNPs with discrete sizes ranging from 2 nm to 60 nm and three block-copolymer PS_{100}-*b*-PAA_{13}, PS_{160}-*b*-PAA_{13} and PS_{250}-*b*-PAA_{13} (the index of polymerization in the PS was varied while keeping that of PAA fixed), they found that the relative sizes of the AuNPs and polymer can affect the structure of the capsules and the interface between the metal surface and the polymer coating (Fig. 8B). In particular, they showed that when the AuNP size was smaller or comparable to the radius of gyration, R_g, of the block copolymer ($R_{Au}/R_g \leq 1$), the particles "dissolve" within the polystyrene-*block*-poly(acrylic acid) (PS-*b*-PAA) micelle core, forming a distribution of polymer capsules containing few AuNPs each; this becomes even more pronounced when the polymer concentration (with respect to that of NPs) is reduced, as control over the shell thickness becomes difficult to achieve (Fig. 8B).[179] Conversely, when the NP size was larger than that of the polymer ($R_{Au}/R_g \gg 1$), the PS-*b*-PAA adsorption is templated by the nanoparticle surface, and a concentric core–shell structure is formed during the encapsulation step. The thickness of the polymer shell is controlled by varying the ratio of polymer to nanoparticle concentration.[179] In a third study the authors expanded this strategy and synthesized two amphiphilic copolymers, [polystyrene-*co*-poly(4-vinyl benzophenone)]-*block*-poly(acrylic acid) [(PS-*co*-PVBP)-*b*-PAA] and [poly(styrene)-*co*-poly(4-vinyl benzophenone)]-*block*-poly(ethylene oxide) [(PS-*co*-PVBP)-*b*-PEO], while introducing a photochemically active benzophenone molecule in the backbone of the copolymer (Fig. 8C).[180] They showed that encapsulation of Au nanoparticles followed by UV-mediated cross-linking provides enhanced colloidal stability to the nanoparticles against pH changes, added salts, heating, and to oxidative etching by dissolved KCN. To demonstrate further functionalization, they reacted the carboxyl groups on the polymer with streptavidin, and quantified the coupling efficiency *via* fluorescence measurements using a dye-labeled biotin molecule as a target. Recently, Li and co-workers introduced a polystyrene-*b*-poly(4-vinylpyridine) (PS-*b*-P4VP) block copolymer where the number of nanoparticles within a micelle core was controlled by varying the relative amounts of nanoparticles, the block co-polymer (PS-*b*-PVP) and the linker used for hydrogen bonding during supramolecular assembly.[181] Here, the pentadecylphenol linker essentially controls the core size of the formed micelles.

In another example Nie and co-workers designed an amphiphilic polymer by chemically substituting 40% of the carboxyl groups of the PAA chain with the 12-carbon aliphatic chain (dodecylamine) *via* carbodiimide chemistry, and used this co-polymer for the growth of gold nanoparticles. The authors suggested that the amphiphilic polymer forms a three-layer coating on the nanoparticles, with one hydrophobic layer resulting from the self-assembly of two polymer chains, intercalating between two carboxyl-rich lateral layers; one of the carboxyl-rich layers coordinates onto the metal surface while the other one interacts with water, promoting dispersion of the nanoparticles in alkaline solutions.[182] With this growth (and coating) route they found that the polymer capsules exhibit pH-dependent conformation, and shedding of the polymer outer layer in acidic pH alters the nanoparticle solubility (NPs become compatible with nonpolar media) along with a decrease in the hydrodynamic radius. They reported that the size of the AuNPs can be controlled from 2 to 15 nm (*in situ* during the growth phase) by varying the Au-to-polymer molar ratios; lower gold-to-polymer ratios provide small NPs, and *vice versa*.

The encapsulation strategy has also been applied to surface functionalize AuNRs, albeit with less frequency. In one study, Kim and co-workers utilized a poly(ethylene oxide)–poly(*n*-butyl acrylate), PEO–PnBA diblock copolymer to encapsulate CTAB-capped AuNRs.[183] In this design, the hydrophobic PnBA chains exhibited strong affinity to the gold–water interface, which resulted in the formation of dense micelle assemblies on the Au surface, while the poly(ethylene oxide) block allowed dispersion of nanorods in water media. We should note that the PEO–PnBA polymer used in this study is different from other more commonly used amphiphilic polymers often based on the PS–PAA motif. Here, switching the hydrophilic block from PAA (an ionic system) to PEO (non-ionic) provided polymer-coated NPs that are insensitive to changes in the ionic strength of the medium.

Finally, we would like to stress that another form of surface-functionalization using charged polymers (*i.e.*, polyelectrolytes) has been applied by a few groups.[184–187] This approach may also be treated as another form of encapsulation within polymeric materials. Here, adsorption of polyelectrolytes, either *via* direct interaction with the metal-rich surface of the nanostructures, or *via* layer-by-layer (LBL) self-assembly, has been used to functionalize citrate-stabilized Au nanoparticles or CTAB-coated nanorods.[186,188,189] For instance, starting with CTAB-capped AuNRs El-Sayed and co-workers applied LBL to prepare NRs with negatively charged surfaces. For this they simply mixed CTAB-nanorods (positively-charged) with a solution of poly(styrene sulfonate), PSS, which promoted the electrostatic adsorption of the polymer onto the NR, producing a dispersion of PSS-modified and negatively charged AuNRs.[190] The materials were further coupled to an antibody and tested for use as photothermal therapy platforms (see below). Layer-by-layer self-assembly of polyelectrolyte materials on glass and metallic surfaces has in fact been widely used by several groups to assemble thin polymer films with various properties, and the above data show that this approach can be easily extended to other nanoscale surfaces.[191–195]

3.2.2. Encapsulation of semiconductor quantum dots and magnetic nanoparticles. Three types of polymers have been targeted by several groups for further modifications: polyacrylic acid (PAA), poly(dimethylaminoethyl methacrylate), PDMA, and poly(maleic anhydride), PMA, even though other systems were also used. These polymers present along their backbones reactive groups that are easy to modify. Reactive groups such as carboxyl and maleic anhydride can allow the insertion (*via* simple transformations) of a hydrophilic and/or hydrophobic block into the overall polymer structure. This allows one to control or alter the balance between the hydrophobic and hydrophilic blocks, and thus the overall behavior of the amphiphilic polymer. In one of the early reports and starting with polyacrylic acid, Wu and co-workers modified ~40% of the carboxyl groups along the chain with octylamine and showed that the resulting amphiphilic polymer can be used to encapsulate CdSe–ZnS QDs.[10] For this system, the hydrophobic octyl side chain interdigitated with the native ligands (often made of TOP/TOPO mixed with a small fraction of phosphonic acids), while the remaining carboxyl groups promoted water compatibility. The resulting QDs were further cross-linked, *via* EDC condensation, with lysine or polyethylene glycol lysine, followed by reaction with antibodies and streptavidin to endow the nanocrystals with biological activity. These encapsulated nanocrystals were the first commercially-offered biocompatible QDs. They have been used in an array of studies and demonstrations over the past decade.[10,196–202] Using a similar approach, Nie and co-workers used a commercially-available high molecular triblock-copolymer made of polybutylacrylate, polyethylacrylate and polymethacrylic acid blocks, on which they grafted a small number of 8-carbon (C-8) alkyl side chains to serve as the hydrophobic modules. Insertion of such alkyl segments allowed the encapsulation of TOP/TOPO–QDs within this triblock copolymer, while the carboxyl groups permitted further coupling to antibodies and tissue labeling.[203] Parak, Pellegrino and co-workers introduced the use of poly(maleic anhydride alt-1-tetradecene) (M_w = 30 000–50 000) as a flexible platform to prepare amphiphilic polymers to encapsulate various inorganic nanocrystals, including luminescent quantum dots and iron oxide nanoparticles (Fig. 9A).[132] The polymer was initially adsorbed onto the hydrophobic QDs in an organic medium (*e.g.*, chloroform solution). Addition of bis(6-aminohexyl) amine initiated the cross-linking of polymer capsules around the nanocrystals. After solvent evaporation, water was used to promote hydrolysis of the unreacted anhydride groups in the polymer capsule, resulting in the dispersion of the QDs in aqueous media; affinity to water is driven by the newly available carboxylic acids along the polymer (and in the capsules). In a follow up study, they coupled ATTO dye molecules pre-modified with the amino group to the alkyl-modified polymer backbone, and used these hybrid complexes to probe the dependence of the energy transfer interactions between QDs and dyes on the environmental conditions.[204] In subsequent studies a few other groups expanded the above idea and introduced polyethylene glycol segments into the amphiphilic polymer structure to improve the bio-compatibility of QDs and reduce non-specific interactions. In one of those studies,

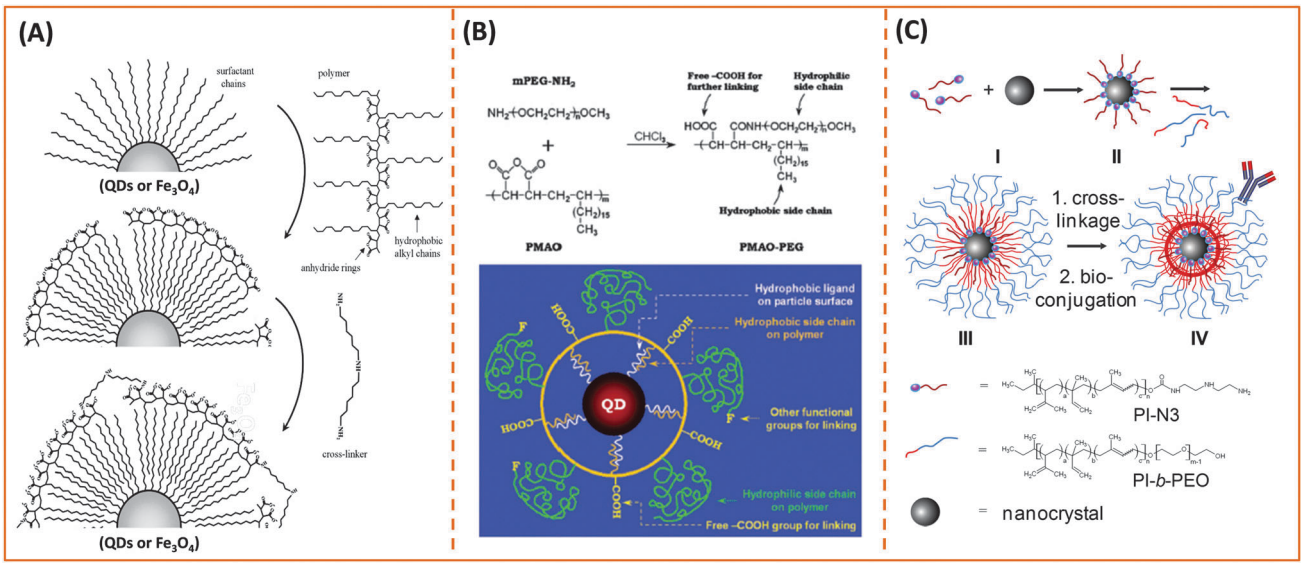

Fig. 9 Representative examples illustrating the phase transfer *via* encapsulation within amphiphilic block-copolymer micelles applied to: (A and B) semiconductor QDs and magnetic nanoparticles using amine-reactive poly(maleic anhydride). (C) A block-copolymer (PI-*b*-PEO) prepared *via* radical polymerization of reactive isoprene groups in the presence of the nanoparticles; the latter approach was also applied to QDs and magnetic nanoparticles.[130,132,209] (Figures are reproduced from the above references with permission from the American Chemical Society.)

Colvin and co-workers grafted lateral PEG chains onto the polymer prior to encapsulation of the nanocrystals (Fig. 9B).[130] They first formed the amphiphilic polymer by reacting poly(maleic anhydride-*alt*-1-octadecene) with amine-modified methoxy-terminated poly(ethylene glycol) (NH_2–PEG–OCH_3, with PEG M_W = 6000–20 000). The nanocrystals (QDs or iron oxide NPs) were mixed with the polymer in chloroform, and following solution homogenization the solvent was evaporated. Addition of buffer to the medium facilitated dispersion of the materials and provided hydrophilic QDs. In another study Mulvaney and co-workers used an amphiphilic polymer, poly(styrene-*co*-maleic anhydride), M_W = 1700, which was synthesized *via* maleic anhydride coupling to either ethanolamine or the amino-PEG derivative Jeffamine M-1000 polyetheramine. The resulting water soluble nanocrystals simultaneously presented PEG as a solubilizing moiety and COOH reactive groups.[205] The authors also reported that the experimental procedure described in ref. 130 (*i.e.* relying on reacting the PEG with the polymer precursor prior to encapsulation) could not be reproduced, whereas the use of Jeffamine M-1000 polyetheramine allowed easier implementation of chemical coupling followed by encapsulation of the nanocrystals.[205] The authors subsequently introduced azide groups into the polymer structure and tested their ability to conjugate the resulting azide-functionalized QDs to cyclooctyne-modified proteins (see below). These studies clearly show that the maleic anhydride motif provides a flexible platform to prepare several tailor-made block co-polymers by introducing hydrophobic and/or hydrophilic moieties (*e.g.*, alkyls and PEG moieties) along with the desired functionalities.

In related approaches, Winnik and co-workers used PEG grafted polyethylenimine (PEI-*g*-PEG) and diblock copolymer poly(ethylene glycol-*b*-2-*N*,*N*-dimethylaminoethyl methacrylate) (PEG-*b*-PDMA) to promote the transfer of QDs to buffer media.[206,207] The authors have, nonetheless, attributed this surface functionalization strategy to the removal of native ligands by ionic anchors present on the polymer. A similar triblock copolymer construct made of poly(poly(ethylene glycol) methyl ether methacrylate)-*block*-poly(2-dimethylaminoethyl methacrylate)-*block*-poly(2-dimethylaminoethyl methacrylate-*co*-octyl methacrylate), [HOOC-PEGMA-*b*-PDMA-*b*-(PDMA-*co*-POMA)], has also been recently used by Gao and co-workers to encapsulate hydrophobic QDs.[208] Weller and co-workers have recently described a few interesting developments in amphiphilic polymer design based on block-copolymers and their use to encapsulate individual or combinations of inorganic nanocrystals within a single capsule (*e.g.*, QDs and iron oxide nanoparticles, see Fig. 9C).[209–212] They further coupled these capsules to target molecules and used the resulting complexes for cellular imaging. In one study they detailed the use of a chemically designed triblock-copolymer to cap CdSe–ZnS QDs *via* partial ligand exchange. The polymer consists of a polyethyleneimine binding block (to promote interaction with the inorganic surface *via* amine binding), a hydrophobic polycaprolactone, and a polyethylene glycol block to facilitate dispersion of the nanoparticles in aqueous media.[210] The authors explored the effects of varying the size of the three blocks and showed that ^{1}H NMR could be used to track the polymer binding onto the QDs combined with a progressive removal of the native TOP/TOPO cap. They also found that changing the polymer-to-nanoparticle molar ratio can allow one to vary/control the number of nanocrystals (QDs, Fe_3O_4 nanoparticles or combination of both) per capsule; capsules containing either one or a few nanocrystals have been made using this route. In a more recent study, they employed *in situ* seeded emulsion polymerization in the presence of the hydrophobic nanocrystals (with their native cap) to prepare nanocrystals encapsulated within an amphiphilic polyisoprene-*block*-poly(ethylene oxide) diblock

(PI-*b*-PEO) copolymer that are also reactive.[213] With this *in situ* strategy, combinations of the surfactants, functional monomers, linkers and the radical initiator are sequentially introduced along with the nanocrystals to promote the encapsulation of one type or a combination of nanocrystals within the same capsule.[213] In a subsequent report they detailed the synthesis of an amphiphilic miktoarm star copolymer made of two PEO and one PI chain, (PI-*b*-$(PEO)_2$ star), with control over the arm size *via* changes in the precursor molecular weights.[211] One of the key features of this polymer is its ability to provide an effective hydrophobic shielding around the nanocrystal surface, which drastically reduces diffusion/permeability of copper and iron ions to the QD surface. In particular, they showed that QDs encapsulated with an azide-modified block copolymer can be used to implement copper-catalyzed click reactions with minimal loss in the PL emission, circumventing previous limitations to using such coupling strategy when smaller surface ligands are used.[211,214] Cyclic molecules such as calix[*n*]arenes (with $n = 4$, 6, and 8) containing carboxylic acid groups were also used to encapsulate luminescent QDs.[215]

4. Use of inorganic nanocrystals in targeted biological applications

4.1. Bioconjugation to target molecules

Conjugation of biomolecules (*e.g.*, proteins and peptides) to the nanoparticle surfaces is critically important for the successful integration of such platforms in various biological systems. A few chemical coupling methodologies have been applied to conjugate hydrophilic nanoparticles (QDs, AuNPs and magnetic NPs) to proteins, peptides and DNAs. They are (1) avidin–biotin bridging; here, proteins or peptides can be pre-modified with biotin groups to facilitate interactions with streptavidin-functionalized QDs or *vice versa*.[127,148,166] (2) 1-Ethyl-3-(3-dimethylaminopropyl)carbodiimide/*N*-hydroxy succinimide) (EDC/NHS), or sulfo-NHS coupling between carboxyl groups on the NPs and amines on the biomolecules, and *vice versa*.[10,127,148] (3) Thiol (–SH) reactive maleimide coupling to cysteine or (sulfhydryl)-modified proteins and peptides, starting with the transformation of the surface reactive groups on the nanocrystals.[216,217] (4) Metal-affinity driven self-assembly between polyhsitidine-appended biomolecules and metal-rich nanocrystals;[161,162,218] this method relies on the affinity between polyhistidine tags and certain transition metal ions (*e.g.*, Ni and Zn), and requires direct interactions between the imidazole groups (on the tag) and the metal-rich surface of nanoparticles. (5) Azide–alkyne Huisgen cycloaddition (or "Click" reaction), which requires access to biomolecules pre-modified with either alkynes or azides, together with azide- or alkyne-functionalized nanoparticles.[145,219–221] The use of avidin binding to the biotin molecule, EDC condensation as well as thiol-to-maleimide coupling strategies were more common in several of the early demonstrations, and this was due to the fact that these protocols have been well established and ubiquitous in biology.[222] Metal-histidine driven self-assembly of QD-bioconjugates is extremely attractive, because it is relatively easy to implement (mixing reagents) and can benefit from the ubiquitous use of polyhistidine expression on proteins. Its use as a conjugation strategy is still somewhat limited, because it requires direct access of the imidazole residues to the inorganic surface of the nanocrystals, although it has been gaining interest in the past few years.[159,162,223,224] The original azide–alkyne Huisgen cycloaddition reaction requires a copper catalyst in particular when using alkyne-modified molecules.[225,226] It has been applied to non-fluorescent NPs such as Fe_3O_4 nanocrystals.[143] However, recent developments have shown that following the ideas originally developed by Bertozzi's group,[227,228] copper-free strain-promoted azide–alkyne cycloaddition (SPAAC) coupling can be effective without requiring the need for a copper catalyst. This advance has made "Click" reaction better suited for coupling onto luminescent QDs, since Cu ions can severely quench the QD PL.[219] A few demonstrations applying this Cu-free click reaction to conjugate proteins to QDs have been reported over the past few years. Texier and co-workers applied this coupling strategy for conjugating cyclooctyne-functionalized QDs to azide-modified biomolecules.[221] They first attached commercially-available carboxy-modified cyclooctyne to the amine-functionalized polyethylene glycol-coated QDs *via* EDC conjugation, and then allowed the resulting QD–cyclooctyne complexes to react with the azide-modified biomolecules at room temperature. This scheme allowed efficient coupling between QDs and biomolecules while preserving the fluorescence properties of the QDs, namely, quantum yield and spectral integrity. Bawendi and coworkers used norbornene–tetrazine to implement cycloaddition reaction and conjugate tetrazine-biomolecules to norbornene-modified QDs (Fig. 10).[219] They first attached commercially available carboxylic-modified norbornene onto a polymeric imidazole ligand (introduced above), *via* amide coupling, and used the resulting norbornene-modified polymer ligand to cap QDs. They then tested the ability of the resulting norbornene-modified QDs to react (*via* cycloaddition reaction) with the tetrazine derivative using one (*in vitro*) solution phase reaction along with another one involving cell membrane (*in vivo*) labeling. In the first example, they reacted the norbornene-modified QDs with a dye modified with a tetrazine derivative [3-(4-benzylamino)-1,2,4,5-tetrazine (BAT)]. They tested the effectiveness of the conjugation using a combination of optical absorption and energy transfer quenching, and indeed, they found that high levels of QD–dye coupling could be achieved with no drastic losses in QD PL since no copper ions were needed; rather large excess of BAT-dye with respect to QDs was required for the coupling, nonetheless. For cellular labeling they explored two configurations. In the first one, they modified the EGF (epidermal growth factor) with BAT, followed by reaction with norbornene-modified QDs to obtain EGF-coated QDs; the cycloaddition reaction was carried out at 37 °C. Then the resulting conjugates were incubated with A431 human carcinoma cells overexpressing EGF receptors (EGFRs) on their membranes. In the second setting, the BAT-modified EGF was first incubated with the A431 cells to provide

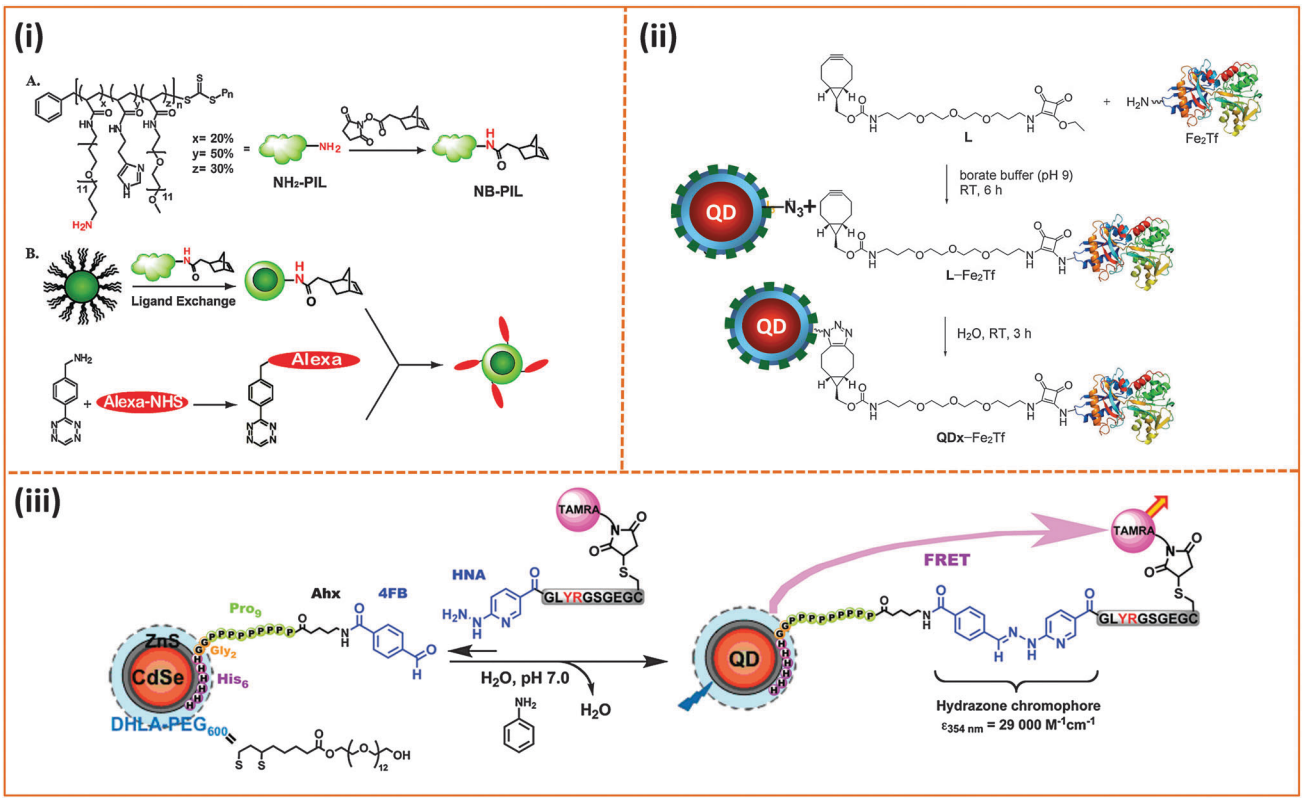

Fig. 10 Three representative bio-conjugation strategies: (i) Coupling of norbornene to the NH_2-functionalized imidazole polymer (A). Diels–Alder reaction between Alexa 594 pre-modified with 3-(4-benzylamino)-1,2,4,5-tetrazine (BAT) and norbornene-modified QDs (B). (ii) Strain-promoted copper-free azide–alkyne cycloaddition between azide-modified QDs and L-Fe_2Tf (L-Fe_2Tf denotes the product resulting from coupling of primary-amine Transferrin with ethyl squaramyl to provide a cyclooctyne conjugate used for the Click reaction). (iii) Hydrazone ligation of aldehyde-functionalized QDs with a peptide pre-modified with a HYNIC residue.[219,220,230] (Figures are adapted from the above references with permission from the American Chemical Society and from Wiley.)

BAT-presenting cells. These cells were then incubated with the norbornene-functionalized QDs. They found that the two approaches provided high levels of fluorescence labeling of the cells, compared with minimal QD fluorescence for control preparations. Liu and co-workers used a polyhistidine- and azide-modified block copolymer, starting from polymaleic anhydride, to cap luminescent QDs.[145] They showed that following ligand exchange the azide groups were accessible for further conjugation to the Baculovirus pre-modified with cyclooctyne through metal-free "Click" reaction. These conjugates were tested in the intracellular uptake by the A549 cell line. The use of click coupling was also implemented by Mulvaney and co-workers.[220] They first introduced azide groups into amphiphilic polymer capsules, then tested their ability to conjugate the azide-functionalized QDs to cyclooctyne-modified transferrin or Alexa Fluor 594, using strain-promoted azide–alkyne cycloaddition (SPAAC) (see Fig. 10).[229] They further demonstrated the biological activities of SPACC-promoted QD-transferrin conjugates by monitoring their uptake in cells expressing a high level of transferrin-receptors on their membranes.[220]

Applying "Click" coupling to QDs and other NPs constitutes a major advance in promoting better integration of these nanoscale platforms into biological systems. One limitation of this approach, however, stems from the fact that an excess amount of target molecules is still needed to achieve saturation in the coupling efficiency. Aniline-catalyzed hydrazone ligation provides an alternative strategy. We have applied the scheme to couple aldehyde-functionalized QDs to a peptide modified with a 2-hydrazinonicotinoyl group (HYNIC); no polymer functionalized nanocrystals were used though.[230] Starting with DHLA–PEG–QDs, the nanocrystals were subsequently self-assembled with a polyhistidine-terminated and aldehyde-modified peptide. The resulting conjugates were reacted with a second HYNIC-modified peptide, and the kinetics of the reaction were monitored optically by tracking the formation of the hydrazone chromophore at 354 nm with time (Fig. 10).[230]

4.2. Use of nanoparticles in biological imaging and sensing

The use of inorganic nanostructures in biology has focused on taking advantage of their unique physical and optical/spectroscopic properties either to improve the performance of more traditional materials or to develop new ideas that exploit their unique photophysical characteristics. These nanocrystals have a large surface area compared to molecular scale probes. Thus, a single nanoparticle can be easily coupled to several biomolecules with potential control over the orientation and spatial arrangements of the biomolecules in the resulting

conjugates. This feature substantially enhances the affinity and biological activity of the resulting conjugates due to, for example, avidity effects. Applications of nanomaterials in biology have increased over the past decade and include use as fluorescent labels for live cells and tissue imaging, drug and gene delivery vehicles, detection of pathogens and soluble heavy metals, sensing of protein–protein, protein–DNA interactions as well as DNA hybridization. In this section, we will focus on a few representative examples where polymer-coated nanocrystals (QDs, AuNPs and magnetic nanoparticles) have been used as platforms for imaging and/or sensing.

4.2.1. Gold nanoparticles. Though no polymer-coating was used, Mirkin and co-workers pioneered the development of colorimetric assays based on changes in the SPR resonance peak when dispersions of oligonucleotide-conjugated AuNPs were mixed with complementary DNA sequences to induce controlled aggregation. In those sensor designs, the authors started with thiol-modified oligonucleotides which were allowed to self-assemble onto citrate-stabilized AuNPs to form the AuNP–DNA conjugates. When mixed with complementary oligonucleotide sequences, the dispersion of AuNP–DNA conjugates experiences a small but measurable change in the solution color, driven by NP aggregation promoted by complementary hybridization between the sequence on the NP and target oligonucleotide added to the medium.[231–233]

AuNPs and AuNRs are very effective fluorescence quenchers of dye and QD emission, with quenching efficiencies exceeding those predicted by the Förster dipole–dipole interaction formalism.[234–236] However, use of polymer coated-AuNPs and AuNRs to develop bio-motivated sensors based on energy transfer has not been actively explored, presumably due to the fact that this surface-functionalization route can increase the separation distance and reduce the quenching efficiencies. Nonetheless, there have been a few reports on sensor design using the direct coordination of thiol-modified dye-labeled DNA and peptides.[233,237,238] More recently the use of metal-histidine coordination to self-assemble fluorescent proteins on AuNPs with very high quenching efficiencies has been explored by a few groups.[162,239] The combination of dyes, fluorescent proteins and QDs with AuNP- or AuNR-quenchers has been utilized by a few groups to develop sensing platforms for targeting protein–protein interactions and competitive binding assays.[231,240,241]

In an early demonstration, Kim and co-workers developed an inhibition assay to detect protein glycosylation based on changes in the PL quenching of QDs when assemblies of carbohydrate-conjugated QDs and lectin-conjugated AuNPs are formed; lectin is known to exhibit high-affinity to manno- and gluco-oligosaccharides.[242] They first conjugated AuNPs to concanavalin A (conA). Then, amine-terminated co-polymer encapsulated QDs (provided from Invitrogen) were conjugated to dextran (polymerized glucose). Sensing of the saccharides was carried out using a competition assay format where the target molecules competed with the QD–dextran conjugate for interactions with conA on the AuNPs. The value of apparent binding constant (K_a) extracted from their titration procedure was similar to the previously reported value $\cong 1.0 \times 10^7\ M^{-1}$. This construct was then applied to probe differences between avidin and its non-glycosylated derivative, neutravidin, and between bovine serum albumin (BSA) and its chemically-modified neoglycosylated form, 22-MB (BSA–α-D-mannopyranosylphenyl isothiocyanate with 22 mannose units per BSA). In both cases, the inhibition of the QD-dextran binding to AuNP–ConA conjugates manifested in a substantial reduction in the QD PL quenching. Furthermore, a correlation between reduction in the PL quenching and the target concentration was observed only for the glycosylated proteins (avidin and 22-MB), which clearly proved that the specificity of the ConA protein on the AuNPs was maintained. They expanded the utility of this sensing scheme and tested its ability to differentiate between glycoproteins having different glycan density profiles per molecule. For this, they used recombinant glucose oxidases expressing different lengths of mannose glycans and found that changes in the PL emission signature closely traced the number of glycan groups present in the target protein.[242] Rotello and co-workers explored the use of AuNPs capped with labile cationic ligands to assemble new platforms that can serve both as delivery vehicles and intercellular probes.[243] These nanoparticles were partially functionalized with a small fraction of thiol-modified fluorescein (FITC-SH). They found that upon assembly on the NPs the fluorescence of the FITC was completely quenched, due to nonradiative energy transfer between FITC and the AuNPs. Addition of glutathione (GSH) to these assemblies promoted the release of the FITC dye from the AuNPs, resulting in the recovery of dye emission. This provided them with an analytical tool, based on changes in the fluorescence emission, to quantify the rate of ligand release from the NP surface. The GSH-induced and concentration-dependent release of the FITC from the AuNP surfaces combined with changes in the fluorescence signal provides a promising drug delivery and sensing platform with potential use in live cells using NPs decorated with a drug or a mixture of drug and fluorophores.[243] In a follow up study, they assembled a new fluorescent protein (GFP)–AuNP conjugate exploiting electrostatic interactions of GFP with the cationic ligands on the gold NPs. This provided a flexible platform to detect specific soluble proteins in buffer media and in human serum, *via* competitive interactions with the surface bound GFP; this format exploits the weak electrostatic interactions driving the NP–GFP conjugate assembly. They applied this platform to sense five serum proteins (human serum albumin, immunoglobulin G, transferrin, fibrinogen and α-antitrypsin), both in buffer and when spiked into human serum. Combining this fluorescence assay with a linear discriminant analysis they were able to identify those soluble proteins with an identification accuracy of 100% in buffer and 97% in human serum.[244]

The large and tunable plasmonic absorption cross section of gold nanostructures (including spherical nanoparticles, nanorods, nanoshells and nanocages) from the visible to the NIR promotes controlled local heating driven by remote laser irradiation in the visible and/or NIR. This process has been exploited by a few groups to develop photothermal platforms, which can ablate cancerous tissues and malignous cells.[245]

We will describe three representative examples where this idea was tested *in vitro* and *in vivo*.

In one early study, El-Sayed and co-workers exploited the pronounced SPR peak of gold nanorods in the NIR to develop AuNR-based therapy platforms that can promote photothermally-induced death of cancer cells. Starting with poly(styrene sulfonate)-coated AuNRs (introduced above) they assembled a few copies of the anti-EGFR (epidermal growth factor receptor) antibody onto the NRs *via* electrostatic physisorption on the negatively charged nanorods. When the NR dispersions were incubated with two malignant epithelial cell lines (HOC 313 clone 8 and HSC 3), only anti-EGFR–AuNR conjugates bound to the membrane of malignant cells expressing EGFR. Exposure to irradiation at 800 nm provided by a CW laser induced a pronounced level of cell death (Fig. 11).[190] They also found that to induce the same level of cell death, malignant cells required about one half of the laser power to induce a similar rate of cell death when the NRs were incubated with a culture of nonmalignant (HaCat) cells. This difference is attributed to the lack of specific interactions of the antibody-AuNRs with the control culture of nonmalignant cells, thus producing much smaller concentration of AuNRs at their membrane and less thermal heating. In the second study, Murphy and co-workers combined layer-by-layer polyelectrolyte adsorption and CTAB-stabilized NRs to assemble

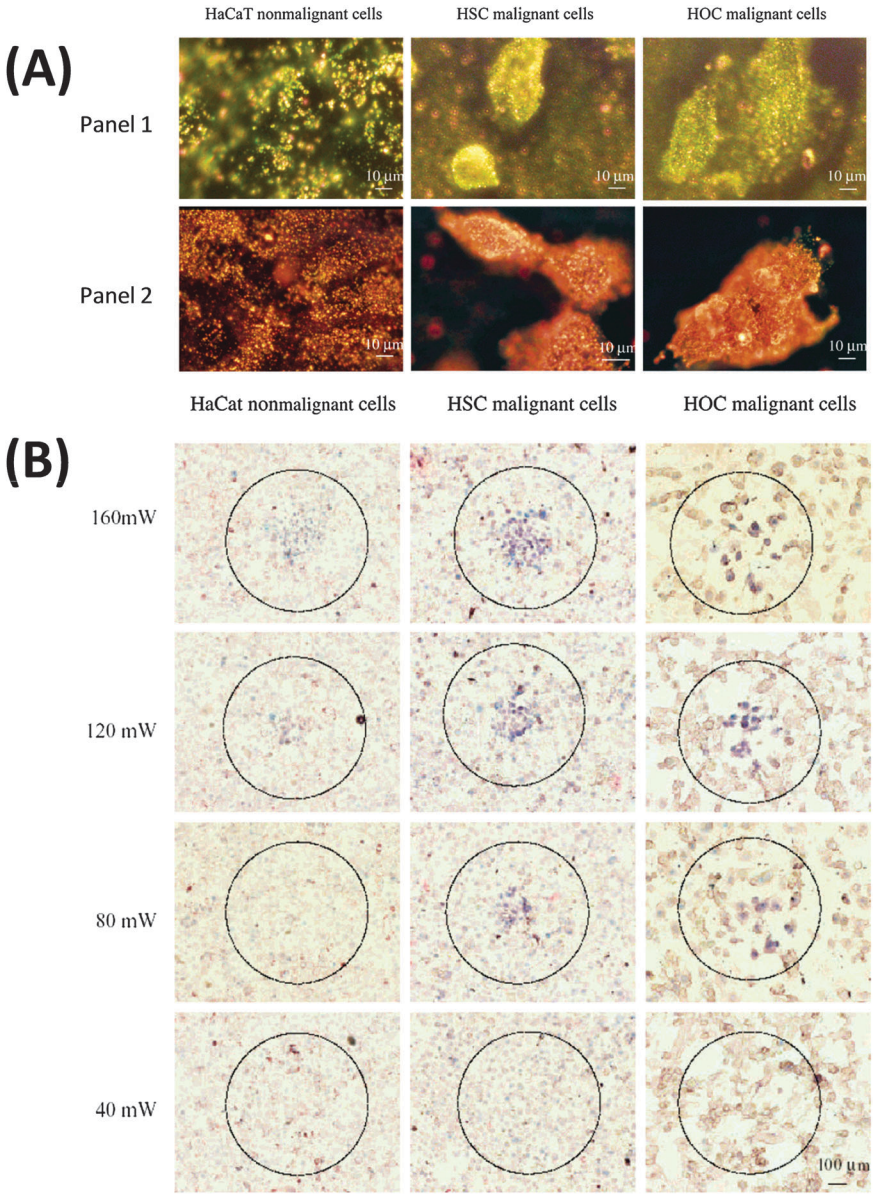

Fig. 11 (A) Light scattering images of cells incubated for 30 min with: anti-EGFR–AuNPs (top), and anti-EGFR–AuNRs (bottom). (B) Typical examples of photothermal therapy of cancer cells (HSC and HOC malignant cells) incubated with anti-EGFR–AuNRs. The circles designate the area exposed to laser irradiation. At a laser power of 80 mW (10 W cm^{-2}), the malignant cells are damaged while the HaCat normal cells are not affected. Higher powers (120 mW and 160 mW) are required to damage HaCat (normal) cells.[190] (Figures are adapted from the above reference with permission from the American Chemical Society.)

a platform that allows remotely-controlled release of molecules embedded within the surface coating layer.[186] To prove this concept, they integrated Rhodamine 6G within a polyelectrolyte coating multilayer using layer-by-layer self-assembly of poly(acrylic acid, sodium salt) (PAA) and poly(allylamine hydrochloride) (PAH) on CTAB–AuNRs. They then showed that upon laser irradiation with a NIR signal, a sizable and power-dependent dye release from the AuNR surfaces takes place. In addition, they found that the rate of dye release was correlated with the number of bilayers adsorbed onto the NR and the time of laser irradiation used (Fig. 12).[186] This design can potentially be applied to promote the drug delivery in cell cultures and tissues. In the third example, Xia and co-workers used gold nanocages as a remote-controlled drug delivery system. They started with poly(vinylpyrrolidone) (PVP)-coated Au-nanocages, grown *via* a galvanic replacement reaction between truncated Ag nanocubes and chloroauric acid ($HAuCl_4$).[246,247] The PVP coating was exchanged with a poly(*N*-isopropylacrylamide) (pNIPAAm) polymer. Because the pNIPAAm copolymer exhibits thermo-sensitive properties (change in conformation with small temperature variations), the PINAM-encapsulated nanocages offer an efficient carrier for the delivery of cargo molecules (drugs and else) to target tissue, followed by remote release *via* laser irradiation. In one example, the authors loaded alizarin–PEG (Dye–PEG),

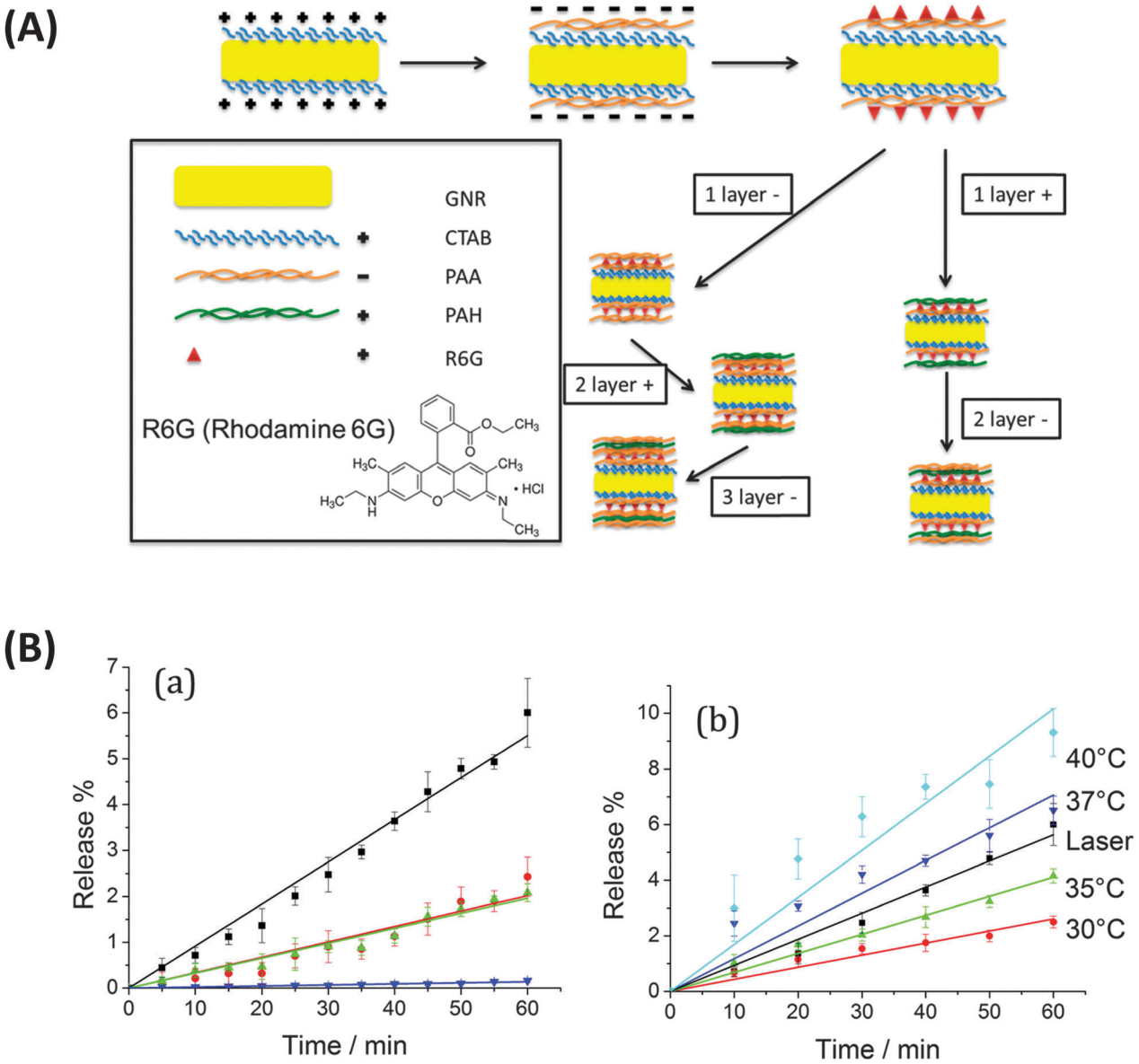

Fig. 12 (A) Schematic of the surface-coating and dye loading onto AuNRs using adsorption of a few polyelectrolyte layers. (B) Percentage of dye release *vs.* laser irradiation time for different samples: (a) AuNR + PAA + R6G + PAA (black); AuNR + PAA + R6G + PAA + PAH (red); AuNR + PAA + R6G + PAH (green); and AuNP + PAA + R6G + PAA (blue); (b) percentage of dye release *vs.* time for AuNR + PAA + R6G + PAA at a given temperature in a water bath. The black curve in the right panel is reproduced from the left panel and refers to the drug release under laser irradiation.[186] (Figures are adapted from the above references with permission from the American Chemical Society.)

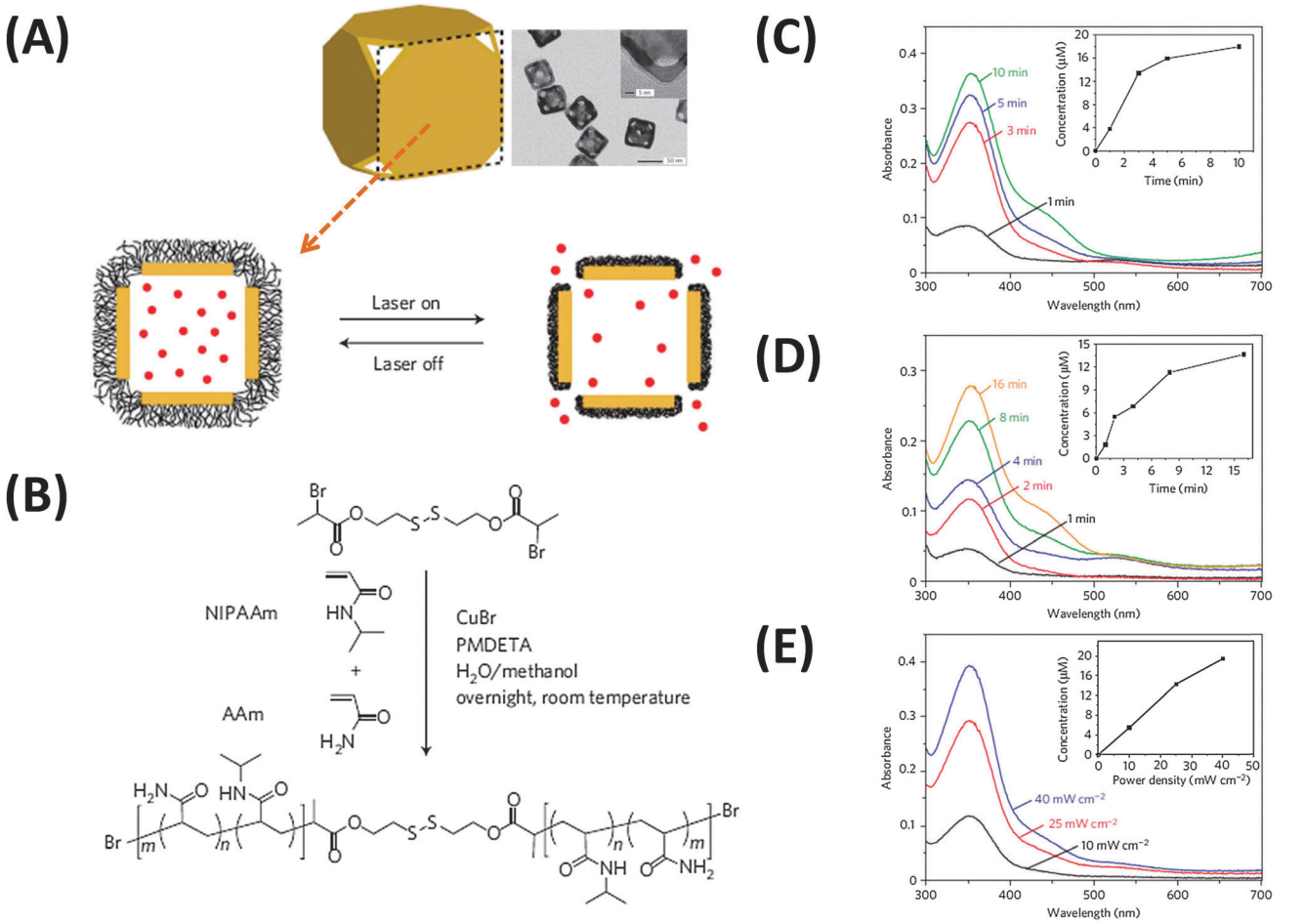

Fig. 13 (A) Schematic illustration of the drug release from Au nanocages upon irradiation with a near-infrared laser source. The absorbed NIR photons are converted into heat, triggering the swelling of the amphiphilic polymer and release the drug molecules. When the laser is turned off, the polymer coating relaxes back to its initial conformation, preventing any further release of the drug. (B) Synthetic scheme of the amphiphilic polymer using RAFT. (C–E) represent the drug release rate under different conditions, namely, upon heating at 42 °C at different times (C), for a given laser power but different irradiation time (D), and for a given irradiation time but different laser power (E).[247] (Figures are adapted from the above reference with permission from Nature Publishing Group.)

or doxorubicin (Dox, a drug) inside the cage by mixing at 42 °C with continuous shaking. They found that NIR photo-irradiation (using a laser power of ~10 mW cm^{-2}) produced enough thermal energy to change the polymer conformation around the cages, releasing the embedded dye or drug. Such release was permitted by the thermally-induced change in the pNIPAAm conformation, opening pores along the cage walls and allowing diffusion of the drug into the surrounding medium (Fig. 13). Here too they measured laser power-dependent release of the drug in the medium.

4.2.2. Quantum dots. The ability to modify the surface ligands on luminescent semiconductor QDs allows chemical tuning of their properties (*e.g.*, using a polymer coating) to target specific receptors on the cell membranes or within intracellular compartments, and potentially affect and control their *in vivo* bio-distribution.[3,8,19] We will focus on few representative examples of copolymer-coated QDs (either encapsulated or cap exchanged) that have been used in biological imaging and sensing. These examples constitute only a small subset of what has been reported in the literature since the first reports proposing the use of QDs as fluorescent platforms in biology.[125,128] In one of the early reports Wu, Bruchez and co-workers used CdSe–ZnS QDs encapsulated within an octylamine-modified polyacrylic acid copolymer and coupled to streptavidin.[10] These conjugates were used to label the breast cancer marker Her2 on the membrane of fixed cells, and to stain microtubule fibers inside the cytoplasm. In particular, they confirmed that, compared to dye labeling, the use of QDs permitted imaging of the target regions with high signal-to-noise ratios and over extended periods of time (Fig. 14). They also showed that the use of distinct color QDs conjugated to either antibody or streptavidin allows labeling of two different cellular targets in the same cell with great resolution, while exciting the specimen with a single excitation source. In another report, Dahan and co-workers investigated the use of QD–glycine conjugates to monitor the lateral diffusion of individual glycine receptors at the surface of neuronal cells; the glycine was assembled *via* biotin-streptavidin binding onto

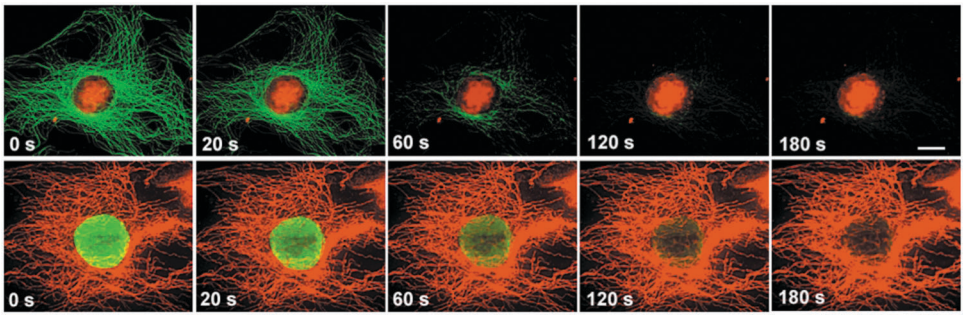

Fig. 14 Side-by-side comparison of the photo-stability of QDs and Alexa 488. Top row: the Nuclei and microtubules of 3T3 cells were respectively labeled with QD 630–streptavidin (red) and Alexa 488 conjugated to anti-mouse IgG (green). Bottom row: microtubules were labeled with QD 630–streptavidin (red) and nuclear antigens were stained green with Alexa 488 conjugated to anti-human IgG.[10] Scale bar, 10 μM. (Figures are adapted from the above reference with permission from the Nature Publishing Group.)

commercially-available QD–streptavidin conjugates.[200] The authors showed that they can track the diffusion of a single QD–glycine conjugate over a long period of time, and obtain information about their dynamic diffusion in the inter-cellular domains. In particular, they observed multiple exchanges between extrasynaptic and synaptic domains in live neurons, where a single QD–glycine receptor conjugate was found to alternate between free and confined diffusion states. In addition, they showed the existence of several membrane domains corresponding to synaptic, perisynaptic and extrasynaptic regions with different receptor diffusion behaviors.

However, the difficulties associated with the controlled delivery of QDs into the cytosols of live cells have limited the effective use of these materials to label and track protein receptors inside the cytosol. Much better success has been achieved in applications focusing on biological processes that occur at the outer surface of the cell (namely, membrane specific phenomena).[200,248,249] Several attempts to achieve cytosolic delivery of QD-conjugates have been reported by various groups, albeit with little to modest success. In one example, Helms and co-workers relied on the ability of pH-dependent conformational change of a polymer coating on the QDs to initiate endosomal disruption and release of the nanocrystals in the cytosol. They first synthesized a cationic core–shell polymer colloid, where the core is made of a pH-buffering proton sponge using poly(ethylene glycol) dimethacrylate (PEGDMA, $M_W \sim 330$ Da) cross-linked poly(2-(diethylamino)-ethyl methacrylate), PDEAEMA, and the shell is made of poly-(2-aminoethyl methacrylate), PAEMA. Then streptavidin-coated QDs (605-SAQDs) were immobilized inside the polymeric colloids *via* multivalent electrostatic interactions between the ammonium ions on the polymer colloid shell and carboxylate functions of the streptavidin side chains. They showed that the QDs encapsulated within this polymer could be delivered into live cells after extended incubation (2–4 hours) *via* endocytosis.[250] Once in the endosome the polymer–QD assemblies experience a chemical shock due to a pH change in acidic conditions, which substantially increases the polymer colloid dimensions, triggering the disruption of the endosomal compartments and measurable release of QDs into the cytosol. Recently, Bawendi and coworkers tried to address the problems associated with the inability to achieve direct delivery of QDs and QD-conjugates into the cytosol of live cells. They designed a microfluidic device that forces live cells to rapidly pass through a constriction in the microfluidic channel.[251] This constriction transiently disrupts the membrane of the cell by opening a few pores and allowing exchange of materials with the extracellular matrix (Fig. 15A). Using this device combined with fluorescence microcopy they were able to track the slow diffusion of fluorescent materials across the cytoplasm (Fig. 15B and C).

Raymo and co-workers explored the ideas of achieving intracellular photo-cleavage of surface bound groups. They started with an amphiphilic polymer ligand presenting multiple copies of DHLA anchoring groups and reactive PEG chains, described in an earlier report,[150] to assemble QD platforms decorated with photo-cleavable 2-nitrobenzyl groups.[252] The nitrobenzyl groups were attached onto the polymer coating using covalent carbodiimide chemistry. They first tested these assemblies in solution, and found that following QD–nitrobenzyl formation the nanocrystal fluorescence signal was drastically quenched, due to electron transfer interactions between the QD and proximal nitrobenzyl groups. Following photolysis of the 2-nitrobenzyl appendages, they measured a large recovery of the QD emission (by more than 60%), a process attributed to a reduction in the rate of electron transfer between nanocrystal and nitrobenzyl groups promoted by the photoinduced release of the organic chromophores from the QDs. These assemblies were then tested in live cells, where they showed that following cellular uptake (*via* endocytosis) and photo-irradiation of the culture, the intracellular fluorescence signal emanating from the QDs increases by ~80% after photo-cleavage of the 2-nitrobenzyl quenchers.[252]

The influence of the QD surface charge distribution on the *in vivo* binding and transport of these materials was recently investigated by Bawendi and coworkers.[163] For this, they compared the interactions of QDs surface ligated with two sets of zwitterion polymers that share the same imidazole anchoring groups: (1) sulfobetaine-functionalized poly(imidazole) ligand, and (2) carboxybetaine-functionalized poly(imidazole) ligand. Here they were able to control the fraction and nature of

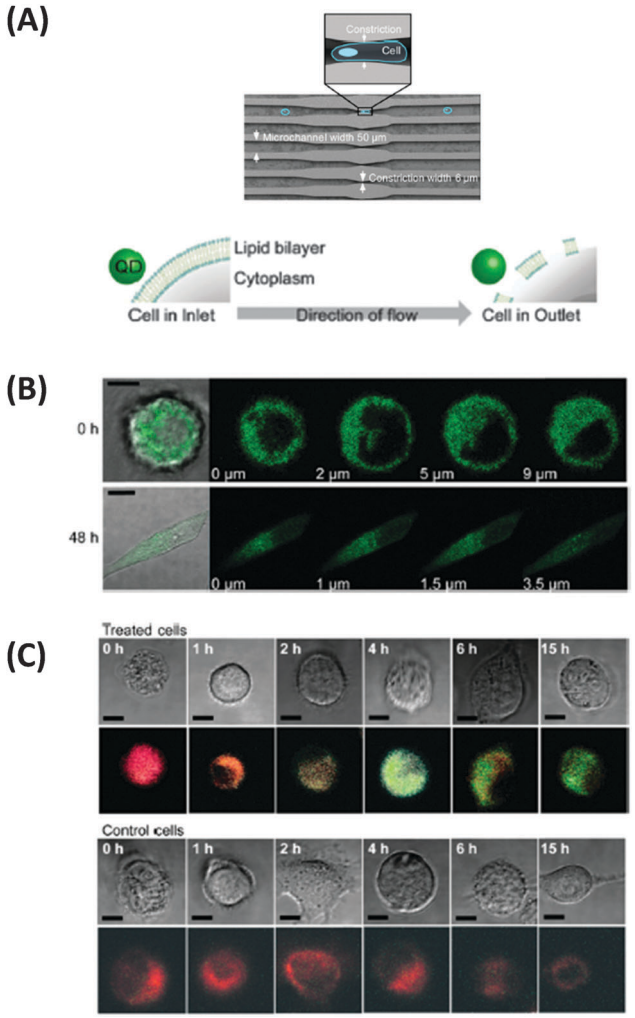

Fig. 15 (A) Schematic diagram of the microfluidic device used for the cell uptake (top), along with the hypothesized method of intracellular entry of QDs (bottom). (B) Overlay of DIC and confocal fluorescence image of representative cells, along with a series of *z*-section fluorescence images of cells with delivered QDs; shown images are immediately after treatment and after 48 h. (C) Confocal microscopy images of live treated and control cells. The observed diffuse staining is limited to the cytoplasm, with no QD fluorescence emanating from the nucleus (dark region within the cell).[251] Scale bar is 10 μm. (Figures are adapted from the above reference with permission from the American Chemical Society.)

exposed charges on the QD surfaces. They evaluated the influence of the spatial charge configuration presented on the QDs coated with these two sets of polymer ligands on the QD interactions with cultured HeLa cells. They found that even for nanocrystals that are neutral or slightly charged, the number of spatially exposed amines (essentially positively charged surface groups) play an important role in determining the level of uncontrolled nonspecific binding to the cells. For instance, they measured significantly higher degrees of nonspecific binding to cells for QDs with coating that possess unconverted tertiary amines. In comparison, polymer coatings that endow QDs with non-exposed amines exhibit little to no binding to cells; these QDs still present a small negative charge on their surfaces. These findings highlight the importance of charge distribution and access of those charges to receptors on cell surfaces. They further complemented their findings by carrying out tumor transport measurements, and showed that non-ionic QDs extravasate from vessels into tumor tissues much faster (an order of magnitude faster) than QDs displaying zwitterionic coating with a net negative surface charge distribution. Overall, this study suggests that effective spatial screening of positively charged groups on the nanoparticles is the best route to minimize nonspecific interactions of such materials with biological media.[163]

The use of QDs as platforms (mostly as exciton donor) to design sensing assemblies based on energy transfer has been explored by several groups over the past decade. Several groups explored the design of sensors to detect enzymatic activity, protein–protein binding, small molecule detection, DNA hybridization and telemorization, using primarily QDs capped with small molecules (compact), as the FRET (fluorescence resonance energy transfer) process requires close proximity between dots and dyes in order to be effective.[160,253,254] However, the use of polymer capped or encapsulated QDs for sensing based on energy transfer interaction has been less explored, since polymer capping has often produced large hydrophilic QDs.[29,255] Nonetheless, a few groups have managed to prepare compact hydrophilic QDs, mainly relying on ligand exchange using multi-coordinating polymers.[7,152,255] For example, Nocera, Bawendi and co-workers have explored two pH sensor designs based on FRET and QD donors. In one example, they conjugated QDs encapsulated within a modified amphiphilic poly(acrylic acid) polymer to a squaraine dye known to exhibit a pH-dependent absorption profile, *via* EDC (1-ethyl-3-(3-dimethylaminopropyl)carbodiimide) condensation. This promoted proximal FRET interactions with high efficiency that vary as a function of the environmental pH. In particular, the authors showed that modulation of the FRET efficiency by varying the solution pH values below and above the pK_a of the dye ($\sim$8.5) produced net ratiometric dependence between the QD and dye emissions. This also provided a simple means to measure the solution pH, by analyzing the ratio of the QD and dye peak intensities, or comparing them to the value at the isosbestic point. Because the ratiometric measurements are potentially not sensitive to fluctuations in the overall collected signals, such an approach can be more accurate and more reliable than 'conventional' chemo- or bio-sensors that utilize one signal response (*i.e.*, either brightening or darkening). This design was further expanded by Snee and co-workers who used a blue emitting CdS–ZnS QD paired with a fluorescein dye to create a ratiometric pH sensor, similar to the one described above. They used a surface-functionalization scheme based on encapsulating the nanoparticles within a thiolated amphiphilic polyacrylic-octylamine 'raft' block-copolymer to promote water transfer of the QDs. Because the thiol on the polymer did not interact directly with the nanoparticle surface, it offered a free target site for attaching a maleimide-activated dye (such as fluorescein or BODIPY), which then provided an acceptor with pH-dependent absorption properties. The resulting

QD–polymer–dye construct exhibited a pH-dependent rate of energy transfer between QD and dye. Subsequently Bawendi and co-workers showed that QDs capped with poly-PEG-imidazole (PEGPIL) exhibit compact lateral extension and the resulting fluorescent platforms were suitable for implementing FRET interactions with proximal dyes. In a recent study, they used PEGPIL–QDs to assemble a FRET-based pH sensing platform.[255] To build the NC-based pH sensor, they coupled a carboxy-X-rhodamine (Rox) to the 3′ overhanging end of a cytosine-rich 35-mer oligonucleotides sequence. This sequence was hybridized with a 16-mer oligonucleotide appended at the 3′-terminus with a thiol group, which could act as a point of attachment for polymer-coated NCs. The use of cytosine-rich oligonucleotide sequences allowed them to exploit a known property of these systems to undergo folding or unfolding in response to changes in pH, depending on the protonation state of the cytosine imino group. They verified that successful conjugation of the oligonucleotide on the QDs is accompanied by changes in the optical absorption and in particular the fluorescence signature of the conjugates compared to QDs and dye alone. When the pH of the buffer solution was varied from 8 to 6, they measured a pronounced change in the relative intensities of the QD and Rox. In particular, they found that at high pH values, low FRET interactions produce a strong emission from the QD combined with a weak contribution from the dye, which is consistent with reduced FRET efficiency and with the expected unfolded configuration of the oligonucleotide hybrid, keeping the donor and acceptor far apart. Conversely, when the buffer pH value is lowered, folding of the oligonucleotide hybrid brings the QD in close proximity with the Rox and enhances the energy transfer efficiency. This produces a composite fluorescence spectrum that shows an increasingly quenched QD signal concomitant with enhancement in the Rox contribution, with a pH-dependent change in the QD and dye contributions to the measured fluorescence. They further applied this construct to probe intracellular pH changes.

4.2.3. Magnetic nanoparticles. The presence of nanoscale magnetic nanoparticles in a solution (or a biological medium) can alter the T2 relaxation time of the water molecules in its immediate vicinity. Such effects depend on the coercivity of the nanoparticle, which also depends on the nanocrystal size and the composition of the magnetic cores. This has been used by several groups to develop magnetic nanoparticles as platforms for enhancing the contrast signal in magnetic resonance imaging (MRI) and/or as sensing platforms to detect molecular events and biological interactions *in vitro* and *in vivo*.[97,102,256] For tissue imaging based on MR, surface-functionalized hydrophilic magnetic NPs (*e.g.*, those made of Fe_3O_4) either as, or attached to targeting bio-receptors (*e.g.*, antibodies) are intravenously-administered to an animal, and then changes in the T2 MR contrast signal are used to visualize the accumulation of these platforms in targeted areas, such as lymph nodes and cancerous tissues. For example, Hyeon and co-workers reported the use of the enhancement in the MR signal to track the accumulation of iron oxide nanoparticles capped with a multifunctional polydopamine polymer ligand (described earlier) in cancer tissue following intravenous administration.[173] They found that the nanoparticles accumulated in the lymph nodes 24 hours after injection through the tail vain of a nude mouse and that these polymer-capped Fe_3O_4 NPs exhibit a longer half-life blood circulation than nanoparticles functionalized with less stable small molecule ligands. Furthermore, they measured relatively high accumulation of nanoparticles in the spleen, liver and lymph nodes 24 hours post intra-venal administration (Fig. 16). Tamil Selvan and co-workers combined NIR-fluorescent dye with Fe_3O_4 nanoparticles to provide a dual-mode magnetic and fluorescent platform.[257] For this they first conjugated the amphiphilic polymer ligand, poly-(isobutylene-*alt*-maleic anhydride) to a NIR-dye (IR-820) along with a few octyl

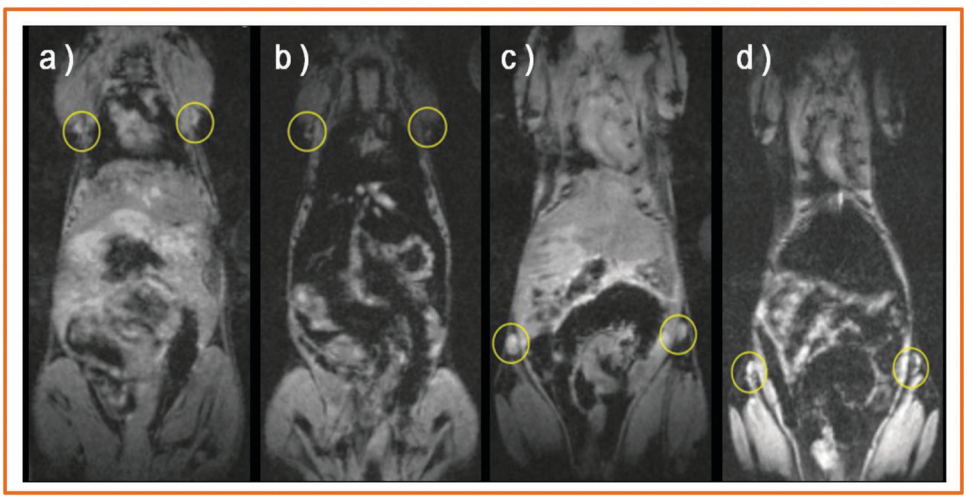

Fig. 16 Comparison of T2-weighted MR images of brachial lymph node (a, b) and inguinal lymph node (c, d) in nude mouse. Shown images are collected before intravenous injection of MIL2-functionalized Fe_3O_4 nanoparticles (a, c) and after 24 h after injection (b, d).[173] (Figures are adapted from the above reference with permission from Wiley.)

amine chains (which constitute the hydrophobic block). The dye-modified block copolymer was then used to encapsulate hydrophobic iron oxide nanoparticles and promote their transfer to water. For fluorescent imaging, they incubated these platforms with HeLa cells for 2 hours at 37 °C, and found that following internalization nearly all the fluorescence signals were accumulated in the perinuclear region of the cells, indicating an intracellular uptake mainly *via* endocytotic pathways (Fig. 17). They also applied these platforms to a murine mouse model and measured high MRI contrast indicating that these dual-mode NPs also provide good negative T2 contrast. In a more recent study, Yang and co-workers assembled a biologically functional dual-mode magnetic and fluorescent platform using Fe_3O_4 NPs, HER2 antibody ($Z_{HER2:342}$) and a NIR-830 dye (NIR-830-HER-2-NPs).[258] The authors showed that these platforms can specifically target primary and metastatic tumors in an orthotopic human ovarian cancer xenograft model.

Apart from imaging, iron oxide nanoparticles (in particular, those rendered hydrophilic and functional using a polymer coating) have also been used to develop magnetic sensors based on changes in the T2-relaxivity; they were further applied to detect full size biomolecules (such as antibody and proteins), as well as small target molecules in solution. For example, Weissleder and co-workers used commercially-available, aminated cross-linked iron oxide nanoparticles (CLIO-NH_2) and conjugated them to either a synthetic oligonucleotide complementary to TTAGGG telomeric repeats, or to a polyclonal anti-hTERT antibody, to provide sensing platforms capable of simultaneously detecting protein levels and enzymatic activities in solution.[259,260] They showed that mixing the two magnetic platforms in the same solution can allow the detection of different amounts of telomerase protein and measure telomerase activity in various cancer and normal cell lines, and furthermore assess the contribution of phosphorylation to the telomerase activity. The NP–oligonucleotide conjugates were prepared by attaching the complementary sequence 5′-CCC-TAA-CCC-TAA-CCC-TAA-3′ directly to the amine groups on the polymer coating of the NPs. Conversely, the NP–anti-hTERT antibody conjugates were formed by coupling protein G (bridging protein) onto the amine groups on the NPs *via* EDC coupling, followed by incubation with a required amount of anti-hTERT. For both constructs interactions of the magnetic platforms with the target molecules (antigen or telomerase) resulted in a sizable decrease in the T2 relaxation of water molecules.

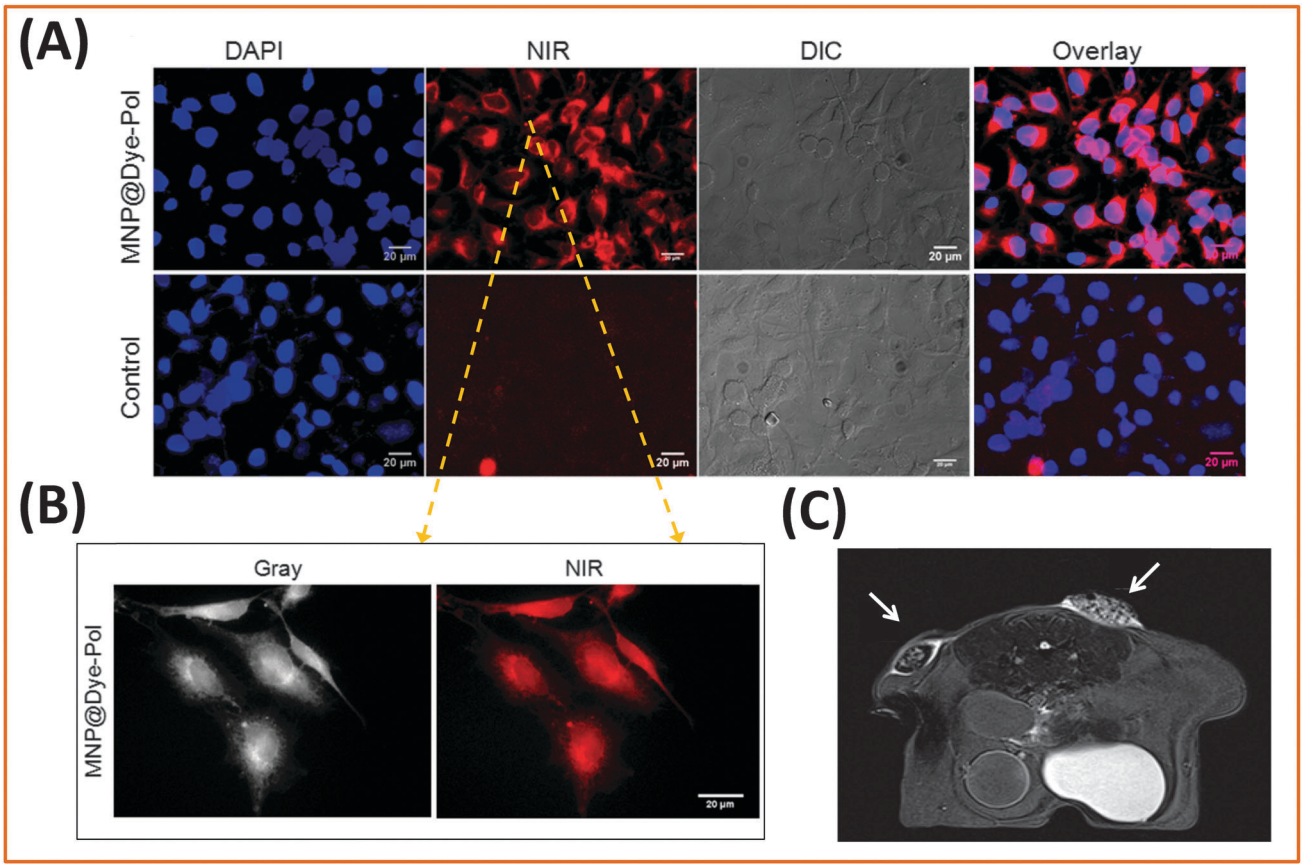

Fig. 17 (A) Labeling of HeLa cells incubated for 2 h with 50 μL of magnetic nanoparticles encapsulated with a dye-conjugated-polymer, MNP@Dye-Pol, (1 mg mL^{-1}). Lower panel shows images of untreated cells (control); (B) higher magnification images. Scale bar: 20 μm; (C) T2-weighted MR imaging of a murine model after subcutaneous injection of 0.7 mM MNP@Dye-Pol fixed in 0.8% agarose. The two arrows indicate distinct sites with a sizable contrast difference; this was attributed to the difference in the molecular weight of the encapsulating polymer used.[257] (Figures are adapted from the above reference with permission from the American Chemical Society.)

In particular, they applied these conjugates to various cell lysates (including breast cancer, lymphoma, HCC, liver metastasis, prostate, insulinoma, melanoma, and melanocytes) obtained from tumor and normal cell lines. They were able to estimate the protein concentrations from changes in T2 values for each set of lysates (Fig. 18). Combining these two sets of relaxation data collected using both magnetic platforms, they found that the HCC cell line had the highest telomerase activity, while the melanoma cell line had the highest amount of telomerase protein. More recently Perez and co-workers extended this sensing idea to calculate the dissociation constant (K_D) for a broad range of protein–ligand (*e.g.*, small drug molecule)

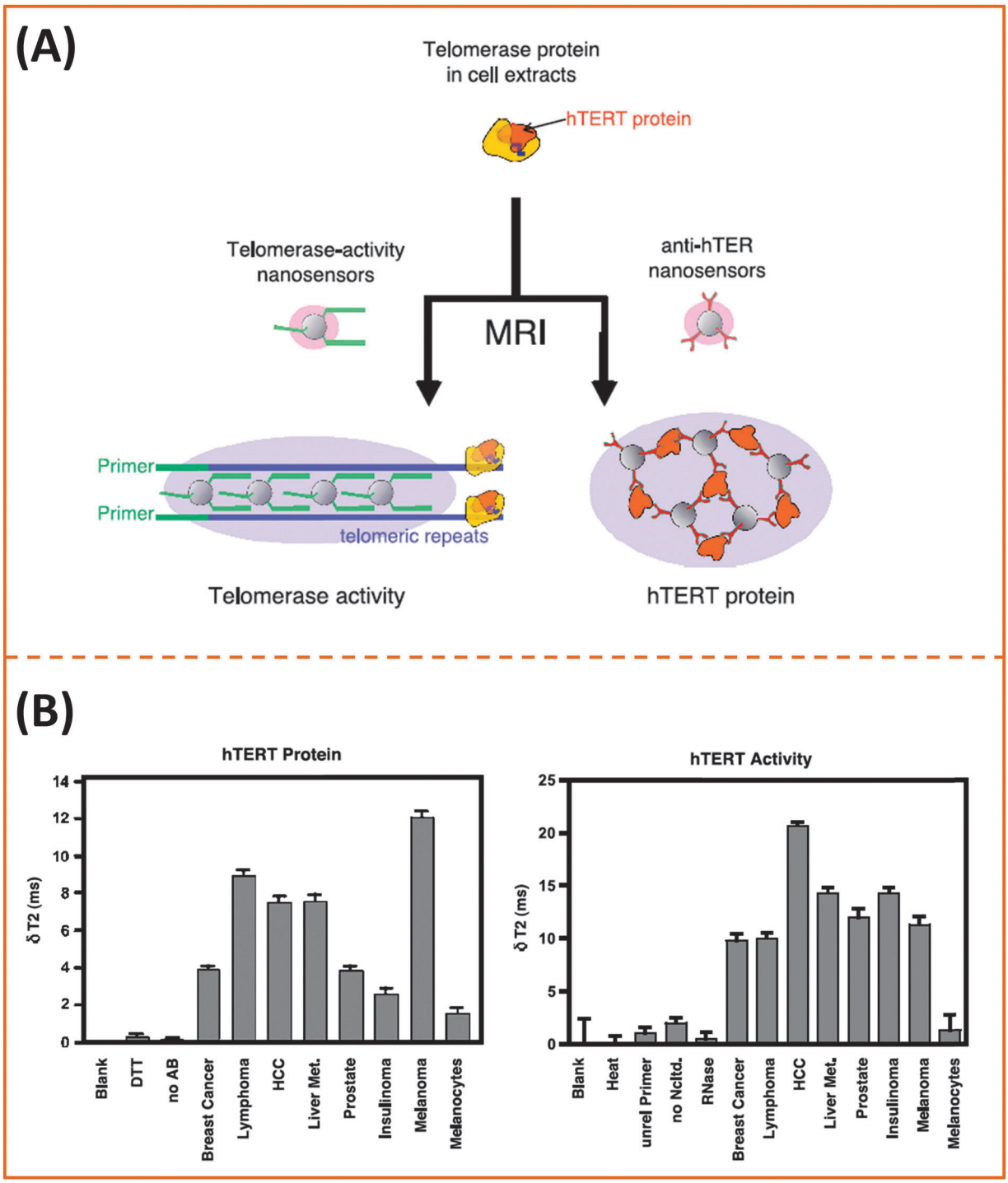

Fig. 18 (A) Schematic diagram of the magnetic nanosensor. (B) Detection of the amounts of telomerase protein (left), and telomerase activity (right) in various cell lysates using the telomerase magnetic nanosensors. Data were collected using a bench top relaxometer.[259] (Figures are adapted from the above reference with permission from Neoplasia Press.)

interactions in solution. They first showed that binding of a protein to a ligand immobilized on a Fe_3O_4 NP resulted in an increase in the T2 relaxation times of water protons in solution, indicating that magnetic relaxation nanosensors, capable of sensing the presence of target proteins (from increases in the water T2 values upon binding to the NPs), can be easily assembled. Furthermore, this transduction mechanism is fully suitable for competition assay format in solution, where increase in the concentration of competing ligand progressively disrupts the binding of specific target protein to the magnetic conjugates; this results in a smaller increase in the T2 MR signal. Thus, mixing increasing concentration of competing ligand with the nanosensor assembly containing the target molecule ligand, a quantitative titration curve can be built to provide an accurate estimate for the value of K_D. They used this sensing scheme to measure the dissociation constant for several protein-to-ligand pairs, including avidin–biotin, protein G–IgG, dextran–concavalin A, and the folic acid–folate receptor. In particular, they showed that for certain target ligands sub-femtomolar concentrations can be measured.[261]

5. Conclusion

We have provided an overview of the strategies developed over the past decade for the surface-functionalization of metal, metal oxide and semiconductor nanostructures with amphiphilic polymers, *via* either encapsulation or cap exchange strategies. We discussed the methods developed to functionalize several types of inorganic nanoparticles with polymeric materials, along with the most commonly used conjugation strategies. We then provided a few representative examples where such polymer-coated inorganic platforms have been used to develop new sensors and for the imaging of cells and/or tissue based on fluorescence or MR contrast. Examples introducing the use of gold nanoparticles and nanorods as laser activated platforms to treat cancerous cells *via* photo-thermal therapy have also been provided.

The remarkable flexibility offered by block-copolymers in terms of size, stereochemistry and conformational control can easily allow their use to surface functionalize inorganic nanocrystals, *via* either of the above strategies. For instance, amphiphilic block copolymers as encapsulating platforms provide the ability to control the micelle size, with extremely low critical micelle concentration easily reachable. Amphiphilic block copolymers also allow one to optimize the hydrophobic block, maximizing the entropy-driven interdigitation of the polymer with the native hydrophobic ligands on the nanoparticles, as well the nature and size of the hydrophilic block for enhanced water affinity. Conversely, the ability to chemically insert large but controllable numbers of metal-coordinating groups with high affinity to a specific metal, metal oxide or metal chalcogenide of choice, can easily provide multidentate ligands with more stable ligand-nanoparticle constructs. Here, the metal-coordinating groups can competitively displace the native ligands on the nanocrystals, while the hydrophilic block promotes water compatibility and reactivity. Thus, as a strategy polymer-coating of nanoparticles can provide dispersions of nanoparticles with great colloidal stability and easy conjugation.

We would also like to provide a critical comparison of the two polymer coating routes. Encapsulation of the inorganic nanocrystals within amphiphilic block copolymers tends to better preserve the photo-physical characteristics (*e.g.*, PL quantum yield for QDs), because it preserves the native ligands. This is beneficial for use in fluorescence imaging, for example. However, preserving such hydrophobic cap can potentially have undesirable effects such as inducing toxicity to biological systems. Furthermore, encapsulation substantially increases the hydrodynamic size of the final hydrophilic nanocrystals. In comparison, ligand exchange provides more compact hydrophilic nanocrystals, as multi-coordination imposes a more extended thinner polymer coating of the nanocrystal surfaces. This is proven by the ability to implement FRET sensing using polymer-capped QDs prepared *via* ligand exchange. However, ligand exchange often results in a slight alteration of the physical properties of the native materials (*e.g.*, lower PL quantum yield of QDs). Also, the chemical design of the polymer ligands can be tedious for some precursors.

Given the wealth of possibilities offered by polymeric materials, we expect that polymer-coating as a strategy to develop fluorescent, magnetic and plasmonic platforms will substantially grow in the future. Groups will continue to explore the use of various amphiphilic polymers to eventually reduce the lateral size of the hydrating layer on the nanoparticles, and introduce multiple orthogonally reactive functions, which should permit easier interfacing with biological systems, such as cells and tissues. One promising design involves the use of zwitterion moieties as the hydrophilic moieties in the amphiphilic polymers. These moieties are much smaller than PEG chains, and tend to exhibit better compatibility with various biological media and reduced nonspecific interactions with serum proteins.

References

1 J. Park, K. J. An, Y. S. Hwang, J. G. Park, H. J. Noh, J. Y. Kim, J. H. Park, N. M. Hwang and T. Hyeon, *Nat. Mater.*, 2004, **3**, 891–895.
2 P. Alivisatos, *Nat. Biotechnol.*, 2004, **22**, 47–52.
3 X. Michalet, F. Pinaud, L. Bentolila, J. Tsay, S. Doose, J. Li, G. Sundaresan, A. Wu, S. Gambhir and S. Weiss, *Science*, 2005, **307**, 538–544.
4 P. Reiss, M. Protiere and L. Li, *Small*, 2009, **5**, 154–168.
5 D. V. Talapin, J. S. Lee, M. V. Kovalenko and E. V. Shevchenko, *Chem. Rev.*, 2010, **110**, 389–458.
6 M. H. M. Dias and P. C. Lauterbur, *Magn. Reson. Med.*, 1986, **3**, 328–330.
7 P. T. Snee, R. C. Somers, G. Nair, J. P. Zimmer, M. G. Bawendi and D. G. Nocera, *J. Am. Chem. Soc.*, 2006, **128**, 13320–13321.

8 H. Mattoussi, G. Palui and H. B. Na, *Adv. Drug Delivery Rev.*, 2012, **64**, 138–166.
9 K. Saha, S. S. Agasti, C. Kim, X. N. Li and V. M. Rotello, *Chem. Rev.*, 2012, **112**, 2739–2779.
10 X. Y. Wu, H. J. Liu, J. Q. Liu, K. N. Haley, J. A. Treadway, J. P. Larson, N. F. Ge, F. Peale and M. P. Bruchez, *Nat. Biotechnol.*, 2003, **21**, 41–46.
11 A. M. Alkilany, S. E. Lohse and C. J. Murphy, *Acc. Chem. Res.*, 2013, **46**, 650–661.
12 F. Aldeek, M. A. H. Muhammed, G. Palui, N. Q. Zhan and H. Mattoussi, *ACS Nano*, 2013, **7**, 2509–2521.
13 Y.-w. Jun, Y.-M. Huh, J.-s. Choi, J.-H. Lee, H.-T. Song, S. Kim, S. Kim, S. Yoon, K.-S. Kim, J.-S. Shin, J.-S. Suh and J. Cheon, *J. Am. Chem. Soc.*, 2005, **127**, 5732–5733.
14 J. H. Lee, Y. M. Huh, Y. Jun, J. Seo, J. Jang, H. T. Song, S. Kim, E. J. Cho, H. G. Yoon, J. S. Suh and J. Cheon, *Nat. Med.*, 2007, **13**, 95–99.
15 S. H. Choi, H. Bin Na, Y. I. Park, K. An, S. G. Kwon, Y. Jang, M. Park, J. Moon, J. S. Son, I. C. Song, W. K. Moon and T. Hyeon, *J. Am. Chem. Soc.*, 2008, **130**, 15573–15580.
16 T. Hyeon, S. S. Lee, J. Park, Y. Chung and H. B. Na, *J. Am. Chem. Soc.*, 2001, **123**, 12798–12801.
17 M. De, P. S. Ghosh and V. M. Rotello, *Adv. Mater.*, 2008, **20**, 4225–4241.
18 H. Mattoussi and J. Cheon, *Inorganic nanoprobes for biological sensing and imaging*, Artech House, Boston, 2009.
19 P. Zrazhevskiy, M. Sena and X. H. Gao, *Chem. Soc. Rev.*, 2010, **39**, 4326–4354.
20 Y. C. Yeh, B. Creran and V. M. Rotello, *Nanoscale*, 2012, **4**, 1871–1880.
21 A. L. Rogach, L. Katsikas, A. Kornowski, D. S. Su, A. Eychmuller and H. Weller, *Ber. Bunsen-Ges.*, 1996, **100**, 1772–1778.
22 N. Gaponik, D. V. Talapin, A. L. Rogach, K. Hoppe, E. V. Shevchenko, A. Kornowski, A. Eychmüller and H. Weller, *J. Phys. Chem. B*, 2002, **106**, 7177–7185.
23 A. L. Rogach, T. Franzl, T. A. Klar, J. Feldmann, N. Gaponik, V. Lesnyak, A. Shavel, A. Eychmüller, Y. P. Rakovich and J. F. Donegan, *J. Phys. Chem. C*, 2007, **111**, 14628–14637.
24 F. Aldeek, L. Balan, J. Lambert and R. Schneider, *Nanotechnology*, 2008, **19**, 475401.
25 D. K. Kim, Y. Zhang, W. Voit, K. V. Rao and M. Muhammed, *J. Magn. Magn. Mater.*, 2001, **225**, 30–36.
26 D. Maity and D. C. Agrawal, *J. Magn. Magn. Mater.*, 2007, **308**, 46–55.
27 C. B. Murray, D. J. Norris and M. G. Bawendi, *J. Am. Chem. Soc.*, 1993, **115**, 8706–8715.
28 F. Aldeek, C. Mustin, L. Balan, T. Roques-Carmes, M. P. Fontaine-Aupart and R. Schneider, *Biomaterials*, 2011, **32**, 5459–5470.
29 I. Medintz, H. Uyeda, E. Goldman and H. Mattoussi, *Nat. Mater.*, 2005, **4**, 435–446.
30 C. M. Tyrakowski and P. T. Snee, *Phys. Chem. Chem. Phys.*, 2014, **16**, 837–855.
31 F. S. Bates and G. H. Fredrickson, *Phys. Today*, 1999, **52**, 32–38.
32 N. Hadjichristidis, S. Pispas and G. Floudas, *Block Copolymers: Synthetic Strategies, Physical Properties, and Applications*, Wiley, 2003.
33 H. Weller, U. Koch, M. Gutierrez and A. Henglein, *Ber. Bunsen-Ges.*, 1984, **88**, 649–656.
34 L. Brus, *J. Phys. Chem.*, 1986, **90**, 2555–2560.
35 S. Laurent, D. Forge, M. Port, A. Roch, C. Robic, L. Vander Elst and R. N. Muller, *Chem. Rev.*, 2008, **108**, 2064–2110.
36 A. L. Efros, M. Rosen, M. Kuno, M. Nirmal, D. J. Norris and M. Bawendi, *Phys. Rev. B: Condens. Matter Mater. Phys.*, 1996, **54**, 4843–4856.
37 D. J. Norris and M. G. Bawendi, *Phys. Rev. B: Condens. Matter Mater. Phys.*, 1996, **53**, 16338–16346.
38 D. J. Norris, A. L. Efros, M. Rosen and M. G. Bawendi, *Phys. Rev. B: Condens. Matter Mater. Phys.*, 1996, **53**, 16347–16354.
39 V. I. Klimov, *Nanocrystal quantum dots*, CRC Press, Boca Raton, 2nd edn, 2010.
40 A. L. Washington, M. E. Foley, S. Cheong, L. Quffa, C. J. Breshike, J. Watt, R. D. Tilley and G. F. Strouse, *J. Am. Chem. Soc.*, 2012, **134**, 17046–17052.
41 J. H. Yu, S. H. Kwon, Z. Petrasek, O. K. Park, S. W. Jun, K. Shin, M. Choi, Y. Il Park, K. Park, H. B. Bin Na, N. Lee, D. W. Lee, J. H. Kim, P. Schwille and T. Hyeon, *Nat. Mater.*, 2013, **12**, 359–366.
42 J. H. Yu, X. Y. Liu, K. E. Kweon, J. Joo, J. Park, K. T. Ko, D. Lee, S. P. Shen, K. Tivakornsasithorn, J. S. Son, J. H. Park, Y. W. Kim, G. S. Hwang, M. Dobrowolska, J. K. Furdyna and T. Hyeon, *Nat. Mater.*, 2010, **9**, 47–53.
43 V. I. Klimov, A. A. Mikhailovsky, S. Xu, A. Malko, J. A. Hollingsworth, C. A. Leatherdale, H. J. Eisler and M. G. Bawendi, *Science*, 2000, **290**, 314–317.
44 M. Kuno, D. P. Fromm, H. F. Hamann, A. Gallagher and D. J. Nesbitt, *J. Chem. Phys.*, 2001, **115**, 1028–1040.
45 K. T. Shimizu, R. G. Neuhauser, C. A. Leatherdale, S. A. Empedocles, W. K. Woo and M. G. Bawendi, *Phys. Rev. B: Condens. Matter Mater. Phys.*, 2001, **63**, 205316.
46 L. S. Li, J. T. Hu, W. D. Yang and A. P. Alivisatos, *Nano Lett.*, 2001, **1**, 349–351.
47 L. Manna, D. J. Milliron, A. Meisel, E. C. Scher and A. P. Alivisatos, *Nat. Mater.*, 2003, **2**, 382–385.
48 N. R. Jana and X. G. Peng, *J. Am. Chem. Soc.*, 2003, **125**, 14280–14281.
49 C. Bouet, B. Mahler, B. Nadal, B. Abecassis, M. D. Tessier, S. Ithurria, X. Xu and B. Dubertret, *Chem. Mater.*, 2013, **25**, 639–645.
50 S. Ithurria, M. D. Tessier, B. Mahler, R. P. S. M. Lobo, B. Dubertret and A. L. Efros, *Nat. Mater.*, 2011, **10**, 936–941.
51 A. I. Ekimov and A. A. Onushchenko, *Sov. Phys. Semicond.-USSR*, 1982, **16**, 775–778.
52 A. I. Ekimov and A. A. Onushchenko, *JETP Lett.*, 1981, **34**, 345–349.
53 A. L. Efros and A. L. Efros, *Sov. Phys. Semicond.-USSR*, 1982, **16**, 772–775.
54 N. F. Borrelli, D. W. Hall, H. J. Holland and D. W. Smith, *J. Appl. Phys.*, 1987, **61**, 5399–5409.

55 D. W. Hall and N. F. Borrelli, *J. Opt. Soc. Am. B*, 1988, **5**, 1650–1654.
56 A. Fojtik, H. Weller, U. Koch and A. Henglein, *Ber. Bunsen-Ges.*, 1984, **88**, 969–977.
57 L. Brus, *J. Phys. Chem.*, 1986, **90**, 2555–2560.
58 Z. A. Peng and X. G. Peng, *J. Am. Chem. Soc.*, 2001, **123**, 183–184.
59 L. H. Qu, Z. A. Peng and X. G. Peng, *Nano Lett.*, 2001, **1**, 333–337.
60 M. V. Kovalenko, M. I. Bodnarchuk, J. Zaumseil, J. S. Lee and D. V. Talapin, *J. Am. Chem. Soc.*, 2010, **132**, 10085–10092.
61 D. V. Talapin, A. L. Rogach, A. Kornowski, M. Haase and H. Weller, *Nano Lett.*, 2001, **1**, 207–211.
62 T. Pons, E. Pic, N. Lequeux, E. Cassette, L. Bezdetnaya, F. Guillemin, F. Marchal and B. Dubertret, *ACS Nano*, 2010, **4**, 2531–2538.
63 C. R. Bullen and P. Mulvaney, *Nano Lett.*, 2004, **4**, 2303–2307.
64 S. Sapra, A. L. Rogach and J. Feldmann, *J. Mater. Chem.*, 2006, **16**, 3391–3395.
65 T. Pons, N. Lequeux, B. Mahler, S. Sasnouski, A. Fragola and B. Dubertret, *Chem. Mater.*, 2009, **21**, 1418–1424.
66 M. D. Regulacio and M. Y. Han, *Acc. Chem. Res.*, 2010, **43**, 621–630.
67 W. J. Cai, L. M. Jiang, D. M. Yi, H. Z. Sun, H. T. Wei, H. Zhang, H. C. Sun and B. Yang, *Langmuir*, 2013, **29**, 4119–4127.
68 E. Cassette, T. Pons, C. Bouet, M. Helle, L. Bezdetnaya, F. Marchal and B. Dubertret, *Chem. Mater.*, 2010, **22**, 6117–6124.
69 I. S. Liu, H.-H. Lo, C.-T. Chien, Y.-Y. Lin, C.-W. Chen, Y.-F. Chen, W.-F. Su and S.-C. Liou, *J. Mater. Chem.*, 2008, **18**, 675–682.
70 C. Bullen and P. Mulvaney, *Langmuir*, 2006, **22**, 3007–3013.
71 B. O. Dabbousi, J. RodriguezViejo, F. V. Mikulec, J. R. Heine, H. Mattoussi, R. Ober, K. F. Jensen and M. G. Bawendi, *J. Phys. Chem. B*, 1997, **101**, 9463–9475.
72 M. A. Hines and P. Guyot-Sionnest, *J. Phys. Chem.*, 1996, **100**, 468–471.
73 P. Reiss, J. Bleuse and A. Pron, *Nano Lett.*, 2002, **2**, 781–784.
74 X. G. Peng, M. C. Schlamp, A. V. Kadavanich and A. P. Alivisatos, *J. Am. Chem. Soc.*, 1997, **119**, 7019–7029.
75 B. Mahler, P. Spinicelli, S. Buil, X. Quelin, J. P. Hermier and B. Dubertret, *Nat. Mater.*, 2008, **7**, 659–664.
76 X. Y. Wang, X. F. Ren, K. Kahen, M. A. Hahn, M. Rajeswaran, S. Maccagnano-Zacher, J. Silcox, G. E. Cragg, A. L. Efros and T. D. Krauss, *Nature*, 2009, **459**, 686–689.
77 H. B. Shen, H. Z. Wang, X. M. Li, J. Z. Niu, H. Wang, X. Chen and L. S. Li, *Dalton Trans.*, 2009, 10534–10540.
78 J. R. Dethlefsen and A. Dossing, *Nano Lett.*, 2011, **11**, 1964–1969.
79 H. B. Shen, H. Z. Wang, Z. J. Tang, J. Z. Niu, S. Y. Lou, Z. L. Du and L. S. Li, *CrystEngComm*, 2009, **11**, 1733–1738.
80 Y. Zhang, Q. Q. Dai, X. B. Li, Q. Z. Cui, Z. Y. Gu, B. Zou, Y. D. Wang and W. W. Yu, *Nanoscale Res. Lett.*, 2010, **5**, 1279–1283.
81 J. Park and S. W. Kim, *J. Mater. Chem.*, 2011, **21**, 3745–3750.
82 X. S. Tang, K. A. Yu, Q. H. Xu, E. S. G. Choo, G. K. L. Goh and J. M. Xue, *J. Mater. Chem.*, 2011, **21**, 11239–11243.
83 A. J. Morris-Cohen, M. D. Donakowski, K. E. Knowles and E. A. Weiss, *J. Phys. Chem. C*, 2009, **114**, 897–906.
84 G. Ennas, A. Musinu, G. Piccaluga, D. Zedda, D. Gatteschi, C. Sangregorio, J. L. Stanger, G. Concas and G. Spano, *Chem. Mater.*, 1998, **10**, 495–502.
85 D. Thapa, V. R. Palkar, M. B. Kurup and S. K. Malik, *Mater. Lett.*, 2004, **58**, 2692–2694.
86 A. N. Christensen, T. R. Jensen, C. R. H. Bahl and E. DiMasi, *J. Solid State Chem.*, 2007, **180**, 1431–1435.
87 S. H. Tolbert, P. Sieger, G. D. Stucky, S. M. J. Aubin, C. C. Wu and D. N. Hendrickson, *J. Am. Chem. Soc.*, 1997, **119**, 8652–8661.
88 F. X. Geng, Z. G. Zhao, H. T. Cong, J. X. Geng and H. M. Cheng, *Mater. Res. Bull.*, 2006, **41**, 2238–2243.
89 T. Douglas and M. Young, *Nature*, 1998, **393**, 152–155.
90 G. Salazar-Alvarez, M. Muhammed and A. A. Zagorodni, *Chem. Eng. Sci.*, 2006, **61**, 4625–4633.
91 C. Pascal, J. L. Pascal, F. Favier, M. L. E. Moubtassim and C. Payen, *Chem. Mater.*, 1999, **11**, 141–147.
92 J. H. Bang and K. S. Suslick, *J. Am. Chem. Soc.*, 2007, **129**, 2242–2243.
93 S. H. Sun and C. B. Murray, *J. Appl. Phys.*, 1999, **85**, 4325–4330.
94 C. R. K. C. B. Murray and M. G. Bawendi, *Annu. Rev. Mater. Sci.*, 2000, **30**, 545–610.
95 F. X. Redl, C. T. Black, G. C. Papaefthymiou, R. L. Sandstrom, M. Yin, H. Zeng, C. B. Murray and S. P. O'Brien, *J. Am. Chem. Soc.*, 2004, **126**, 14583–14599.
96 Y. W. Jun, Y. Y. Jung and J. Cheon, *J. Am. Chem. Soc.*, 2002, **124**, 615–619.
97 Y.-w. Jun, J.-H. Lee and J. Cheon, *Angew. Chem., Int. Ed.*, 2008, **47**, 5122–5135.
98 V. F. Puntes, K. M. Krishnan and P. Alivisatos, *Appl. Phys. Lett.*, 2001, **78**, 2187–2189.
99 V. F. Puntes, P. Gorostiza, D. M. Aruguete, N. G. Bastus and A. P. Alivisatos, *Nat. Mater.*, 2004, **3**, 263–268.
100 N. R. Jana, Y. Chen and X. Peng, *Chem. Mater.*, 2004, **16**, 3931–3935.
101 S. Sun, H. Zeng, D. B. Robinson, S. Raoux, P. M. Rice, S. X. Wang and G. Li, *J. Am. Chem. Soc.*, 2003, **126**, 273–279.
102 J. Cheon and J. H. Lee, *Acc. Chem. Res.*, 2008, **41**, 1630–1640.
103 J. R. Lai, K. V. P. M. Shafi, A. Ulman, K. Loos, N. L. Yang, M. H. Cui, T. Vogt, S. Estournes and D. C. Locke, *J. Phys. Chem. B*, 2004, **108**, 14876–14883.
104 R. Qiao, C. Yang and M. Gao, *J. Mater. Chem.*, 2009, **19**, 6274–6293.
105 S. Sun, *Adv. Mater.*, 2006, **18**, 393–403.
106 M. Brust, M. Walker, D. Bethell, D. J. Schiffrin and R. Whyman, *J. Chem. Soc., Chem. Commun.*, 1994, 801–802.
107 J. Turkevich, P. C. Stevenson and J. Hillier, *Discuss. Faraday Soc.*, 1951, 55–75.
108 G. Frens, *Nat. Phys. Sci.*, 1973, **241**, 20–22.

109 X. P. Sun, S. J. Dong and E. K. Wang, *Polymer*, 2004, **45**, 2181–2184.
110 A. Pucci, M. Bernabo, P. Elvati, L. I. Meza, F. Galembeck, C. A. D. Leite, N. Tirelli and G. Ruggeri, *J. Mater. Chem.*, 2006, **16**, 1058–1066.
111 G. Maiorano, S. Sabella, B. Sorce, V. Brunetti, M. A. Malvindi, R. Cingolani and P. P. Pompa, *ACS Nano*, 2010, **4**, 7481–7491.
112 N. Wangoo, C. R. Suri and G. Shekhawat, *Appl. Phys. Lett.*, 2008, **92**, 133104.
113 D.-H. Tsai, F. W. DelRio, A. M. Keene, K. M. Tyner, R. I. MacCuspie, T. J. Cho, M. R. Zachariah and V. A. Hackley, *Langmuir*, 2011, **27**, 2464–2477.
114 E. Oh, K. Susumu, R. Goswami and H. Mattoussi, *Langmuir*, 2010, **26**, 7604–7613.
115 M. A. Muhammed, F. Aldeek, G. Palui, L. Trapiella-Alfonso and H. Mattoussi, *ACS Nano*, 2012, **6**, 8950–8961.
116 S. E. Lohse, J. R. Eller, S. T. Sivapalan, M. R. Plews and C. J. Murphy, *ACS Nano*, 2013, **7**, 4135–4150.
117 X. Ye, L. Jin, H. Caglayan, J. Chen, G. Xing, C. Zheng, V. Doan-Nguyen, Y. Kang, N. Engheta, C. R. Kagan and C. B. Murray, *ACS Nano*, 2012, **6**, 2804–2817.
118 T. K. Sau and C. J. Murphy, *J. Am. Chem. Soc.*, 2004, **126**, 8648–8649.
119 H. Hakkinen, *Nat. Chem.*, 2012, **4**, 443–455.
120 D. A. Fleming and M. E. Williams, *Langmuir*, 2004, **20**, 3021–3023.
121 H. Hiramatsu and F. E. Osterloh, *Chem. Mater.*, 2004, **16**, 2509–2511.
122 O. C. Compton and F. E. Osterloh, *J. Am. Chem. Soc.*, 2007, **129**, 7793–7798.
123 S. Liu, G. Y. Chen, P. N. Prasad and M. T. Swihart, *Chem. Mater.*, 2011, **23**, 4098–4101.
124 W. H. Liu, A. B. Greytak, J. Lee, C. R. Wong, J. Park, L. F. Marshall, W. Jiang, P. N. Curtin, A. Y. Ting, D. G. Nocera, D. Fukumura, R. K. Jain and M. G. Bawendi, *J. Am. Chem. Soc.*, 2010, **132**, 472–483.
125 W. C. W. Chan and S. M. Nie, *Science*, 1998, **281**, 2016–2018.
126 H. T. Uyeda, I. L. Medintz, J. K. Jaiswal, S. M. Simon and H. Mattoussi, *J. Am. Chem. Soc.*, 2005, **127**, 3870–3878.
127 W. Liu, M. Howarth, A. B. Greytak, Y. Zheng, D. G. Nocera, A. Y. Ting and M. G. Bawendi, *J. Am. Chem. Soc.*, 2008, **130**, 1274–1284.
128 M. Bruchez, M. Moronne, P. Gin, S. Weiss and A. P. Alivisatos, *Science*, 1998, **281**, 2013–2016.
129 H. Mattoussi, J. M. Mauro, E. R. Goldman, G. P. Anderson, V. C. Sundar, F. V. Mikulec and M. G. Bawendi, *J. Am. Chem. Soc.*, 2000, **122**, 12142–12150.
130 W. W. Yu, E. Chang, J. C. Falkner, J. Y. Zhang, A. M. Al-Somali, C. M. Sayes, J. Johns, R. Drezek and V. L. Colvin, *J. Am. Chem. Soc.*, 2007, **129**, 2871–2879.
131 F. Zhang, E. Lees, F. Amin, P. R. Gil, F. Yang, P. Mulvaney and W. J. Parak, *Small*, 2011, **7**, 3113–3127.
132 T. Pellegrino, L. Manna, S. Kudera, T. Liedl, D. Koktysh, A. L. Rogach, S. Keller, J. Radler, G. Natile and W. J. Parak, *Nano Lett.*, 2004, **4**, 703–707.
133 A. N. Lukyanov and V. P. Torchilin, *Adv. Drug Delivery Rev.*, 2004, **56**, 1273–1289.
134 R. Levy, N. T. K. Thanh, R. C. Doty, I. Hussain, R. J. Nichols, D. J. Schiffrin, M. Brust and D. G. Fernig, *J. Am. Chem. Soc.*, 2004, **126**, 10076–10084.
135 M. C. Daniel and D. Astruc, *Chem. Rev.*, 2004, **104**, 293–346.
136 J. M. Kogot, H. J. England, G. F. Strouse and T. M. Logan, *J. Am. Chem. Soc.*, 2008, **130**, 16156–16157.
137 P. Dash and R. W. J. Scott, *Chem. Commun.*, 2009, 812–814.
138 X. Zhang, M. R. Servos and J. Liu, *J. Am. Chem. Soc.*, 2012, **134**, 7266–7269.
139 K. E. Sapsford, W. R. Algar, L. Berti, K. B. Gemmill, B. J. Casey, E. Oh, M. H. Stewart and I. L. Medintz, *Chem. Rev.*, 2013, **113**, 1904–2074.
140 K. O. Aruda, M. Tagliazucchi, C. M. Sweeney, D. C. Hannah, G. C. Schatz and E. A. Weiss, *Proc. Natl. Acad. Sci. U. S. A.*, 2013, **110**, 4212–4217.
141 P. D. Jadzinsky, G. Calero, C. J. Ackerson, D. A. Bushnell and R. D. Kornberg, *Science*, 2007, **318**, 430–433.
142 J. R. Reimers, Y. Wang, B. O. Cankurtaran and M. J. Ford, *J. Am. Chem. Soc.*, 2010, **132**, 8378–8384.
143 H. B. Na, G. Palui, J. T. Rosenberg, X. Ji, S. C. Grant and H. Mattoussi, *ACS Nano*, 2012, **6**, 389–399.
144 N. Chan, M. Laprise-Pelletier, P. Chevallier, A. Bianchi, M.-A. Fortin and J. K. Oh, *Biomacromolecules*, 2014, **15**, 2146–2156.
145 P. Zhang, S. Liu, D. Gao, D. Hu, P. Gong, Z. Sheng, J. Deng, Y. Ma and L. Cai, *J. Am. Chem. Soc.*, 2012, **134**, 8388–8391.
146 G. P. Mitchell, C. A. Mirkin and R. L. Letsinger, *J. Am. Chem. Soc.*, 1999, **121**, 8122–8123.
147 Z.-J. Zhu, Y.-C. Yeh, R. Tang, B. Yan, J. Tamayo, R. W. Vachet and V. M. Rotello, *Nat. Chem.*, 2011, **3**, 963–968.
148 K. Susumu, H. T. Uyeda, I. L. Medintz, T. Pons, J. B. Delehanty and H. Mattoussi, *J. Am. Chem. Soc.*, 2007, **129**, 13987–13996.
149 J. S. Kang and T. A. Taton, *Langmuir*, 2012, **28**, 16751–16760.
150 I. Yildiz, E. Deniz, B. McCaughan, S. F. Cruickshank, J. F. Callan and F. M. Raymo, *Langmuir*, 2010, **26**, 11503–11511.
151 I. Yildiz, B. McCaughan, S. F. Cruickshank, J. F. Callan and F. M. Raymo, *Langmuir*, 2009, **25**, 7090–7096.
152 G. Palui, H. B. Na and H. Mattoussi, *Langmuir*, 2012, **28**, 2761–2772.
153 L. Liu, X. H. Guo, Y. Li and X. H. Zhong, *Inorg. Chem.*, 2010, **49**, 3768–3775.
154 E. Giovanelli, E. Muro, G. Sitbon, M. Hanafi, T. Pons, B. Dubertret and N. Lequeux, *Langmuir*, 2012, **28**, 15177–15184.
155 M. Sun, L. Yang, P. Jose, L. Wang and J. Zweit, *J. Mater. Chem. B*, 2013, **1**, 6137–6146.
156 G. Palui, T. Avellini, N. Zhan, F. Pan, D. Gray, I. Alabugin and H. Mattoussi, *J. Am. Chem. Soc.*, 2012, **134**, 16370–16378.
157 G. Bucher, C. Y. Lu and W. Sander, *ChemPhysChem*, 2005, **6**, 2607–2618.

158 X. J. Chen, J. Lawrence, S. Parelkar and T. Emrick, *Macromolecules*, 2013, **46**, 119–127.
159 K. E. Sapsford, T. Pons, I. L. Medintz, S. Higashiya, F. M. Brunel, P. E. Dawson and H. Mattoussi, *J. Phys. Chem. C*, 2007, **111**, 11528–11538.
160 A. R. Clapp, I. L. Medintz, J. M. Mauro, B. R. Fisher, M. G. Bawendi and H. Mattoussi, *J. Am. Chem. Soc.*, 2004, **126**, 301–310.
161 K. E. Sapsford, T. Pons, I. L. Medintz, S. Higashiya, F. M. Brunel, P. E. Dawson and H. Mattoussi, *J. Phys. Chem. C*, 2007, **111**, 11528–11538.
162 F. Aldeek, M. Safi, N. Zhan, G. Palui and H. Mattoussi, *ACS Nano*, 2013, **7**, 10197–10210.
163 H. S. Han, J. D. Martin, J. Lee, D. K. Harris, D. Fukumura, R. K. Jain and M. Bawendi, *Angew. Chem.*, 2013, **52**, 1414–1419.
164 Y. Sahoo, H. Pizem, T. Fried, D. Golodnitsky, L. Burstein, C. N. Sukenik and G. Markovich, *Langmuir*, 2001, **17**, 7907–7911.
165 S.-W. Kim, S. Kim, J. B. Tracy, A. Jasanoff and M. G. Bawendi, *J. Am. Chem. Soc.*, 2005, **127**, 4556–4557.
166 H. Wei, N. Insin, J. Lee, H.-S. Han, J. M. Cordero, W. Liu and M. G. Bawendi, *Nano Lett.*, 2011, **12**, 22–25.
167 L. Sandiford, A. Phinikaridou, A. Protti, L. K. Meszaros, X. Cui, Y. Yan, G. Frodsham, P. A. Williamson, N. Gaddum, R. M. Botnar, P. J. Blower, M. A. Green and R. T. M. de Rosales, *ACS Nano*, 2012, **7**, 500–512.
168 C. J. Xu, K. M. Xu, H. W. Gu, R. K. Zheng, H. Liu, X. X. Zhang, Z. H. Guo and B. Xu, *J. Am. Chem. Soc.*, 2004, **126**, 9938–9939.
169 E. Amstad, T. Gillich, I. Bilecka, M. Textor and E. Reimhult, *Nano Lett.*, 2009, **9**, 4042–4048.
170 J. Xie, K. Chen, H.-Y. Lee, C. Xu, A. R. Hsu, S. Peng, X. Chen and S. Sun, *J. Am. Chem. Soc.*, 2008, **130**, 7542–7543.
171 K. Cheng, S. Peng, C. Xu and S. Sun, *J. Am. Chem. Soc.*, 2009, **131**, 10637–10644.
172 W. Wang, X. Ji, H. B. Na, M. Safi, A. Smith, G. Palui, J. M. Perez and H. Mattoussi, *Langmuir*, 2014, **30**, 6197–6208.
173 D. Ling, W. Park, Y. I. Park, N. Lee, F. Li, C. Song, S.-G. Yang, S. H. Choi, K. Na and T. Hyeon, *Angew. Chem., Int. Ed.*, 2011, **50**, 11360–11365.
174 C. C. Lu, L. R. Bhatt, H. Y. Jun, S. H. Park and K. Y. Chai, *J. Mater. Chem.*, 2012, **22**, 19806–19811.
175 A. Graillot, D. Bouyer, S. Monge, J. J. Robin, P. Loison and C. Faur, *J. Hazard. Mater.*, 2013, **260**, 425–433.
176 P. Aggarwal, J. B. Hall, C. B. McLeland, M. A. Dobrovolskaia and S. E. McNeil, *Adv. Drug Delivery Rev.*, 2009, **61**, 428–437.
177 C. Tassa, S. Y. Shaw and R. Weissleder, *Acc. Chem. Res.*, 2011, **44**, 842–852.
178 Y. J. Kang and T. A. Taton, *Angew. Chem., Int. Ed.*, 2005, **44**, 409–412.
179 Y. Kang and T. A. Taton, *Macromolecules*, 2005, **38**, 6115–6121.
180 Y. Chen, J. Cho, A. Young and T. A. Taton, *Langmuir*, 2007, **23**, 7491–7497.
181 W. K. Li, S. Q. Liu, R. H. Deng, J. Y. Wang, Z. H. Nie and J. T. Zhu, *Macromolecules*, 2013, **46**, 2282–2291.
182 B. A. Kairdolf and S. M. Nie, *J. Am. Chem. Soc.*, 2011, **133**, 7268–7271.
183 D. H. Kim, A. Wei and Y.-Y. Won, *ACS Appl. Mater. Interfaces*, 2012, **4**, 1872–1877.
184 A. Elbakry, A. Zaky, R. Liebkl, R. Rachel, A. Goepferich and M. Breunig, *Nano Lett.*, 2009, **9**, 2059–2064.
185 A. Elbakry, E. C. Wurster, A. Zaky, R. Liebl, E. Schindler, P. Bauer-Kreisel, T. Blunk, R. Rachel, A. Goepferich and M. Breunig, *Small*, 2012, **8**, 3847–3856.
186 J. Huang, K. S. Jackson and C. J. Murphy, *Nano Lett.*, 2012, **12**, 2982–2987.
187 A. Gole and C. J. Murphy, *Chem. Mater.*, 2005, **17**, 1325–1330.
188 K. S. Mayya, B. Schoeler and F. Caruso, *Adv. Funct. Mater.*, 2003, **13**, 183–188.
189 H.-C. Huang, S. Barua, D. B. Kay and K. Rege, *ACS Nano*, 2009, **3**, 2941–2952.
190 X. H. Huang, I. H. El-Sayed, W. Qian and M. A. El-Sayed, *J. Am. Chem. Soc.*, 2006, **128**, 2115–2120.
191 G. Decher, *Science*, 1997, **277**, 1232–1237.
192 J. B. Schlenoff, H. Ly and M. Li, *J. Am. Chem. Soc.*, 1998, **120**, 7626–7634.
193 L. L. Rouhana, M. D. Moussallem and J. B. Schlenoff, *J. Am. Chem. Soc.*, 2011, **133**, 16080–16091.
194 W. B. Stockton and M. F. Rubner, *Macromolecules*, 1997, **30**, 2717–2725.
195 C. Tedeschi, H. Möhwald and S. Kirstein, *J. Am. Chem. Soc.*, 2001, **123**, 954–960.
196 S. K. Chakraborty, J. A. J. Fitzpatrick, J. A. Phillippi, S. Andreko, A. S. Waggoner, M. P. Bruchez and B. Ballou, *Nano Lett.*, 2007, **7**, 2618–2626.
197 B. C. Lagerholm, M. M. Wang, L. A. Ernst, D. H. Ly, H. J. Liu, M. P. Bruchez and A. S. Waggoner, *Nano Lett.*, 2004, **4**, 2019–2022.
198 D. R. Larson, W. R. Zipfel, R. M. Williams, S. W. Clark, M. P. Bruchez, F. W. Wise and W. W. Webb, *Science*, 2003, **300**, 1434–1436.
199 S. Courty, C. Luccardini, Y. Bellaiche, G. Cappello and M. Dahan, *Nano Lett.*, 2006, **6**, 1491–1495.
200 M. Dahan, S. Levi, C. Luccardini, P. Rostaing, B. Riveau and A. Triller, *Science*, 2003, **302**, 442–445.
201 D. S. Lidke, P. Nagy, R. Heintzmann, D. J. Arndt-Jovin, J. N. Post, H. E. Grecco, E. A. Jares-Erijman and T. M. Jovin, *Nat. Biotechnol.*, 2004, **22**, 198–203.
202 M. J. Roberti, M. Morgan, G. Menendez, L. I. Pietrasanta, T. M. Jovin and E. A. Jares-Erijman, *J. Am. Chem. Soc.*, 2009, **131**, 8102–8107.
203 X. H. Gao, Y. Y. Cui, R. M. Levenson, L. W. K. Chung and S. M. Nie, *Nat. Biotechnol.*, 2004, **22**, 969–976.
204 M. T. Fernández-Argüelles, A. Yakovlev, R. A. Sperling, C. Luccardini, S. Gaillard, A. Sanz Medel, J.-M. Mallet, J.-C. Brochon, A. Feltz, M. Oheim and W. J. Parak, *Nano Lett.*, 2007, **7**, 2613–2617.
205 E. E. Lees, T. L. Nguyen, A. H. A. Clayton, P. Mulvaney and B. W. Muir, *ACS Nano*, 2009, **3**, 1121–1128.

206 M. F. Wang, M. Zhang, J. Li, S. Kumar, G. C. Walker, G. D. Scholes and M. A. Winnik, *ACS Appl. Mater. Interfaces*, 2010, **2**, 3160–3169.
207 M. F. Wang, N. Felorzabihi, G. Guerin, J. C. Haley, G. D. Scholes and M. A. Winnik, *Macromolecules*, 2007, **40**, 6377–6384.
208 J. Qian and X. H. Gao, *ACS Appl. Mater. Interfaces*, 2013, **5**, 2845–2852.
209 E. Pöselt, C. Schmidtke, S. Fischer, K. Peldschus, J. Salamon, H. Kloust, H. Tran, A. Pietsch, M. Heine, G. Adam, U. Schumacher, C. Wagener, S. Förster and H. Weller, *ACS Nano*, 2012, **6**, 3346–3355.
210 E. Poselt, S. Fischer, S. Foerster and H. Weller, *Langmuir*, 2009, **25**, 13906–13913.
211 J. Ostermann, J. P. Merkl, S. Flessau, C. Wolter, A. Kornowksi, C. Schmidtke, A. Pietsch, H. Kloust, A. Feld and H. Weller, *ACS Nano*, 2013, **7**, 9156–9167.
212 H. Kloust, E. Poselt, S. Kappen, C. Schmidtke, A. Kornowski, W. Pauer, H. U. Moritz and H. Weller, *Langmuir*, 2012, **28**, 7276–7281.
213 H. Kloust, C. Schmidtke, A. Feld, T. Schotten, R. Eggers, U. E. A. Fittschen, F. Schulz, E. Pöselt, J. Ostermann, N. G. Bastús and H. Weller, *Langmuir*, 2013, **29**, 4915–4921.
214 H. Kloust, C. Schmidtke, J. P. Merkl, A. Feld, T. Schotten, U. E. A. Fittschen, M. Gehring, J. Ostermann, E. Poselt and H. Weller, *J. Phys. Chem. C*, 2013, **117**, 23244–23250.
215 T. Jin, F. Fujii, E. Yamada, Y. Nodasaka and M. Kinjo, *J. Am. Chem. Soc.*, 2006, **128**, 9288–9289.
216 E. Oh, K. Susumu, J. B. Blanco-Canosa, I. L. Medintz, P. E. Dawson and H. Mattoussi, *Small*, 2010, **6**, 1273–1278.
217 M. Zhou, E. Nakatani, L. S. Gronenberg, T. Tokimoto, M. J. Wirth, V. J. Hruby, A. Roberts, R. M. Lynch and I. Ghosh, *Bioconjugate Chem.*, 2007, **18**, 323–332.
218 A. R. Clapp, E. R. Goldman and H. Mattoussi, *Nat. Protoc.*, 2006, **1**, 1258–1266.
219 H.-S. Han, N. K. Devaraj, J. Lee, S. A. Hilderbrand, R. Weissleder and M. G. Bawendi, *J. Am. Chem. Soc.*, 2010, **132**, 7838–7839.
220 C. Schieber, A. Bestetti, J. P. Lim, A. D. Ryan, T.-L. Nguyen, R. Eldridge, A. R. White, P. A. Gleeson, P. S. Donnelly, S. J. Williams and P. Mulvaney, *Angew. Chem., Int. Ed.*, 2012, **51**, 10523–10527.
221 A. Bernardin, A. Cazet, L. Guyon, P. Delannoy, F. Vinet, D. Bonnaffe and I. Texier, *Bioconjugate Chem.*, 2010, **21**, 583–588.
222 G. T. Hermanson, *Bioconjugate techniques*, Academic Press, San Diego, 1996.
223 I. L. Medintz, T. Pons, K. Susumu, K. Boeneman, A. M. Dennis, D. Farrell, J. R. Deschamps, J. S. Melinger, G. Bao and H. Mattoussi, *J. Phys. Chem. C*, 2009, **113**, 18552–18561.
224 J. M. Kogot, H. J. England, G. F. Strouse and T. M. Logan, *J. Am. Chem. Soc.*, 2008, **130**, 16156–16157.
225 R. Huisgen, G. Szeimies and L. Möbius, *Chem. Ber.*, 1967, **100**, 2494–2507.
226 F. Amblard, J. H. Cho and R. F. Schinazi, *Chem. Rev.*, 2009, **109**, 4207–4220.
227 J. M. Baskin, J. A. Prescher, S. T. Laughlin, N. J. Agard, P. V. Chang, I. A. Miller, A. Lo, J. A. Codelli and C. R. Bertozzi, *Proc. Natl. Acad. Sci. U. S. A.*, 2007, **104**, 16793–16797.
228 P. V. Chang, J. A. Prescher, E. M. Sletten, J. M. Baskin, I. A. Miller, N. J. Agard, A. Lo and C. R. Bertozzi, *Proc. Natl. Acad. Sci. U. S. A.*, 2010, **107**, 1821–1826.
229 J. C. Jewett and C. R. Bertozzi, *Chem. Soc. Rev.*, 2010, **39**, 1272–1279.
230 J. B. Blanco-Canosa, I. L. Medintz, D. Farrell, H. Mattoussi and P. E. Dawson, *J. Am. Chem. Soc.*, 2010, **132**, 10027–10033.
231 C. A. Mirkin, R. L. Letsinger, R. C. Mucic and J. J. Storhoff, *Nature*, 1996, **382**, 607–609.
232 Z. Li, R. C. Jin, C. A. Mirkin and R. L. Letsinger, *Nucleic Acids Res.*, 2002, **30**, 1558–1562.
233 R. Elghanian, J. J. Storhoff, R. C. Mucic, R. L. Letsinger and C. A. Mirkin, *Science*, 1997, **277**, 1078–1081.
234 C. J. Breshike, R. A. Riskowski and G. F. Strouse, *J. Phys. Chem. C*, 2013, **117**, 23942–23949.
235 F. Aldeek, X. Ji and H. Mattoussi, *J. Phys. Chem. C*, 2013, **117**, 15429–15437.
236 T. Pons, I. L. Medintz, K. E. Sapsford, S. Higashiya, A. F. Grimes, D. S. English and H. Mattoussi, *Nano Lett.*, 2007, **7**, 3157–3164.
237 E. Dulkeith, M. Ringler, T. A. Klar, J. Feldmann, A. M. Javier and W. J. Parak, *Nano Lett.*, 2005, **5**, 585–589.
238 Y. Liu, K. Yehl, Y. Narui and K. Salaita, *J. Am. Chem. Soc.*, 2013, **135**, 5320–5323.
239 E. Petryayeva and U. J. Krull, *Langmuir*, 2012, **28**, 13943–13951.
240 J. Griffin, A. K. Singh, D. Senapati, P. Rhodes, K. Mitchell, B. Robinson, E. Yu and P. C. Ray, *Chem. – Eur. J.*, 2009, **15**, 342–351.
241 W. Q. Li, C. Y. Sun, F. Wang, Y. C. Wang, Y. W. Zhai, M. Liang, W. J. Liu, Z. M. Liu, J. Wang and F. Sun, *Nano Lett.*, 2013, **13**, 2477–2484.
242 E. Oh, D. Lee, Y. P. Kim, S. Y. Cha, D. B. Oh, H. A. Kang, J. Kim and H. S. Kim, *Angew. Chem., Int. Ed.*, 2006, **45**, 7959–7963.
243 A. Chompoosor, G. Han and V. M. Rotello, *Bioconjugate Chem.*, 2008, **19**, 1342–1345.
244 M. De, S. Rana, H. Akpinar, O. R. Miranda, R. R. Arvizo, U. H. F. Bunz and V. M. Rotello, *Nat. Chem.*, 2009, **1**, 461–465.
245 X. Q. An, F. Zhan and Y. Y. Zhu, *Langmuir*, 2013, **29**, 1061–1068.
246 S. E. Skrabalak, L. Au, X. D. Li and Y. N. Xia, *Nat. Protoc.*, 2007, **2**, 2182–2190.
247 M. S. Yavuz, Y. Cheng, J. Chen, C. M. Cobley, Q. Zhang, M. Rycenga, J. Xie, C. Kim, K. H. Song, A. G. Schwartz, L. V. Wang and Y. Xia, *Nat. Mater.*, 2009, **8**, 935–939.
248 N. Anikeeva, T. Lebedeva, A. R. Clapp, E. R. Goldman, M. L. Dustin, H. Mattoussi and Y. Sykulev, *Proc. Natl. Acad. Sci. U. S. A.*, 2006, **103**, 16846–16851.
249 F. Pinaud, X. Michalet, G. Iyer, E. Margeat, H. P. Moore and S. Weiss, *Traffic*, 2009, **10**, 691–712.

250 A. R. Bayles, H. S. Chahal, D. S. Chahal, C. P. Goldbeck, B. E. Cohen and B. A. Helms, *Nano Lett.*, 2010, **10**, 4086–4092.
251 J. Lee, A. Sharei, W. Y. Sim, A. Adamo, R. Langer, K. F. Jensen and M. G. Bawendi, *Nano Lett.*, 2012, **12**, 6322–6327.
252 S. Impellizzeri, B. McCaughan, J. F. Callan and F. M. Raymo, *J. Am. Chem. Soc.*, 2012, **134**, 2276–2283.
253 I. L. Medintz, A. R. Clapp, H. Mattoussi, E. R. Goldman, B. Fisher and J. M. Mauro, *Nat. Mater.*, 2003, **2**, 630–638.
254 R. C. Somers, R. M. Lanning, P. T. Snee, A. B. Greytak, R. K. Jain, M. G. Bawendi and D. G. Nocera, *Chem. Sci.*, 2012, **3**, 2980–2985.
255 E. R. Kay, J. Lee, D. G. Nocera and M. G. Bawendi, *Angew. Chem., Int. Ed.*, 2013, **52**, 1165–1169.
256 N. Lee and T. Hyeon, *Chem. Soc. Rev.*, 2012, **41**, 2575–2589.
257 S. K. Yen, D. Jańczewski, J. L. Lakshmi, S. B. Dolmanan, S. Tripathy, V. H. B. Ho, V. Vijayaragavan, A. Hariharan, P. Padmanabhan, K. K. Bhakoo, T. Sudhaharan, S. Ahmed, Y. Zhang and S. Tamil Selvan, *ACS Nano*, 2013, **7**, 6796–6805.
258 M. Satpathy, L. Wang, R. Zielinski, W. Qian, M. Lipowska, J. Capala, G. Y. Lee, H. Xu, Y. A. Wang, H. Mao and L. Yang, *Small*, 2014, **10**, 544–555.
259 J. M. Perez, J. Grimm, L. Josephson and R. Weissleder, *Neoplasia*, 2008, **10**, 1066–1072.
260 J. Grimm, J. M. Perez, L. Josephson and R. Weissleder, *Cancer Res.*, 2004, **64**, 639–643.
261 O. J. Santiesteban, C. Kaittanis and J. M. Perez, *Angew. Chem., Int. Ed.*, 2012, **51**, 6728–6732.